PHILOSOPHICAL TRANSACTIONS OF THE ROYAL SOCIETY A MATHEMATICAL, PHYSICAL & ENGINEERING SCIENCES

Plane Nets in Crystal Chemistry

M. O'Keeffe and B. G. Hyde

Phil. Trans. R. Soc. Lond. A 1980 **295**, 553-618
doi: 10.1098/rsta.1980.0150

PLANE NETS IN CRYSTAL CHEMISTRY

By M. O'Keeffe† and B. G. Hyde‡§

† *Department of Chemistry, Arizona State University, Tempe, Arizona* 85281, *U.S.A.*

‡ *Gorlaeus Laboratories, R.U. Leiden, P.B.* 75, *Leiden, The Netherlands*

(*Communicated by J. S. Anderson, F.R.S. – Received* 10 *May* 1979)

CONTENTS

§ Present address: Research School of Chemistry, The Australian National University, Box 4, P.O., Canberra, A.C.T. 2600, Australia.

In the present paper we consider not only the simplest periodic nets (such as arise from the equivalent circle packings of Niggli, Fejes Tóth and others) but also less regular ones, ignored by mathematicians but nevertheless of widespread occurrence and usefulness in crystal chemistry.

After a general introduction including some mathematical theorems a catalogue of about 30 nets gives, in most cases, the plane group short symbol, and the unit cell parameters and the coordinates of the nodes in terms of unit spacing between nearest nodes. Examples of their occurrence in compounds of established structure are given in each case.

The related concepts of the dual of a simple net and primary and secondary nets in less simple cases are then treated briefly.

Transformations between nets are discussed, also with crystal structure examples: first in the case that there is no change in the shape of the unit cell, and using a proposed 'compatibility' principle. It transpires that compatible nets are simply derivable from one another, and that in most classes the simplest member is a regular net ($\mathbf{4^4}$, $\mathbf{3^6}$, or $\mathbf{6^3}$). A few of the transformations are relatively well known, but most are new. Together they emphasise the fact that crystal structures do not constitute a massive collection of unrelated types, but rather a group of patterns largely derivable one from another by a few simple, geometrical–crystallographic operations. Here, as elsewhere in the paper, it frequently occurs that transformations are equivalent to the regular incorporation of 'point defects' (missing atoms = 'vacancies' or additional atoms = 'interstitials'). Hence 'point defects' may be readily generated (even in very small concentrations) by cooperative operations, without any need for long-range diffusion of single atoms. This possibility is not generally considered in theories of diffusion in solids.

Another type of transformation involves slip, and does result in a change in the shape of the unit cell, sometimes by a homogeneous deformation. It allows transformation between *different* (compatibility) classes of nets.

§ 9 deals with the (hexagon–pentagon–triangle) net description of 'tetrahedrally closed packed' alloy structures – Frank–Kasper and Friauf–Laves phases – and transformations relating them. The **β-U_3O_8** and related nets discussed in § 10 are somewhat similar, but also contain quadrangles.

In § 11 a different type of operation is used to relate structures: adjacent planes are combined by collapse to form a composite net on a single plane. This produces further crystal structure relations that were not previously available, e.g. between **ReO_3**, **HTB** and the **pyrochlore** framework.

Finally, in § 12, some conclusions are drawn, and some of the more novel points developed in the paper are summarized and emphasized.

'*Handeln vom Netz, nicht von dem, was das Netz beschreibt.*'
L. Wittgenstein: *Tractatus Logico-Philosophicus*

1. Introduction

The difficulty of assimilating fully the nature and details of crystal structures and structural relations has led to a number of different geometrical descriptions being employed. One of the most powerful and frequently used describes structures as connected coordination polyhedra. Relations which may then be seen are alternative ways of connecting or orienting the same polyhedra, or alternative polyhedra with identical arrays of vertices (i.e. alternative ways of occupying the various interstices in a given array). However, there is an implicit rigidity which is a drawback in this approach. It may inhibit consideration of structures which, often, are not exactly of the ideal type; and of the possibility that there may be a more or less continuous sequence of real structures between two or more ideal types of the same stoichiometry (or even of different stoichiometries). Most such sequences will involve distortion of the coordination polyhedra themselves; a process that may be difficult to visualize. Certain arrays of corner-connected polyhedra can be deformed without deforming the polyhedra or changing the topology of the structure. But this may also be difficult to visualize and is, in any case, restricted to a relatively few structure types. Most notable perhaps in this connection are the ReO_3(DO_9) structure type (Glazer 1972; O'Keeffe & Hyde 1977) and the ideal cristobalite ($C9$) structure (O'Keeffe & Hyde 1976).

An alternative and complementary approach considers structures as stackings of two-dimensional packings of atoms, i.e. layers. Such a description of structures based on closest packing is indeed very familiar, but it is likely to be even more useful for describing those structures in which the coordination polyhedra are ill-defined or undefinable, or those relations or transformations that involve distortion of the coordination polyhedra.

Previous work relevant to this topic includes that of Wells (1954*a*, *b*, 1970), who discussed some plane nets as a prelude to a discussion of three-dimensional nets; but who focused attention mainly on their connectivity. Frank & Kasper (1958, 1959), Shoemaker & Shoemaker (1968), Sinha (1972) and others have given accounts of nets in some of the more important and common alloy structures. Pearson (1972) considers inorganic and alloy structures but, apart from the closest-packed case, the discussion of the more ionic ('inorganic') crystal structures in terms of layers is much less well-developed than the coordination polyhedron approach. In our view this is unfortunate: the net description can be rewarding, and deserves to be more fully developed and widely used. Accordingly, in this paper we will attempt to redress the balance by also emphasizing 'inorganic' structures and the nets they contain. However, alloy structures cannot, and should not, be excluded. Their customary separation is artificial, unnecessary and detrimental to an appreciation of crystal science as a whole. In inorganic structures the conventional cation/anion radius ratio is usually less than one: in many alloys, the corresponding atom radius ratio is greater than one, and hence a wider variety of nets (and polyhedra) is observed. However, it should also be observed that a large number of structures are common to both alloys and inorganic crystals and, of course, any purely geometrical descriptions and correspondences are equally valid for both types of material.

We first describe some of the simpler and more important two-dimensional arrays, together with some example of structures containing them.† We then discuss transformations between

† When specific references are not given, reference for alloy structures may be made to Schubert (1964) or to Pearson (1972) and for ionic crystal structures to Wyckoff (1963) and Povarennykh (1972).

PHILOSOPHICAL TRANSACTIONS OF THE ROYAL SOCIETY A MATHEMATICAL, PHYSICAL & ENGINEERING SCIENCES

the nets, together with examples of relations between crystal structures. This aspect is usually ignored, but we believe that it is here that the greatest power of the nets approach is manifested. The approach yields some valuable insights into particularly geometrical factors determining structure and structural relations. Previous articles (Hyde *et al.* 1972, 1974) dealt briefly with only the simplest nets, and the topological relations between a few structures based on them.

2. Definitions and nomenclature

A planar array of atoms may be represented by an array of circles in a plane. Niggli (1926, 1928) systematically derived and discussed all the possible packings of equivalent circles (see also Haag, 1929). An excellent account of the mathematical aspects of this and related topics has been given by Fejes Tóth (1964). However, many of the more interesting patterns that we wish to discuss have not been formally described before – in part at least, because they do not appear to arise naturally in a formal mathematical treatment.

If the centres of contiguous (or almost contiguous) circles are joined with straight lines, these form a two-dimensional *net*, and the plane will be covered with polygons forming a *tessellation*. The centres of the circles are now referred to as *atoms* or *vertices* and the lines joining vertices are *bonds* or *edges*.

The terms 'vertices' and 'edges' are more appropriate to the formal description of patterns; atoms and bonds to the description of crystal structures. To emphasize the latter we often draw small circles, representing atom positions, at the nodes/vertices of the nets. We will also use the terms 'net' and 'tessellation' interchangeably according to whether we wish to emphasize the topological or metrical aspects of the geometrical pattern.

Vertices are conveniently described by the Schläfli symbol which specifies the not-necessarily-regular polygons meeting at the vertex in cyclic order (Cundy & Rollet 1961). *Regular* tessellations are those composed of congruent regular polygons and the symbol for the vertex figure can also serve as the symbol for the tessellation. The three regular tessellations (figures 2–4) are thus $\mathbf{3^6}$, $\mathbf{4^4}$, and $\mathbf{6^3}$. Note that we use bold face symbols to specify a net or tessellation and symbols in ordinary type to specify a type of vertex (atom).

Semi-regular tessellations employ more than one kind of regular polygon, but all vertices are congruent. They are analogous to the Archimedean solids and sometimes referred to as Archimedean tessellations. There are eight semi-regular nets or tessellations, namely $\mathbf{3^4.6}$; $\mathbf{3^3.4^2}$; $\mathbf{3^2.4.3.4}$; **3.6.3.6**; **3.4.6.4**; $\mathbf{4.8^2}$; $\mathbf{3.12^2}$ and **4.6.12** (figures 5–12).

Even with just two regular polygons (e.g. squares and equilateral triangles) an infinite number of tessellations is possible. For obvious reasons, our interest is mainly in those patterns which are periodic in two dimensions and with a small number of vertices in the repeat unit (unit cell). There appears to be no systematic nomenclature for such patterns. We have devised one that is a little cumbersome and often we prefer to employ trivial names.

The basic topological property of an infinite tessellation on the Euclidean plane is that the sum of the number of vertices and polygons is equal to the number of edges, $V+P = E$ (Coxeter, 1961). From this, and the fact that each edge joins two vertices and separates two polygons, one can derive a useful relationship between the fractions of the various types of polygon and the number of polygons meeting at a vertex. Specifically, if ϕ_n is the fraction of polygons in a tessellation that are n-gons and f_i is the fraction of vertices at which i polygons meet,

$$1/\Sigma\, n\phi_n + 1/\Sigma\, if_i = \tfrac{1}{2}, \qquad (1)$$

a result that does not appear to be well known although it is extensively used by Wells (1954*a*, *b*) for the special cases of constant i.

An example of the use of this formula is provided by the large class of 4-connected nets ($i = 4$) involving triangles, quadrangles, and pentagons. For these, one must have the number of triangles equal to the number of pentagons (see also Smith (1968) for related formulae).

3. Tessellations involving irregular polygons

There is no way to cover the plane with regular figures if pentagons (or indeed heptagons and many other polygons with more sides, but of less interest here) are to be included. However, nature has devised a number of very elegant arrangements of atoms corresponding to tessellations of 'almost' regular figures in which pentagons and, to a lesser extent, heptagons are conspicuous. Some of these are described below. In order to arrive at a unique metrical description of such patterns, we have (except as noted below) considered the arrangement of regular figures that most nearly cover the plane without overlap and with the same symmetry as the real pattern. There will be two complementary classes of vertex: those like 3.5.3.5 which will have gaps between the edges of some of the polygons, and those like 3.5.4.5, where the corners of the polygons cannot quite meet. In these cases, the centre of gravity of the polygon corners is taken as the atom position. This procedure gives coordinates very close to those found in nature in many instances.

It is known (see, for example, Cundy & Rollet 1961; MacMahon 1921) that the plane can be covered by equal-sided (but not regular) pentagons with two angles of $\frac{1}{2}\pi$ (MacMahon's net no. 18 below). (More specifically, the angles in order are $\frac{1}{2}\pi$, $[\frac{3}{4}\pi - (\frac{1}{2})\arccos\frac{3}{4}]$ (twice), $\frac{1}{2}\pi$, $[\frac{1}{2}\pi + \arccos\frac{3}{4}]$.) But these cannot be combined with regular polygons to cover the plane. Equation (1) shows that any tessellation of pentagons must have incongruent vertices. Many, but not all, of the patterns involving pentagons can be reproduced only if the other polygons are also irregular and a study of plane coverings with irregular polygons soon becomes very complex. There is however, an important class of nets (e.g. numbers 20, 23, 24, 25 below) made from equilateral triangles, squares and pentagons of equal sides with angles of $\frac{2}{3}\pi$, $\{\frac{1}{6}\pi + \arccos[\frac{1}{2}(\sqrt{3}-1)]\}$, $\{\frac{1}{2}\pi + \arcsin[\frac{1}{2}(\sqrt{3}-1)]\}$ (twice) and $\{\frac{1}{6}\pi + \arccos[\frac{1}{2}(\sqrt{3}-1)]\}$.

In this context, it is useful to consider tessellations involving vertices $n_1 . n_2 \ldots n_j \ldots$ (i.e., vertices common to n_1-gon, n_2-gon, ... n_j-gon ...). The angular defect of a vertex k is then defined as δ_k, where

$$\delta_k = 2\pi[1 - \Sigma(\tfrac{1}{2} - 1/n_j)]. \tag{2}$$

Clearly, δ_k is the difference between 2π and the sum of the angles of (possibly partly overlapping) regular polygons meeting at a vertex. For a tessellation of convex polygons

$$\Sigma f_k \delta_k = 0, \tag{3}$$

so that only appropriate combinations of vertices with positive and negative δ can yield a tessellation.† Therefore, any tessellation involving pentagons must have at least two kinds of

† Equation (3) is just a special case of the general result that the integral curvature of a space is equal to $2\pi\chi$, where χ is the Euler–Poincaré characteristic of the space (Coxeter 1961). For the Euclidean plane $\chi = 0$. The corresponding expression for convex polyhedra ($\chi = 2$) is Descartes' formula (Coxeter 1948): $\Sigma\delta_k = 4\pi$.

vertex, and any tessellations of congruent n-gons must have $n \leqslant 6$.† This may be seen by inspection of table 1 which lists the angular defects in degrees at some likely vertices (atoms) with small values of $|\delta_k|$, which is useful for deciding the ratios in which vertices must appear.

TABLE 1. ANGULAR DEFECTS (IN DEGREES) AT SOME COMMON VERTICES

vertex	$360\delta/2\pi$	vertex	$360\delta/2\pi$
5^3	36	3.6.4.6. or $3.4.6^2$	-30
$3^2.4.6$ or 3.4.3.6	30	$5^3.3$	-24
$3^2.5^2$ or 3.5.3.5	24	7^3	$-25\frac{5}{7}$
4.7^2	$12\frac{6}{7}$	$4^3.5$	-18
5.8^2	18	$5^2.8$	-9
$3.4^2.5$ or 3.4.5.4	12	$3.4.7.4$ or $3.4^2.7$	$-8\frac{4}{7}$
5.6^2	12	$3.4.5^2$ or 3.5.4.5	-6
$3^4.5$	12		

4. DESCRIPTION OF SOME NETS

We now enumerate the basic properties of some nets and, for the less familiar, provide examples of their occurrence. Some of course are sufficiently well known that detailed discussion here would be superfluous.

A convenient and complete specification is to give the unit cell and coordinates of the vertices; this proves very useful in discussing transformations between nets. We give the two-dimensional space group short symbol and vertex (atom) positions according to the Wyckoff notation as specified in the International Tables for X-ray Crystallography (Henry & Lonsdale 1965). The only invariant complexes are the regular nets and **3.6.3.6**; for all the other nets numerical values of the coordinates are calculated as described below. The lattice parameters are calculated for (shortest) edge lengths of unity. The density, ρ, is the fraction of the plane covered by circles of unit diameter. The numbers A and B are defined below (§ 7).

The essential topology of the net can often be described by specifying what we term a *minimum figure*. This is an extension of the Schläfli notation for regular and semi-regular nets. The minimum figure is specified by providing in cyclic order, the symbol for each vertex of a polygon. Many of the nets in this paper can be specified in this way. The symbolism is best illustrated by example. Consider the net shown in figure 16 commonly called the **β-W** net. The vertices of each of the triangles in the net are 3.6.3.6, $3^2.6^2$, and $3^2.6^2$. It is easy to show that there is only one net, the one under discussion, in which every triangle is of this type. Accordingly, we symbolize the net by [**3.6.3.6**, $(\mathbf{3^2.6^2})^2$]. A second example must suffice. In the net in figure 22(*a*), all triangles have the same sequence of vertex symbols [$(3.5.4.5)^2$, 3.5.3.5]. This symbol again completely specifies the net if it is understood that every triangle has the same sequence of vertices.

It might be remarked that although we require polygons in the minimum figure to be similar in type and sequence of vertices, they may well be different in their edge sharing. In this latter sense, it may be seen that even in the semi-regular net **3^4.6** (figure 5) there are two types of triangles (namely, those sharing edges with three triangles and those sharing edges with two triangles and a hexagon) although all vertices are, of course, equivalent. It

† It should be noted that the Euler condition $V+P=E$, and equivalently equations (1)–(3), is a necessary but not a sufficient condition for the existence of a tessellation. Thus **5^2.10** is compatible with this condition but does not exist. A complete enumeration of impossible tessellations with one type of vertex and satisfying the Euler condition is **$3^2.6^2$**, **3^2.4.12**, **3.4.3.12**, **$3.4^2.6$**, **3.8.24**, **3.9.18**, **3.10.15**, **5^2.10**.

might also be remarked that it is easy to devise nets that cannot be uniquely defined by the order of vertices of a polygon even though all polygons with the same number of edges are equivalent in the local sense of having the same types of vertex in the same order. The two nets of figure 1 can readily be seen to have equivalent triangles, quadrangles and hexagons in this

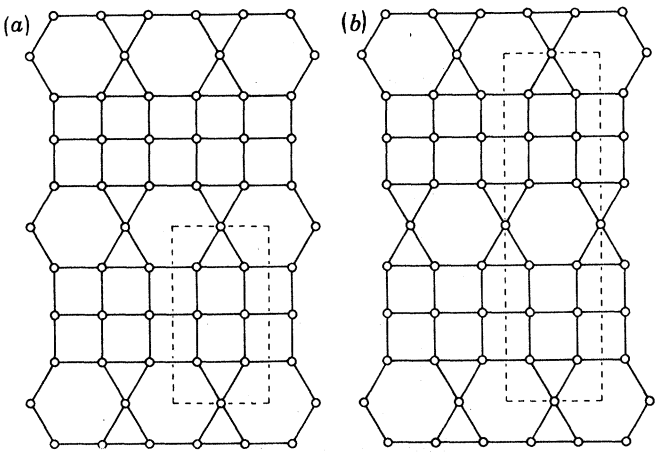

FIGURE 1 (*a*) AND (*b*). Two topologically different nets with nodes of the same kind.

sense. The shortcomings of the Schläfli notation are apparent in its application to polyhedra also. There are, for example, two distinct convex polyhedra with the symbol 3.4^3 (Miller 1930). For moderately complex nets (tessellations) the most economical description of the topology appears to be a drawing of the repeat unit.

(*a*) *Regular nets*

(1) $\mathbf{3^6}$. *p6m*; $a = 1$. 3^6 in 1 (*a*). $\rho = \sqrt{\frac{1}{12}}\,\pi = 0.9069$. $B = 1$. Figure 2.

This is the well-known triangular net formed by closest packing of equal circles in a plane. The closest packing of equal spheres is obtained by stacking $\mathbf{3^6}$ nets of unit spheres a distance of $\sqrt{\frac{2}{3}}$ apart. The basic properties of structures formed by stacking these nets have been known since Barlow's researches of the last century and are now to be found in elementary texts.

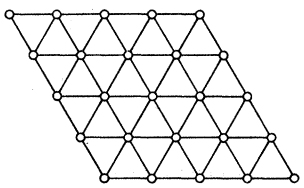

FIGURE 2. Net 1 ($\mathbf{3^6}$).

(2) $\mathbf{4^4}$. *p4m*; $a = 1$. 4^4 in 1 (*a*). $\rho = \frac{1}{4}\pi = 0.7854$. $A = 1$. Figure 3.

This is another entirely familiar net occurring most notably in cubic closest packing (face-centred cubic), in simple cubic and in body-centred cubic three-dimensional arrays.

(3) $\mathbf{6^3}$. *p6m*; $a = \sqrt{3}$. 6^3 in 2 (*b*). $\rho = \sqrt{\frac{1}{27}}\,\pi = 0.6046$. $B = 2$. Figure 4.

This is the honeycomb net familiar in graphite and as cation layers in ionic crystals such as corundum (Al_2O_3). Another example of its occurrence is provided by the B net in AlB_2.

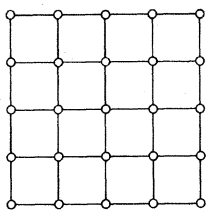

FIGURE 3. Net 2 (4^4).

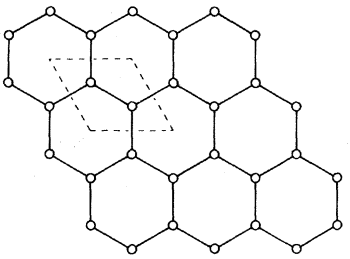

FIGURE 4. Net 3 (6^3).

(b) Semi-regular nets

(4) $\mathbf{3^4.6}$. $p6$; $a = \sqrt{7}$. $3^4.6$ in $6(d)$, $x = \frac{3}{7}$, $y = \frac{1}{7}$. $\rho = \frac{\sqrt{3}}{7}\pi = 0.7773$. $B = 2$. Figure 5.

This is the only one of the regular and semi-regular tessellations lacking a mirror plane The enantiomorph of the tessellation given above is obtained by putting atoms in $6(d)$ with $x = \frac{1}{7}$, $y = \frac{3}{7}$. The I atoms in $[C_5H_5NH]Ag_5I_6$ are arranged on alternating enantiomorphs o $\mathbf{3^4.6}$. (Geller 1972). Other examples of its occurrence are in the anion nets of $KOsF_6$ and Pr_7O_{12}.

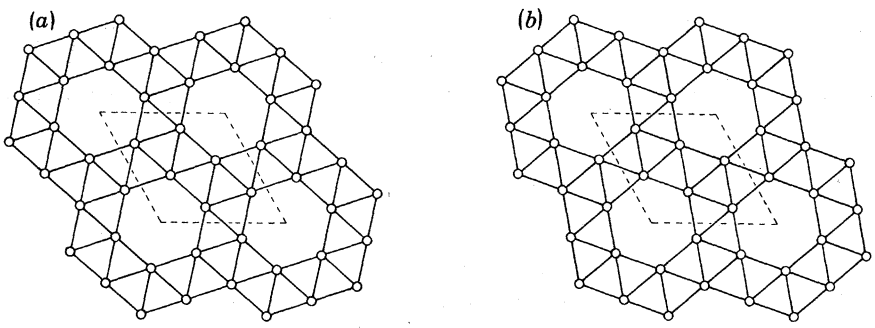

FIGURE 5 (*a*) AND (*b*). Two enantiamorphs of net 4 ($\mathbf{3^4.6}$).

(5) $\mathbf{3^3.4^2}$. *cmm*; $a = 1$, $b = 2+\sqrt{3}$. $3^3.4^2$ in $4(e)$, $y = (1+\sqrt{3})/(4+2\sqrt{3})$. $\rho = \pi/(2+\sqrt{3}) = 0.8418$. Figure 6.

This net is intermediate between $\mathbf{3^6}$ and $\mathbf{4^4}$ and is the only regular or semi-regular tessellation without a four-fold or six-fold axis. It is of some importance in the description of structures intermediate between close-packed and simple cubic (Hyde *et al.* 1972). A puckered (non-planar) approximation to this net occurs parallel to $\{10\bar{1}1\}$ in hexagonal close-packing. [The corresponding nets in cubic close-packing are $\mathbf{4^4}$ or $\mathbf{3^6}$. In mixed stackings, if *4* represents a

row of squares, and *3* represents a row of triangles (directions parallel to the close-packed rows), then h = *4.3* or *3.4* and c = *4.4* or *3.3*. So

$$\begin{aligned} hc &= \ldots 4.3.3.4.4.3.3.4\ldots, \\ h^2c &= \ldots 4.3.4.4.3.4.4.3\ldots \quad \text{or} \quad \ldots 3.4.3.3.4.3.3\ldots, \\ hc^2 &= \ldots 4.3.3.3.4.4.4.3\ldots, \\ h^2c^2 &= \ldots 4.3.4.4.4.3.4.4.4\ldots] \end{aligned}$$

It also occurs in structures such as that of TlI and, somewhat distorted in SnS. $3^3.4^2$ packings of equal spheres can be stacked at the 'closest packing' spacing of $\sqrt{\frac{2}{3}}$.

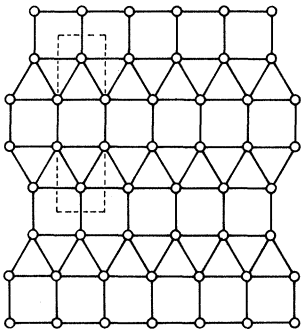

FIGURE 6. Net 5 ($3^3.4^2$).

(6) $3^2.4.3.4$. $p4g$; $a = (2+\sqrt{3})^{\frac{1}{2}}$. $3^2.4.3.4$ in $4(c)$, $x = 1-\frac{1}{4}[(2-\sqrt{3})/(2+\sqrt{3})]^{\frac{1}{2}} = 0.1830$. $\rho = \pi/(2+\sqrt{3}) = 0.8418$. $A = 1$. Figure 7.

This net is of equal density to the previous one. It is the densest packing of equal circles with four-fold symmetry, in which all circles are equivalent. (An example with the same density and with four-fold symmetry but with non-equivalent circles is no. 12 given below.) It is of great importance in alloy structures and has been discussed in that connection particularly by Frank & Kasper (1959) and by Pearson (1972). The $CuAl_2$ ($C16$) structure is a well-known example in which (001) Al nets of this type are stacked with the origins of successive layers displaced by $\frac{1}{2}\frac{1}{2}$. $3^2.4.3.4$ nets of unit spheres can approach within $\sqrt{\frac{2}{3}}$ (the distance apart of 3^6 layers in closest packing) in this configuration. Other examples of its occurrence include the structures of Pt_3Ge, TlSe, $CoGa_3$, U_3Si_2, PdS, Pb_3O_4, the Ln nets in $LnAu_6$ and K in $K_3W_5O_{15}$ (tetragonal tungsten bronze). Again it is of importance in being transitional between 3^6 and 4^4.

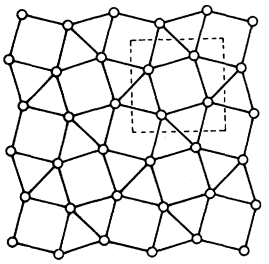

FIGURE 7. Net 6 ($3^2.4.3.4$).

(7) **3.6.3.6.** $p6m$; $a = 2$. 3.6.3.6 in 3 (c). $\rho = \frac{\sqrt{3}}{8}\pi = 0.6802$. $B = 1$. Figure 8.

This net is known to crystal chemists as the kagome net (Frank & Kasper 1958) after the three-way bamboo weave, and is found extensively in ornament. It is the only quasi-regular tessellation (Fejes Tóth 1964; all edges as well as vertices are equivalent) and again is of very wide occurrence in alloy structures, e.g. (0001) planes of Fe in W_6Fe_7, Zn in $MgZn_2$ and $CaZn_5$. In oxide chemistry it occurs, notably as (111) layers of oxygen in the $ReO_3(DO_9)$ and NbO structures, and in some network silicates, e.g. cymrite, $BaAlSi_3O_8(OH)$; and also very frequently in cation planes (e.g. in the structures of spinel, NbO and pyrochlore).

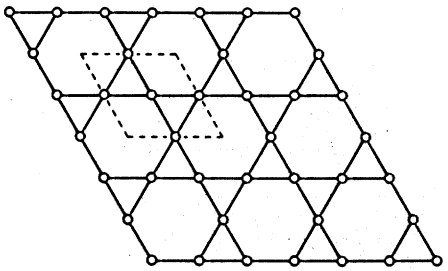

FIGURE 8. Net 7 (**3.6.3.6**), the kagome net.

(8) **3.4.6.4.** $p6m$; $a = 1+\sqrt{3}$. 3.4.6.4 in 6 (e), $x = 1/(3+\sqrt{3})$. $\rho = 3^{\frac{1}{2}}\pi/(4+2\sqrt{3}) = 0.7290$. $B = 2$. Figure 9.

This is another net often found in ornament. It occurs notably as a pattern of anions in the hexagonal tungsten bronze (HTB) structure and in the $BaSiF_6$ structure, and also appears in alloy structures such as those of $BaFe_2Al_9$ and Hf_9Mo_4B. The centres of the squares (tungsten ion positions in HTB) are on a kagome net.

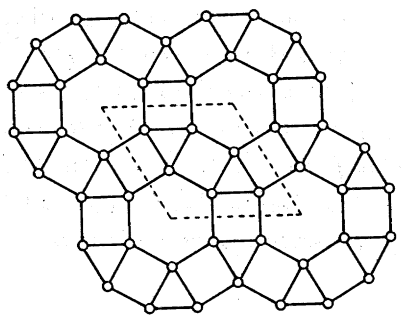

FIGURE 9. Net 8 (**3.4.6.4**).

(9) **4.8²**. $p4m$; $a = 1+\sqrt{2}$. 4.8² in 4 (e), $x = 1/(2+2\sqrt{2})$. $\rho = \pi/(3+2\sqrt{2}) = 0.5390$. $A = 1$. Figure 10.

This is familiar as a tiling pattern but, in common with the next two, is of less frequent occurrence in ionic crystals owing to the large size of the polygons and low packing density. Wells (1954*c*) has indicated the occurrence of this and the next two nets in hydrogen-bonded crystals of organic molecules. It is more often found in alloy structures, for example those of UB_{12} and Mg_2Ga_5.

PHILOSOPHICAL TRANSACTIONS OF THE ROYAL SOCIETY A MATHEMATICAL, PHYSICAL & ENGINEERING SCIENCES

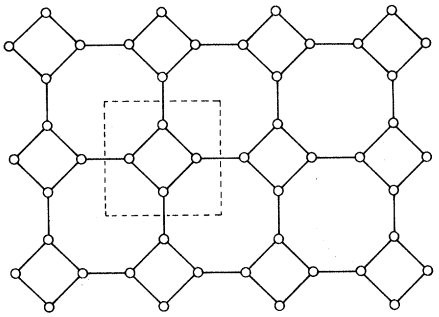

FIGURE 10. Net 9 (**4.8²**).

(10) **3.12²**. $p6m$; $a = 2+\sqrt{3}$. 3.12² in 6(*e*), $x = (1-1/\sqrt{3}) = 0.4226$. $\rho = 3\frac{1}{2}\pi/(7+4\sqrt{3}) = 0.3907$. $B = 2$. Figure 11.

This net has some interest as being that of the least dense stable circle packing (Niggli 1926).

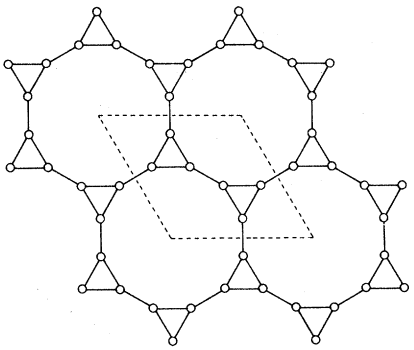

FIGURE 11. Net 10 (**3.12²**).

(11) **4.6.12**. $p6m$; $a = 3+\sqrt{3}$. 4.6.12 in 12(*f*), $x = (3\sqrt{3}+3)^{-1}$, $y = x+\frac{1}{3}$. $\rho = \pi/(3+2\sqrt{3}) = 0.4860$. $B = 1$. Figure 12.

As with the previous net, the low density and large polygons render this net relatively unimportant in the description of ionic crystal structures, however an example of its occurrence (slightly puckered) is as the Si net of a $Si_{12}O_{20}$ layer in the mineral pyrosmalite.

(*c*) *Non-regular nets with regular polygons*

There are a number of important nets in which only regular polygons occur but in which more than one type of vertex occurs. The possibilities are endless. We have restricted ourselves largely to those nets that are of interest either by virtue of their frequent occurrence or because of their importance to the subsequent discussion of transformations between nets. As long as the restriction is to nets with regular polygons, the positions of the vertices are completely determined. Nets are named by a minimum figure and/or trivial name.

(12) **[3³.4², (3².4.3.4)²]**, **U_6Mn**. $p4g$; $a = (3+\sqrt{3})/\sqrt{2} = 3.346$. 3².4.3.4 in 8(*d*), $x = (6+\sqrt{12})^{-1} = 0.1057$, $y = 3\frac{1}{2}x = 0.1830$; 3³.4² in 4(*c*), $x = (6+\sqrt{12})^{-1} = 0.1057$. $\rho = \pi/(2+\sqrt{3}) = 0.8418$. $A = 3$. Figure 13.

This is one of the simplest combinations of 3².4.3.4 and 3³.4² vertices and appears to be the only simple combination with square symmetry. Successive layers can be stacked in the same

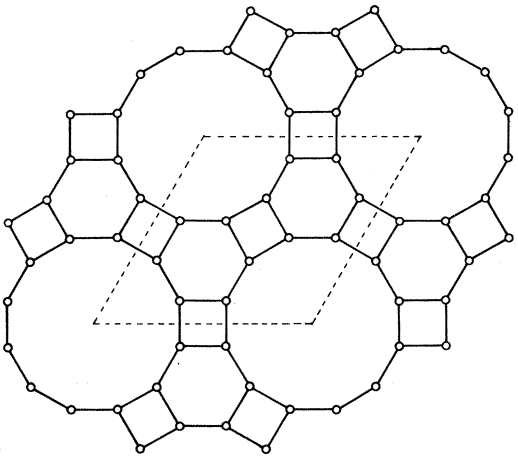

FIGURE 12. Net 11 (**4.6.12**).

way as **3².4.3.4** in $CuAl_2$; there is then one site of eightfold coordination for every six atoms. Filling this site, one has approximately the structure of U_6Mn. The {111} anion nets in bixbyite (Mn_2O_3), in the mineral natrolite, and in $NaZn(OH)_3$ and the Cd nets in As_2Cd_3 also approximate this net. In Zr_5Al_3 and W_5Si_3 they are slightly distorted with the two kinds of atom segregated to the two types of nodes.

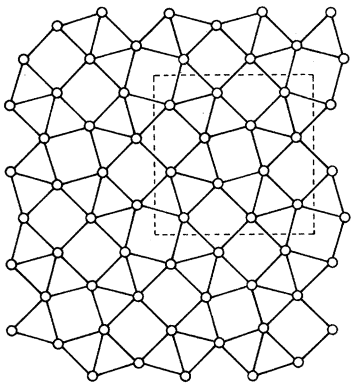

FIGURE 13. Net 12 (U_6Mn).

(13) **[(3³.4²)², (3².4.3.4)²]**. *pgg*; $2b = a = 4(2+\sqrt{3})^{\frac{1}{2}}$. $3^3.4^2$ in 4(*c*), $x = 0.4665$, $y = \frac{1}{4}$; $3^2.4.3.4$ in 4(*c*), $x = 0.2165$, $y = 0.3840$. $\rho = \pi/(2+\sqrt{3}) = 0.8418$. Figure 14.

This net may be considered the simplest member of a family of nets obtained by intergrowth of **3³.4²** and **3².4.3.4**. Reference to the figure will show that there are zig-zag chains of $3^3.4^2$ (labelled β) and $3^2.4.3.4$ (labelled α) parallel to b. In an obvious notation, this net may be signified ...αβ... Examples of its occurrence are in Ni_4B_3 and in $SrNb_2O_6$ and one form of $CaTa_2O_6$ (Jahnberg 1963). Two related examples may also be cited: ...ααβ... (figure 15*a*) contains the same vertices in the same proportions as the U_6Mn net, although the two nets are topologically quite distinct. This net may be found in '$Pd_{4.8}P$' and $LaNb_3O_9$ (Sturm & Gruen 1975). The combination ...αββ... (figure 15*b*) occurs, slightly puckered, and parallel

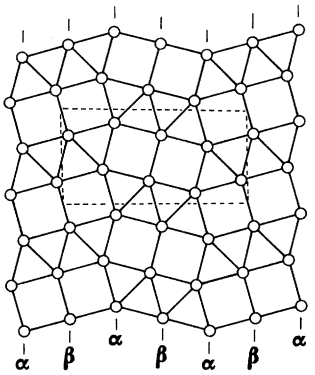

FIGURE 14. Net 13.

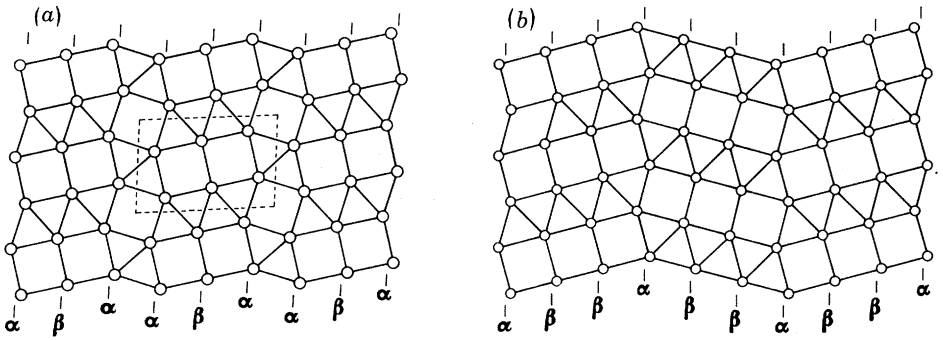

FIGURE 15 (*a*) AND (*b*). Two examples of intergrowth of $3^3.4^2$ and $3^2.4.3.4$. α and β refer to chains of $3^2.4.3.4$ and $3^3.4^2$ nodes respectively.

to (031) (setting *Pnma*), in compounds with the *cementite* (Fe_3C) structure [but ...αα... parallel to (010)].

(14) **[3.6.3.6, $(3^2.6^2)^2$], β-W**. *pmm*; $a = \sqrt{3}$, $b = 2$. 3.6.3.6 in 1(*b*); $3^2.6^2$ in 2(*h*), $y = \frac{1}{4}$. $\rho = \frac{\sqrt{3}}{8}\pi = 0.6802$. Figure 16.

This is a simple example of a hexagon and triangle net with two types of vertex and is found, for example, as the Cu net in Cu_3AsS_4, and the Au net in $PrAu_6$ (Moreau & Parthé 1974). Somewhat distorted (so that $a = b$) and alternating with 4^4 nets it occurs in the so-called 'β-W' structure of, e.g. Cr_3Si. This is also the arrangement of cations in the garnet structure. The metrically square net with $a = b$ we refer to as no. 14*.

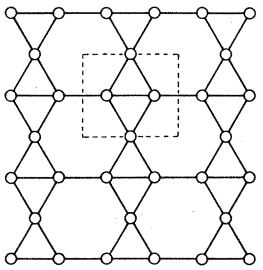

FIGURE 16. Net 14 (β-W).

(15) Kagome tiling. $p2$; $a = b = \sqrt{13}$, $\alpha = 2 \arctan(\frac{3\sqrt{3}}{5}) = 92.20°$. $\rho = \frac{11}{30\sqrt{3}}\pi = 0.6651$. Figure 17.

This net is discussed by Frank & Kasper (1959) and is mainly of interest in a discussion of alloy structures (cf. also $SmAu_6$; Moreau & Parthé 1974). It will be encountered later in discussing transformations between nets. It contains four $3^2.6^2$, two 6^3 and five 3.6.3.6 vertices and is best described by the diagram.

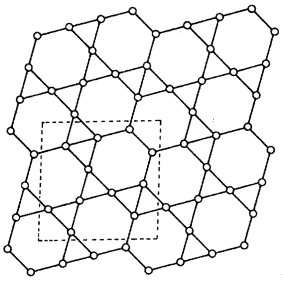

FIGURE 17. Net 15 (kagome tiling).

(16) (*a*) **[$(3^2.4.3.4)^2$, $(3.4.6.4)^2$]**. $p6m$; $a = 2+\sqrt{3}$. $3^2.4.3.4$ in 6(*e*), $x = (1+\sqrt{3})/(3+2\sqrt{3})$; 3.4.6.4 in 6(*d*), $x = 1/(2+\sqrt{3})$. $\rho = 0.7813$. $B = 1$. Figure 18(*a*).

This net is a simple combination of $3^2.4.3.4$ and 3.4.6.4 vertices. It is not one that we have discovered in nature.

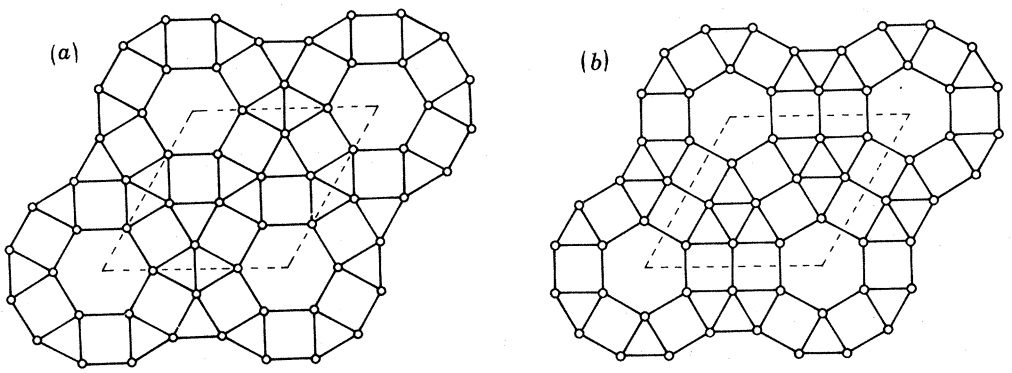

FIGURE 18. (*a*) Net 16(*a*), (*b*) Net 16(*b*).

(*b*) **[$(3^3.4^2)^2$, $(3.4.6.4)^2$]**. $p6m$; $a = 2+\sqrt{3}$. $3^3.4^2$ in 6(*e*), $x = (1+\sqrt{3})/(3+2\sqrt{3})$; 3.4.6.4 in 6(*e*), $x = 1/(3+2\sqrt{3})$. $\rho = 0.7813$. $B = 1$. Figure 18(*b*).

This net is closely analogous to the previous one. It occurs slightly distorted in the structure of $PbNb_2O_6$ (Mahe 1967).

(17) (Not named) $p4g$; $a = \sqrt{8}+\sqrt{6}$. $3^2.4.3.4$ in 8(*d*), $x = 1/(2+\sqrt{3})$, $y = 0$; $3^2.4.3.4$ in 8(*d*), $x = y = (1+\sqrt{3})/(8+4\sqrt{3})$; 3.4.6.4 in 8(*d*), $x = (1+\cos(\frac{1}{12}\pi))/(\sqrt{8}+\sqrt{6})$, $y = (\sin(\frac{1}{12}\pi))/(\sqrt{8}+\sqrt{6})$; 3.4.6.4 in 4(*c*), $x = (1+\sqrt{3})/(4+\sqrt{12})$. $\rho = 0.7894$. Figure 19.

This net is included as an example of an intergrowth of **3.4.6.4** and **$3^2.4.3.4$** with square symmetry (compare no. 16*a* and below, p. 610 for intergrowths with different symmetry). Also of interest is the net obtained when the hexagons are centred (by adding 3^6 nodes at

2(*b*): 0, $\frac{1}{2}$; $\frac{1}{2}$, 0). One then has an intergrowth of $\mathbf{3^6}$ and $\mathbf{3^2.4.3.4}$ with square symmetry, and the density is $\rho = 15\pi/(28+16\sqrt{3}) = 0.8458$. This is the densest net with square symmetry that we have discovered.

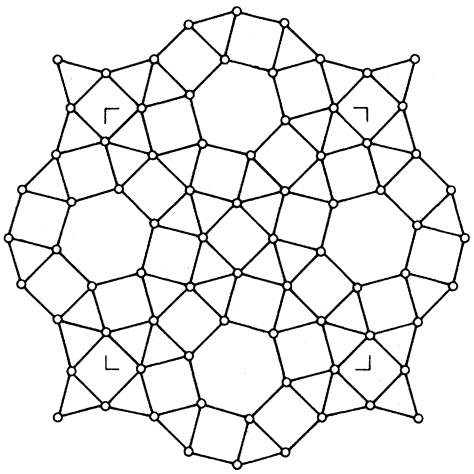

FIGURE 19. Net 17.

(*d*) *Nets with pentagons and heptagons*

We now describe some nets involving irregular polygons. At this stage, it does not appear fruitful to attempt to be either systematic or exhaustive. Even with pentagons alone, there are unlimited possibilities. Pentagon-only nets can be derived as the duals of the five-connected nets described above (i.e., derived by joining the centres of the polygons of those nets). One such, the dual of $\mathbf{3^2.4.3.4}$, is topologically equivalent to MacMahon's net mentioned above; the others appear to be of less interest. The nets we describe are all of considerable importance in crystal chemistry. As already discussed, there is some arbitrariness in assigning coordinates and cell dimensions and for some less common nets we give the coordinates found in crystal structures.

(18) $\mathbf{[(5^3)^2, 5^4, 5^3, 5^4]}$, MacMahon's net. *p4g*; $a = (4+\sqrt{7})^{\frac{1}{2}} = 2.578$. 5^4 in 2(*a*); 5^3 in 4(*c*), $x = 0.637$. $\rho = 0.709$. $A = 3$. Figure 20.

We have already discussed this net above. The coordinates are for pentagons of equal edge. It occurs as an oxygen and a vanadium net in $K_2V_3O_8$ and in the isostructural $Ba_2TiSi_2O_8$

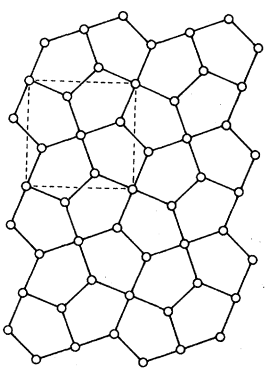

FIGURE 20. Net 18 (MacMahon's net).

(Moore 1967). The minerals of the melilite group, $(Ca, Na)_2(Mg, Al, Si)_3O_7$, and many othe compounds with the same structure have the same cation positions as $K_2V_3O_8$ so that th smaller ions (Mg, Al, Si) in melilite are also on this net, and indeed have very nearly the cc ordinates given above. The structures of many of the transition metal pnictides and chalcc genides can be described in terms of stacking of puckered versions of these nets with cation at the 5^4 vertices and anions at the 5^3 vertices (Jeitschko 1974).

(19) **[5^4, $3^2.5^2$, $(3.5.4.5)^2$, $3^2.5^2$]**. $p4m$; $a = 3$. 5^4 in $1(a)$; $3^2.5^2$ in $4(d)$, $x = \frac{1}{3}$; 3.5.4.5 in $4(e)$ $x = 0.2765$. $A = 1$. Figure 21.

This simple net occurs as the Mn array in Th_6Mn_{23}. It is of some importance as the proto type of families of more complex nets, and because it is simply derived from $\mathbf{4^4}$. The coord nates in this instance are chosen as follows: the $3^2.5^2$ vertices are arranged to divide the ce edge into equal lengths, so that one triangle edge and two pentagon edges are $\frac{1}{3}a$. This required for subsequent derivation of other nets from this one. The coordinates of the 3.5.4. vertices are then a compromise between having equilateral triangles ($x = \frac{1}{\sqrt{12}}$) and havin the edge of the square equal to $\frac{1}{3}a$ [$x = \frac{1}{6}(3-\sqrt{2})$].

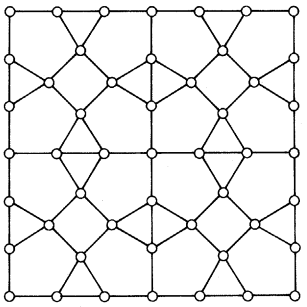

FIGURE 21. Net 19.

(20) **[$(3.5.4.5)^2$, 3.5.3.5]**. $p4g$; $a = \sqrt{\frac{3}{2}+(\frac{5}{2}+\sqrt{5})^{\frac{1}{2}}} = 3.4010$. 3.5.3.5 in $2(b)$; 3.5.4.5 in $8(d)$ $x = 0.064$, $y = 0.208$. $\rho = 0.679$. $A = 1$. Figure 22*a*.

This is another simple tessellation involving pentagons that is of wide occurrence in crystal To illustrate the method of deriving the coordinates, the 'best' covering of the plane wit regular polygons of the same edge-length is shown in figure 22*b*. The Hg atoms in Mn_2Hg have this arrangement with $x = 0.063$, $y = 0.204$. In this compound the Mn atoms are centre over the pentagons in a $\mathbf{3^2.4.3.4}$ net. The oxygen atoms (O_5) in the primary (001) layers c $K_2V_3O_8$ are on this net: the potassium atoms in this compound are arranged as are the M atoms in Mn_2Hg_5 (i.e. on a $\mathbf{3^2.4.3.4}$ net centring the pentagons). Another example of it occurrence is as the W net in the tetragonal tungsten bronze structure (see below). An alter native derivation of the coordinates of the vertices of this net is obtained by making all edg lengths equal. One then has squares and equilateral triangles combined with the pentagon described earlier (with angles of $\frac{2}{3}\pi$, $\{\frac{1}{12}\pi + \arccos\frac{1}{2}(\sqrt{3}-1)\}$, $\{\frac{1}{2}\pi + \arcsin\frac{1}{2}(\sqrt{3}-1)\}$ (twice) and $\{\frac{1}{12}\pi + \arccos\frac{1}{2}(\sqrt{3}-1)\}$). For these conditions, $a = 3.248$ and $x = 0.080$, $y = 0.203$, i.e very close to the configuration shown in figure 22*a*.

(21) **[5.4^3, 5.4.3.4, 5.4^3, $(5.4.3.4)^2$]**, tetragonal tungsten bronze. $p4g$; $a = \sqrt{2+(\frac{5}{2}+\sqrt{5})^{\frac{1}{2}}+\sqrt{\frac{3}{2}}} = 4.815$. 5.4^3 in $8(d)$, $x = 0.071$, $y = 0.154$; 5.4.3.4 in $8(d)$, $x = 0.353$, $y = 0$; 5.4.3. in $4(c)$, $x = 0.200$. $\rho = 0.6775$. $A = 1$. Figure 23.

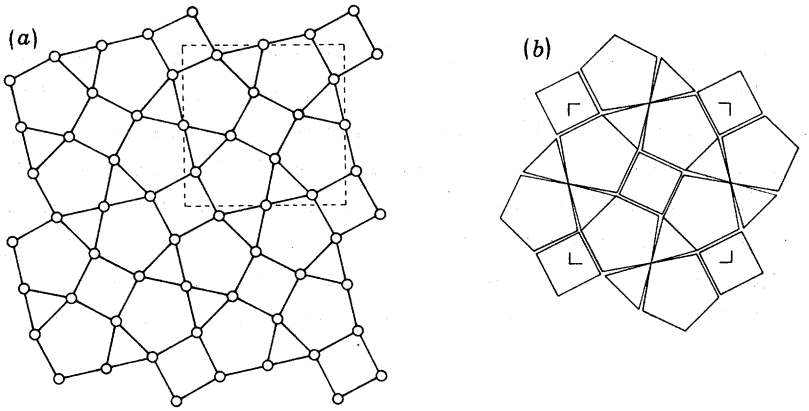

FIGURE 22. (*a*) Net 20. (*b*) Regular polygons corresponding to those of net 20 arranged to cover the plane as well as possible.

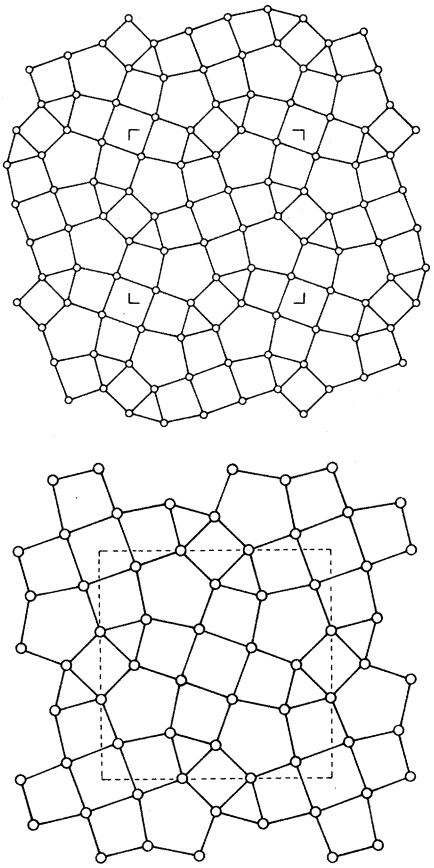

FIGURE 23. Net 21 (tetragonal tungsten bronze).

This is the primary oxygen net of tetragonal tungsten bronze, $K_3W_5O_{15}$. The coordinates given above were determined from the 'best-covering' of regular polygons and are very close to those originally determined by Magnéli (1949). A large and important group of oxides has since been discovered with related structures based on the same net (see e.g. Jamieson *et al.* 1968).

(22) **[$(5^3.3)^2$, 5^3, $5^3.3$, 5^3]**. $p31m$; $a = 2.803$. 5^3 in $2(b)$; $5^3.3$ in $3(c)$, $x = 0.291$. $\rho = 0.5771$. $B = 5$. Figure 24.

The coordinates correspond to a 'best-covering' by polygons. This is the major (0001) net of (five-eighths of) the oxygen atoms in α-U_3O_8. U and the remainder of the O atoms are on $\mathbf{3^6}$ nets centred over the pentagons. The same arrangement prevails in the Th_3Pd_5: the Pd atoms are at the vertices of this pentagon-triangle net and the Th atoms on a $\mathbf{3^6}$ net centred over the pentagons. The K and V atoms of $K_3V_5O_{14}$ have the same arrangement as the Th and Pd atoms of Th_3Pd_5. Other examples of the occurrence of this net are in $Na_2Nb_4O_{11}$ and $CaTa_4O_{11}$ (Jahnberg 1970). Often it occurs with different types of atoms at the different sorts of vertices. Examples are provided by the structures of Fe_2P and $SrCl_2 \cdot 6H_2O$.

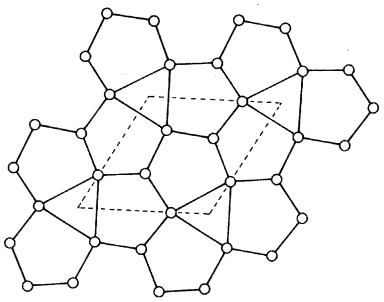

FIGURE 24. Net 22.

(23) **[$(3.4.5.4)^2$, $(3.5.4.5)^2$]**. $p31m$; $a = 3.297$. 3.4.5.4 in $3(c)$, $x = -0.175$; 3.5.4.5 in $6(d)$, $x = 0.175$, $y = 0.478$. $\rho = 0.751$. $B = 1$. Figure 25.

This and the following two nets may be constructed from the same polygons as described for net 20 (in different proportions). The net occurs parallel to (111) in β-Mn and as oxygen nets in $K_3V_5O_{14}$ and in the related compounds $Ba_3Si_4Ta_6O_{26}$ and '$Ba_3Si_4Ta_6O_{23}$' (Shannon & Katz 1970). The centres of the squares and those triangles not at the origin are the V positions in $K_3V_5O_{14}$ and are of course the vertices of the previous net (no. 22).

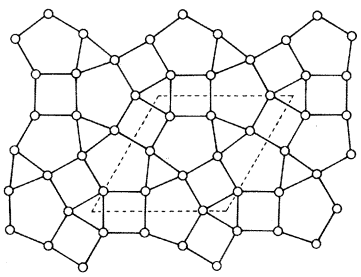

FIGURE 25. Net 23.

(24) **[3.5.3.5 $(3.4.5^2)^2$]**. cmm; $a = 2.732$, $b = 3.861$. 3.5.3.5 in $2(a)$, $3.4.5^2$ in $8(f)$, $x = 0.317$, $y = 0.129$. $\rho = 0.745$. Figure 26.

This is the anion net of β-U_3O_8 and Nb_3O_7F-II (Lundberg 1971) and the primary net in Mn_8Si_2C (Spinat *et al.* 1975). It is closely related to net 22 (the net for α-U_3O_8). In making the comparison with no. 22, we will want to consider this net as metrically hexagonal, i.e. with

$b/a = \sqrt{3}$ rather than $b/a = (2+12^{\frac{1}{2}})/(1+\sqrt{3})$, given above. We will then label the net no. 24*.

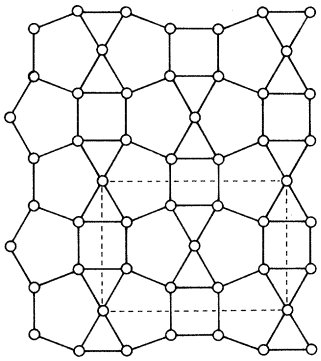

FIGURE 26. Net 24.

(25) **[3.4.5.4, $(3.4.5^2)^2$]**. *pmg*; $a = 2.732$, $b = 2.297$. 3.4.5.4 in $2(c)$, $y = 0.069$; $3.4.5^2$ in $4(d)$, $x = 0.567$, $y = 0.287$. $\rho = 0.751$. Figure 27.

This net is closely related to the two preceding. Examples of its occurrence are in $CeCu_2$ (somewhat distorted) and in UVO_5 (Chevalier & Gasperin 1970).

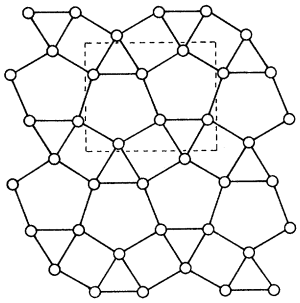

FIGURE 27. Net 25.

(26) **[$(4.7^2)^2$, $(7^3)^2$, $(4.7^2)^2$, 7^3]**. *p4g*; 7^3 in $4(c)$, $x = 0.087$: 4.7^2 in $8(d)$, $x = 0.170$, $y = 0.042$. $A = 3$. Figure 28.

This net is included as a simple (and very symmetrical) net involving heptagons. It occurs in the borides with the ThB_4 structure and in YB_2C. The coordinates are those for ThB_4.

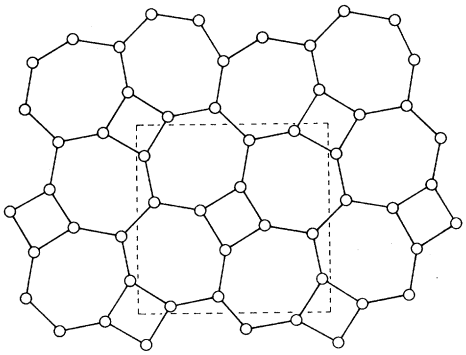

FIGURE 28. Net 26.

PHILOSOPHICAL TRANSACTIONS OF THE ROYAL SOCIETY A MATHEMATICAL, PHYSICAL & ENGINEERING SCIENCES

The centres of the heptagons are at the vertices of **3².4.3.4**. Such a net of Th atoms occurs i
ThB_4.

(27) **[9³, (3.9²)², 9³, (3.9²)², 9³, (3.9²)²]**. $p3m1$; $a = 1+\sqrt{3}$. 9^3 in $1(b)$; 3.9^2 in $3(d)$, $x = (1+2\sqrt{3})/(3+3\sqrt{3}) = 0.545$. $\rho = 0.486$. $B = 1$. Figure 29.

This net is probably the simplest containing enneagons. The coordinates are chosen so tha all edges are equal (and the triangles equilateral); they are close to those observed in crystals It occurs as a Ru net in Ru_7B_3 and in the many isostructural compounds and as S nets i compounds with the La_3CuSiS_7 structure (Flahaut & Laruelle 1970). Both of these closel related structure types may be described elegantly as a stacking of nets (but more elegantl in terms of coordination polyhedra (Hyde *et al.* 1974)).

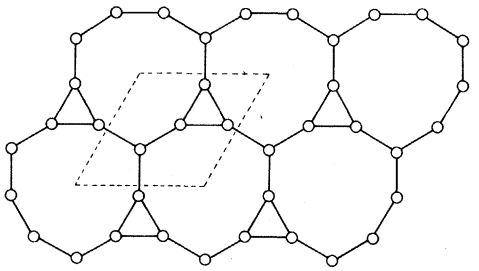

FIGURE 29. Net 27.

(*e*) *Some other nets containing heptagons and octagons*

There are several nets occurring in borides that can be considered as derived from **6³**. Thes are three-connected and contain pentagons and heptagons as well as hexagons. Equation (1 shows that for such nets $\phi_5 = \phi_7$. Simple possibilities are:

(i) $\phi_5 = \phi_7 = 0$. This is just the **6³** net of YB_2 ($\equiv AlB_2$).

(ii) $\phi_5 = \phi_7 = \frac{1}{2}$. An example of a net fulfilling this condition is shown in figure 30(*a*) an is the B net of $YCrB_4$ (Kuz'ma 1970). Y and Cr atoms are over the centres of the heptagon and pentagons respectively. The same net (plane group *pgg*) occurs in ScB_2C_2.

(iii) $\phi_5 = \phi_7 = \frac{1}{3}$. The net shown in figure 30(*b*) fulfills this condition. This is the B ne in Y_2LnB_6 (Kuz'ma & Svarichevskaya 1972). It also has symmetry *pgg*.

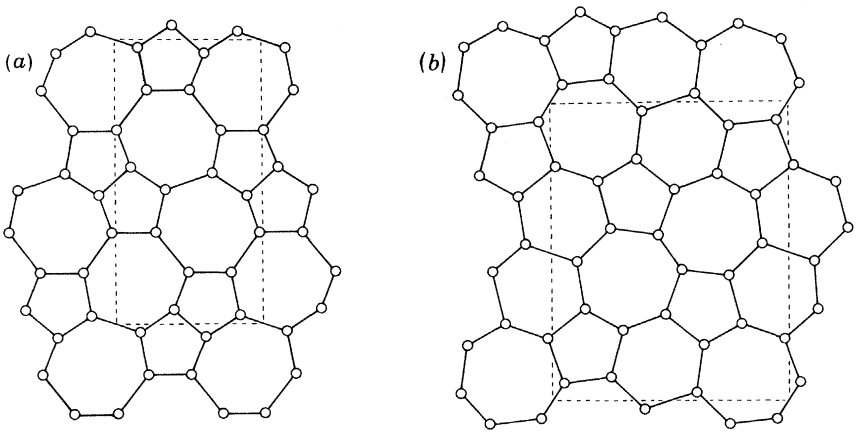

FIGURE 30. (*a*) The B net of $YCrB_4$. (*b*) The B net of Y_2LnB_6.

Other examples of nets made up of equal numbers of heptagons and pentagons are given by Wells (1954*a*).

Included here is a simple net of octagons and pentagons (figure 31). The symmetry is *cmm* and it contains 5.8^2 and $5^2.8$ vertices in the ratio 1:2 (compare table 1). An example of its occurrence is as the Si net in the layer silicate okenite, $CaSi_2O_5 \cdot 2H_2O$.

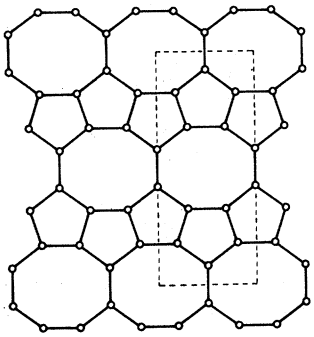

FIGURE 31. A net with $5^2.8$ and 5.8^2 vertices.

5. DUALS, AND PRIMARY AND SECONDARY NETS

In the present context a crystal structure is a sequential stacking of appropriate nets. Packing considerations imply that the nodes in one net will, in projection, usually appear at or near the centres of the polygons in the adjacent net. The geometrical concept of the *dual* of a net is relevant here. Coxeter (1961) defines the dual of a regular net $\mathbf{n^m}$ as another net (it is, in fact, $\mathbf{m^n}$) whose edges are the perpendicular bisectors of the edges of $\mathbf{n^m}$. This construction is equivalent to joining the centres of adjacent polygons in $\mathbf{n^m}$; a procedure which is less ambiguous in the case of non-regular nets.

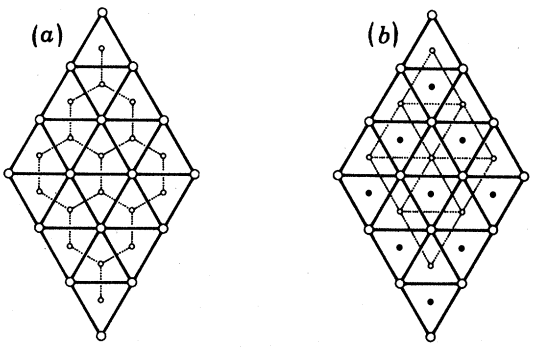

FIGURE 32. (*a*) The Al net (large circles) and the B net (small circles) in AlB_2. (*b*) The W net (large circles) and the C net (small open circles) in WC. Filled circles represent sites occupied by B in AlB_2 but empty in WC.

In the simplest structures, for example, those based on a close-packed array of one species of atom, the main nets are regular, $\mathbf{3^6}$ or $\mathbf{4^4}$, and the subsidiary nets (of 'interstitial' atoms) are their duals (e.g. AlB_2, figure 32*a*) or, more commonly, an incompletely occupied dual (e.g. WC, figure 32*b*). (Partial occupancy of the nodes of a dual by atoms is obviously quite common.) In this latter case the 'interstitial' net is often the dual of a net formed by combining

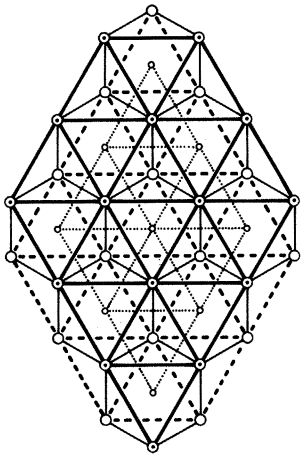

FIGURE 33. 3^6 interstitial net (dotted lines) as the dual of 6^3 formed by superposition of two 3^6 nets (full and broken heavy lines).

both adjacent nets, one above and one below. For example, in close-packed structures this combined net may be 6^3, and the appropriate dual 3^6 (e.g. NaCl, figure 33).

In more complicated structures the concepts analogous to a net and its dual are the primary and secondary nets, introduced by Frank & Kasper (1958). In a *primary* net or layer the node intervals correspond to atoms in contact: in the structures of the Frank–Kasper phases it is a relatively dense tessellation of triangles and pentagons and/or hexagons. Intermediate layers, in which the atoms are more widely spaced, are *secondary* nets. They are not duals, since they connect the centres of only the larger polygons of the primary net. (The smaller ones are usually centred by atoms at the nodes of the other nearest primary net.) They are tessellations of large squares and/or triangles. Several examples are given in the figures of § 9. The structures of $CuAl_2$, and Mn_2Hg_5 provide simpler examples: in the first, the primary nets are Al in $3^2.4.3.4$ and the secondary nets, produced by centring the squares, are Cu in 4^4; in the second, the primary nets are Hg in type no. 20 and the secondary nets, produced by centring the pentagons, are Mn in $3^2.4.3.4$.

6. Non-regular nets: the segregation of different atoms to different nodes

Only the simpler structures consist of regular and/or semi-regular nets in each of which all nodes are identical. This is not the case with non-regular nets in which, not surprisingly, it is commonly (but not invariably) observed that, if more than one type of atom is present, the different species are accommodated at the different types of node. Examples have already been given in §4.

7. Transformations between nets: compatibility

The stacking of nets often provides a concise and convenient description of crystal structures. However, it is our thesis that a major advantage of this approach is that an understanding of transformations between nets leads correspondingly to relations between crystal structures. Accordingly we now explore some ways in which nets are related.

In an attempt to devise a systematic approach, it is convenient at the outset to divide nets into two main groups, namely those belonging to the square system and those belonging to the hexagonal system. Several non-regular nets may not strictly belong to either system but are conveniently idealized. Thus, no. 14* is considered pseudo-square and no. 24* pseudo-hexagonal. The very few simple nets that do not belong to either system, most notably $3^3.4^2$, are often transitional between a member of each system. (They are, of course, rectangular or oblique.)

Nets belonging to the cubic or hexagonal systems are further subdivided into what we term classes of *compatible* nets. These are simply nets for which there exists a common super-cell with the same density of atoms. Transformations between compatible nets involve only movements of atoms in the common super-cell and thus require no macroscopic shape change other than a uniform expansion or contraction. These transformations often involve rotation of a group of atoms, such as at the corners of a polygon, combined with a uniform displacement from the centre of rotation. Applied to crystal structures this type of motion may often in turn be identified with rotation of a coordination polyhedron or group of polyhedra about a symmetry axis.

It may readily be shown that for nets of the same symmetry system to be compatible, the number of atoms, N, in the unit cell of each net must be expressible as

$$N = A(p^2+q^2), \text{ square system,}$$

$$N = B(p^2+pq+q^2), \text{ hexagonal system.}$$

Here p and q are integers and A or B are non-zero integers that are the same for two compatible nets.

One finds then that there are various classes of compatible nets characterized by the value of A or B, where these are either equal to unity or to another integer such that A has no factors of the form p^2+q^2 (square system) and B has no factors of the form p^2+pq+q^2 (hexagonal system).

TABLE 2. NETS LISTED BY COMPATIBLE CLASS†

square system	hexagonal system
$A = 1$: 2(4^4), 6, 9, 19, 20, 21.	$B = 1$: 1(3^6), 7, 11, 16, 17, 23, 27.
$A = 3$: 12, 14*, 18, 26.	$B = 2$: 3(6^3), 4, 8, 10.
	$B = 5$: 22, 24*.

† The net numbers are those used in the text, § 4.

Interestingly, most of the more common nets fall into three classes, the simplest member of which is one of the three regular nets. In table 2, the nets previously described are sorted into compatible groups.

The advantage of this method is that transformations between nets of a compatible class are usually easy to find and to describe. They may often be combined with transformations between the simple members of each class (which will involve a change in shape of the unit cell) to transform a net of one class into a net of another class. We first discuss transformations within a class.

(*a*) *Square system*

(i) $A = 1$

The prototype of this class is the square net **4⁴**: we will now show how other nets in the class may be derived from it. Figure 34 shows the atomic displacements that transform **4⁴** to **3².4.3.4** (Bursill & Hyde 1972). In the figure we have emphasized two aspects of the transformation. In the first place, it is considered as rotations of square groups of atoms by $\frac{1}{12}\pi$ rad. The second, identical transformation converts squares of atoms into 60° rhombuses. In discussing crystal structure transformations, either of these descriptions may be the more appropriate according to whether one wishes to emphasize the rotation of coordination polyhedra or the collapse of empty polyhedra.

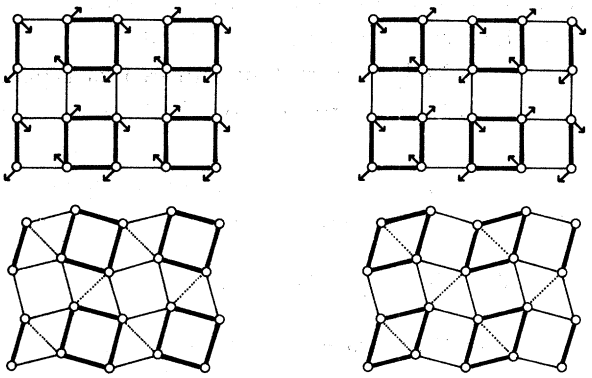

FIGURE 34. Transformation from **4⁴** to **3².4.3.4**.

Consider the three-dimensional lattice complex, with symbol J (Fisher *et al.* 1973) which is the anion arrangement in the ReO_3 and perovskite structures, and the Cu arrangement in Cu_3Au. It may be described as a network of corner-connected octahedral groups of atoms, centred by cations in ReO_3 and perovskite and empty in Cu_3Au, or as primary **4⁴** nets interleaved by secondary **4⁴** nets of half the density. Transformation of the superimposed primary layers of **4⁴** to superposed **3².4.3.4** corresponds to rotation of these octahedra about four-fold axes. Just such a transformation produces the T_2 phase of **$NaNbO_3$** from 'cubic perovskite'.†

Structures related by the same operation are **Cu_3Au** and **Ir_3Si** (≈ low-temperature **Pt_3Si**), with **U_3Si** (= high-temperature **Pt_3Si**) having an intermediate configuration. (In low **Pt_3Si** there is a small monoclinic distortion, $\beta = 88.1°$). But now the rotations along a given axis that operate on the primary **4⁴** nets are alternately clockwise and anticlockwise, so that alternate **3².4.3.4** product nets differ in orientation by $\frac{1}{2}\pi$ rad, and are stacked anti-symmetrically (figure 35). (By contrast, in the structure of U_3Si_2 they superpose.)

The structure of $CdAu_3$ is a variant of the **Cu_3Au** type which contains (001) antiphase boundaries (**R** = $\frac{1}{2}$[110]) at intervals of 2**c**(**Cu_3Au**). (This operation converts alternate (001) layers of corner-shared octahedra to edge-shared square pyramids. At the same time, the Cd atoms go very slightly off-centre.) If the complete [**Au_6**] octahedra are rotated (exactly as in **$CuAu_3$**), **$CdAu_3$** transforms to **$ZnAu_3$**(R2). Interestingly, $ZnAu_3$ itself has both structure types [(H) and (R2)].

Another simple example of a three-dimensional array based on **4⁴** nets is the primitive cubic

† Chemical formulae in bold face represent structure types, not compounds.

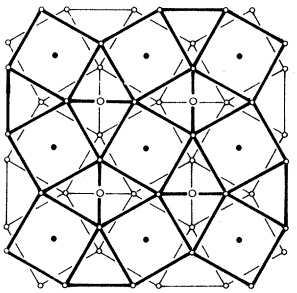

FIGURE 35. Stacking of **3².4.3.4** nets of Ir in Ir_3Si (at $z = \frac{1}{4}, \frac{3}{4}$). Small filled circles are Ir on a secondary **4⁴** net at $z = 0, \frac{1}{2}$ and the larger open circles are Si positions at $z = 0, \frac{1}{2}$.

array, for example in CsCl; transformation of the anion nets to **3².4.3.4** produces low-temperature **TlSe** (and also **KHF_2**). (High-temperature TlSe is **CsCl** type.) Again, the major nets of **3².4.3.4** are stacked alternately obverse and reverse. The cation array (also **4⁴** in **CsCl**) remains **4⁴**, but consists of two subarrays – each **4⁴** on doubled edge. One, presumably Tl^{I}, is in square, 30° antiprisms, [Se_8]; while the smaller Tl^{III} is in a [Se_4] tetrahedron – both slightly compressed in the **c** direction. (If the Tl^{I} is substituted by Se we have a hypothetical $TlSe_3$ = anti-low-**Pt_3Si**.)

Starting from the same 2×2 supercell of **4⁴**, other nets can be derived by varying the angle of rotation. The product depends to some extent on the degree of contraction or dilation accompanying the rotation operation. (Throughout, for convenience, we will keep the shortest bond length constant.) Thus, **4⁴** → **3².4.3.4** requires a reduction in area of $\frac{1}{4}(2+\sqrt{3})$. The nets we will generate next involve an increase in area.

Figures 36 (*a*) and (*b*) show how rotation of squares by arctan $\frac{1}{2} = 26.56°$ produces a net (*b*) that can be described as **4⁴** with one-fifth of the atoms missing. Clearly the area has increased by $\frac{5}{4}$. Such a net is known in crystals, occurring for example as (very slightly distorted) the primary (001) net of Ni in $Ni_{12}P_5$, as the (001) Ni net in $MoNi_4$, and as the cation net in Ti_4O_5 (Watanabe *et al.* 1970). It forms the starting point for deriving two other commonly occurring nets. By collapsing the small squares in figure 36 (*b*) to rhombuses, or rotating half the large squares (rather as in **4⁴** → **3².4.3.4**) the net in figure 36 (*c*) is produced. It is one in which half the large squares have been converted into regular octagons, and is found, for example, as the primary (001) net of Ni in Ni_3P, which is of the **Fe_3P** type. (Two [PNi_8] cubes in $Ni_{24}P_{10}$ [at 000 and $\frac{1}{2}\frac{1}{2}\frac{1}{2}$] lose their P and collapse to rhombic antiprisms. The composition change is $Ni_{24}P_{10} - 2P \rightarrow Ni_{24}P_8 = 8Ni_3P$, an elegant method of accommodating changes in stoichiometry.) Clearly, it is also simply related to **4.8²**, figure 36 (*d*), which is of wide occurrence in crystals, including chalcogenides such as $Pd_{17}Se_{15}$. The net in figure 36 (*c*) transforms to **4.8²** by appropriate rotations of the octagons; conversely, **4.8²** → figure 36 (*c*) by collapsing all the squares or rotating half the octagons.

Continuing the operation of rotating squares in **4⁴** to **4⁴** + one-fifth 'vacancies' up to a rotation angle of 45° one gets **4.8²** [figure 36 (*d*)] directly (rather than by the circuituous route just described). The increase in area over **4⁴** is $\frac{3}{4} + \frac{1}{\sqrt{2}} = 1.457$, so that it could be formally described as **4⁴** with 31.37% 'vacancies'.

A minor variation of the net in figure 36 (*c*) is shown in figure 36 (*e*). In this net, the octagons and large squares are all converted into irregular but congruent octagons. Such an arrangement is to be found in the structure of β-V_3S.

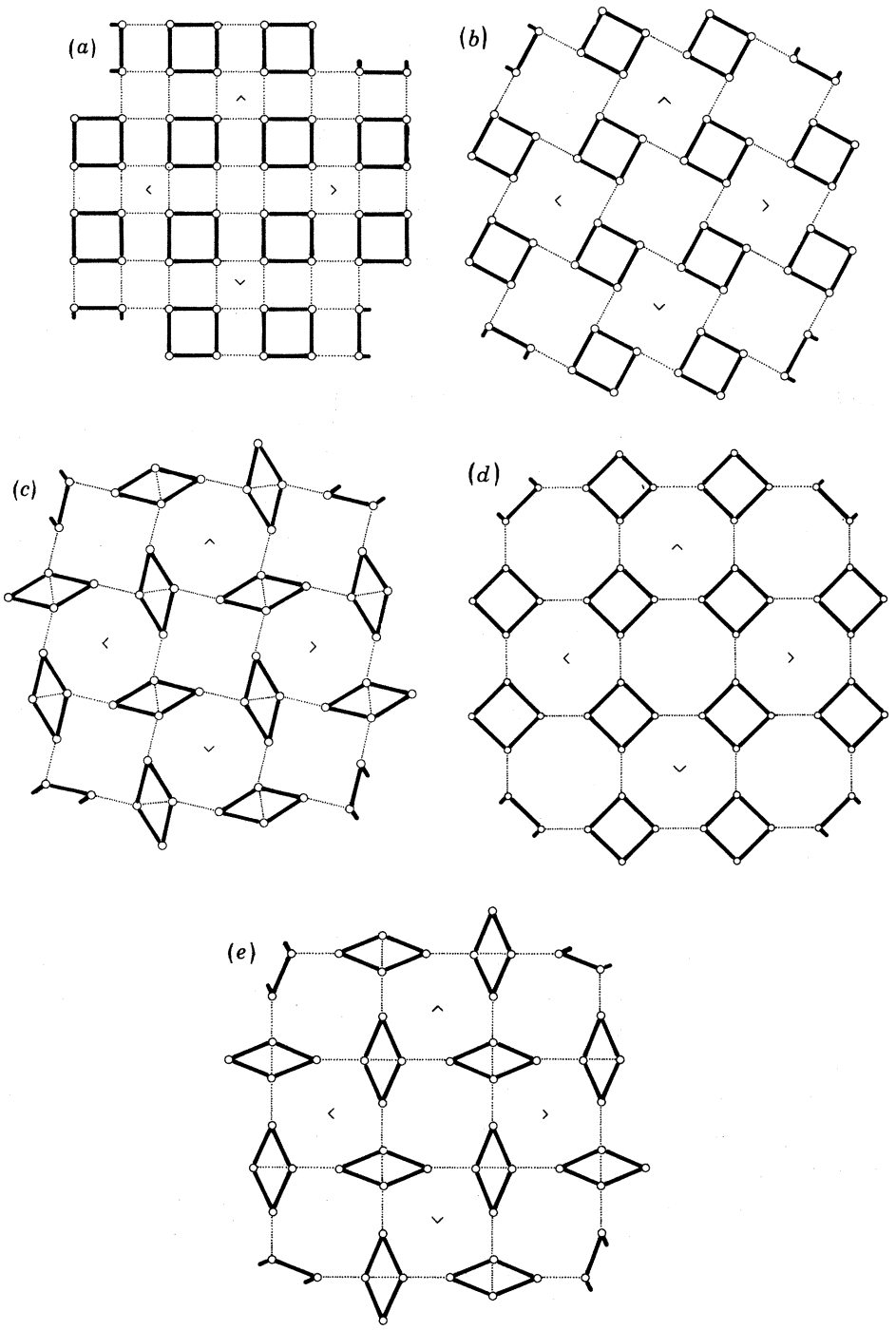

FIGURE 36. Transformations of 4^4 (see text).

If the 'vacant site' in figure 36 (*b*) is filled, 4^4 is regenerated. The reverse operation [figure 36 (*b*) → figure 36 (*a*)] will then generate interstitial atoms in a 4^4 net. Thus, local fluctuations in density, commonly termed point-defects are readily produced by rotation mechanisms – in this example and in many others – and normal atom diffusion is not essential.

The next group of nets is also derived from 4^4 by rotating square groups of atoms, but with

PHILOSOPHICAL TRANSACTIONS OF THE ROYAL SOCIETY A MATHEMATICAL, PHYSICAL & ENGINEERING SCIENCES

a different periodicity of the rotation centres. The super-cell of $\mathbf{4^4}$ now has an edge length of $2\sqrt{2}$, and there are two kinds of squares to be rotated: those at the origin and those at the centre of the cell in figure 37 (*a*). Rotation of the former by 45° gives the net of figure 37 (*b*), which is found, for example, in the (001) nets at $z/c = 0, \frac{1}{2}$ in Ca_3Ag_8 (with Ca at 3.4.3.6 and Ag at 3.6.4.6), in $Pd_{17}Se_{15}$ [(001) nets of Se at $z/c = \frac{1}{2}$] and, somewhat puckered, as the primary (001) oxygen net in narsarsukite ($NaTiSi_4O_{11}$).

Alternatively, both sets of squares can be rotated, but in opposite directions. If the rotations are $\pm \arctan \frac{1}{2}$ the net of figure 37 (*c*) results. This is analogous (in the sense of having the same density) to the net of figure 36 (*b*), '$\mathbf{4^4}$ with one-fifth vacancies'. Again, it is a common net in crystals, occurring as the primary (001) net of Hg in Pd_2Hg_5 and W in W_5Si_3. If an atom is put into the centre of the octagon, one has the Hg net of Mn_2Hg_5 (net 20, see also figure 37 (*d*) and below). And, if two silicon atoms are placed in each distorted octagon, one has the primary (001) nets of W_5Si_3. These three structure types are thus rather elegantly related. In Ti_5Te_4 the same net [figure 37 (*c*)] has [Te_4] squares at 00 and [Ti_4] squares at $\frac{1}{2}\frac{1}{2}$ (at $z/c = 0$, vice versa at $z/c = \frac{1}{2}$). The difference in size between the squares slightly distorts the net.

Continuing the rotations that produced figure 37 (*c*) until the rotation angle is 45°, one will of course regain the $\mathbf{4.8^2}$ net.

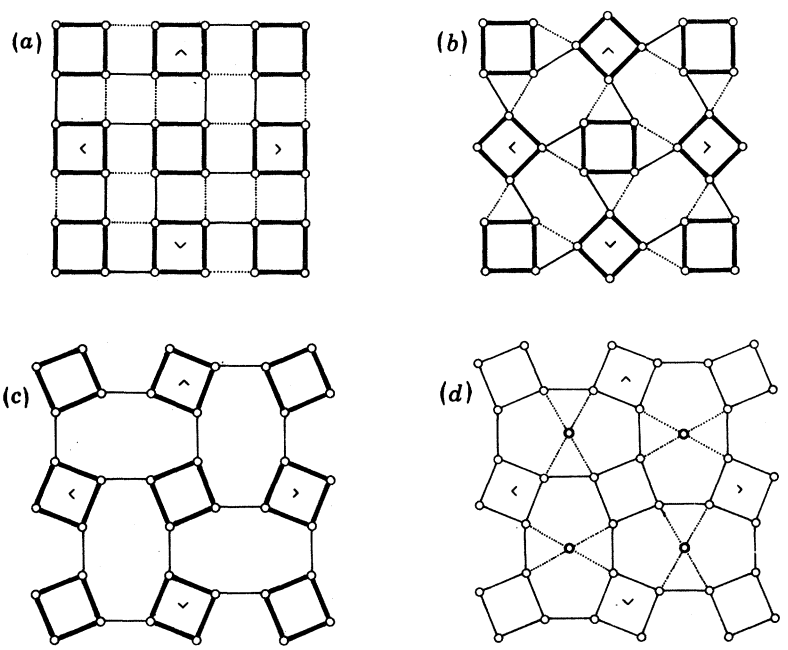

FIGURE 37. (*a*)–(*c*). Transformations of $\mathbf{4^4}$ (see text). (*d*) The Hg net of Mn_2Hg_5 (net 20). The heavy circles represent atoms added to the net shown in (*c*).

So far, we have divided the $\mathbf{4^4}$ net into square groups that are rotated relative to each other. A further variant is provided by changing the array of rotation centres so that isolated atoms are left with their positions unaltered. Figure 38 shows three possibilities: starting from $\mathbf{4^4}$ in figure 38 (*a*), net 19 is generated in (*b*) whereas, from $\mathbf{4^4}$ in (*c*), net 20 is generated in (*d*). Note that in figure 38 (*d*) the stationary, single atoms centre the distorted octagons of figure 37 (*c*). Hence, there is again a 'vacancy'/'interstitial' complementarity between figures 37 (*c*) and 38 (*d*); but they are both derived from the same array ($\mathbf{4^4}$), *and therefore from each other*, without

adding or subtracting any atoms! In figure 38 (*f*) we show an interesting net obtained from **4⁴** [in figure 38 (*e*)] by rotating isolated squares of atoms with rotation centres on an approximately **3².4.3.4** net in a 6×6 supercell of **4⁴**. The derived net, containing hexagons, pentagons, squares, and triangles, is in fact the (001) array of Mo atoms at octahedron centres in the Mo_5O_{14} structure (cf. below).

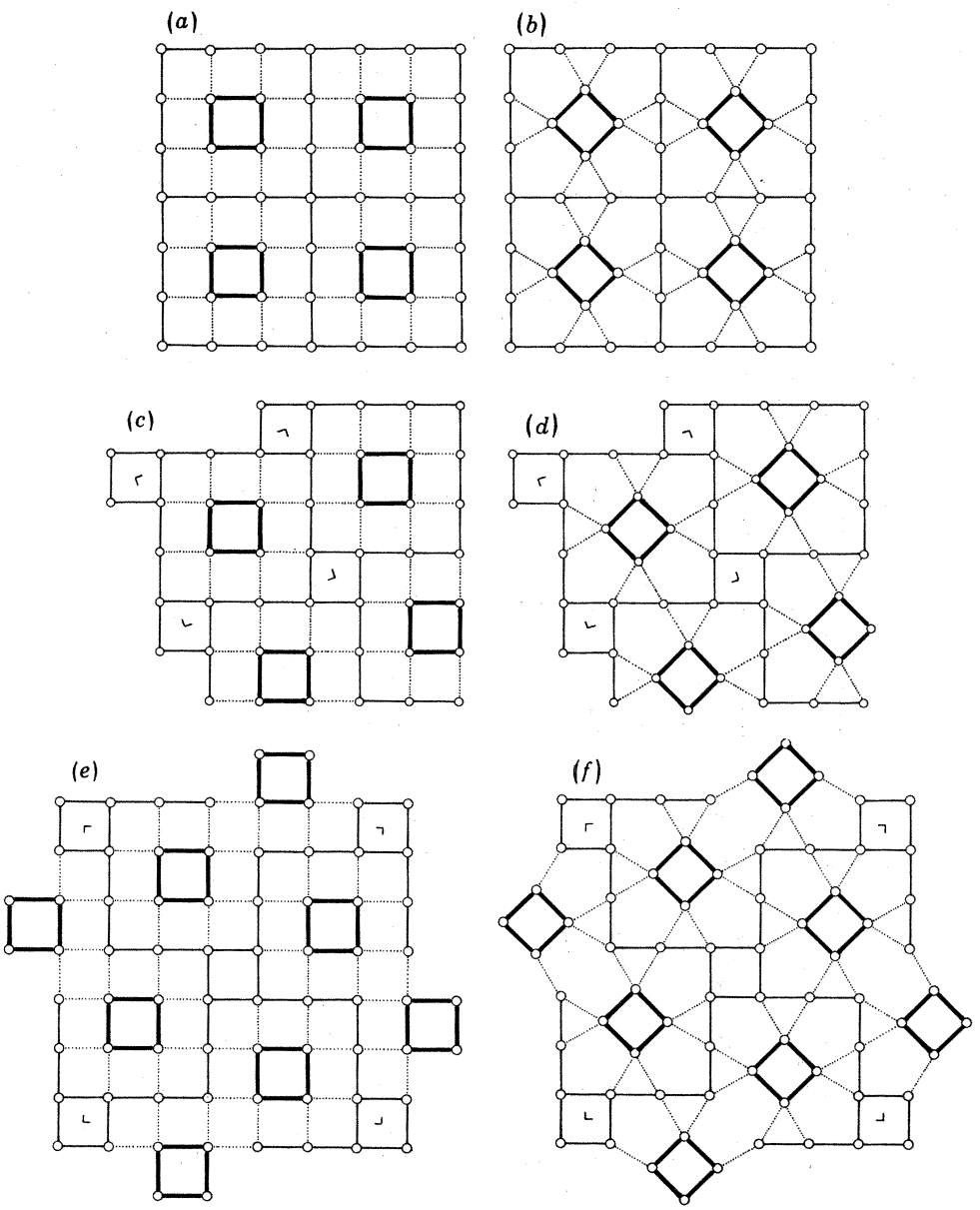

FIGURE 38. Further transformations of **4⁴**: to net 19 in (*b*), net 20 in (*d*) [≡ figure 37 (*d*)], and the (001) array of Mo in Mo_5O_{14} in (*f*).

The final net in this class in table 2 is no. 21, the primary anion net of tetragonal tungsten bronze (TTB). A formal derivation of the TTB anion net from **4⁴** by rotation of isolated squares is shown in figure 39 (*a*). In making the transformation, some bonds common to a square and a triangle have been omitted to make pentagons, a somewhat artificial procedure. In this

instance, it is more fruitful to consider the transformations of actual crystal structures in which there is a network of corner-connected octahedra of anions with cations at their centres: the arbitrariness in omitting lines then disappears. Elsewhere (Hyde & O'Keeffe 1973*a*) we have, in this way, discussed the derivation of several 'bronze'-type structures from $\mathbf{ReO_3}$ which is based on 4^4 anion nets. In figure 39(*b*) a (001) layer of $\mathbf{ReO_3}$ is related to a (001) layer of tetragonal bronze type. Groups of four cations are rotated (the transformation being that of 4^4 to net 20 described above), and hence groups of four octahedra.

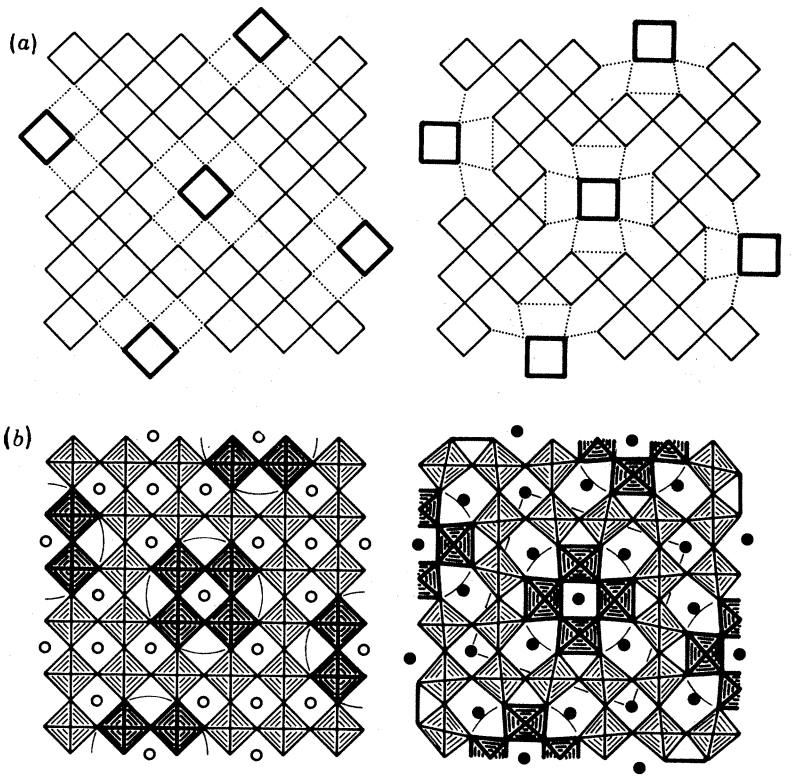

FIGURE 39. (*a*) Derivation of net 21 from 4^4. (*b*) Derivation of the tetragonal tungsten bronze structure from that of ReO_3.

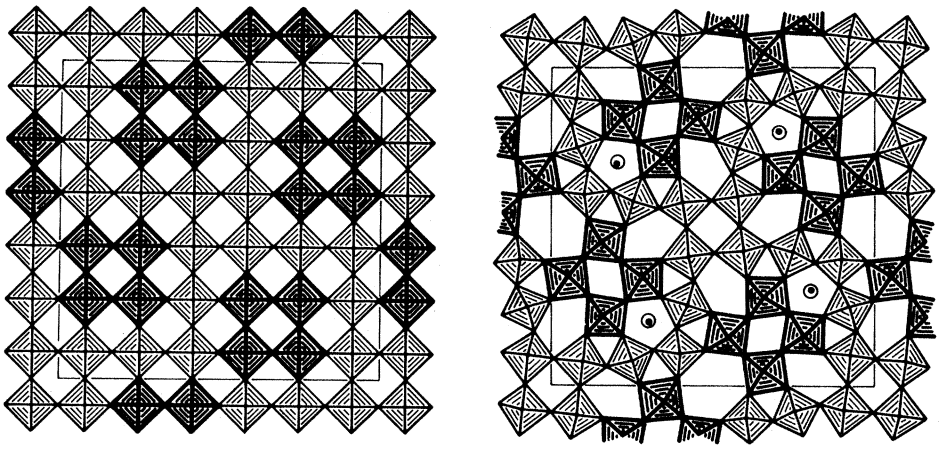

FIGURE 40. Derivation of the Mo_5O_{14} structure from that of ReO_3.

There is good evidence, largely from high resolution electron microscopy (Iijima & Allpress 1974*a*) that in these instances the structural correspondences are more than formal. Crystals containing coherent domains of both structure types and even isolated rotation faults (Bursill & Hyde 1972) have been observed.

Clearly one should be able to derive $\mathbf{Mo_5O_{14}}$ from $\mathbf{ReO_3}$ in a similar manner by using the transformation of figure 38(*c*) as a guide. This is shown in figure 40.

As a final example of the rotation of groups of squares (or octahedra in crystal structures) we show, in figure 41, how the network of corner-connected octahedra in $Nb_4W_7O_{31}$ (Iijima & Allpress 1974*b*) may be derived from $\mathbf{ReO_3}$ in a manner similar to that in figures 39 and 40. It can be seen that this structure is closely related to **TTB** and in fact is obtained simply by omitting one-quarter of the rotations used to derive **TTB** from $\mathbf{ReO_3}$.

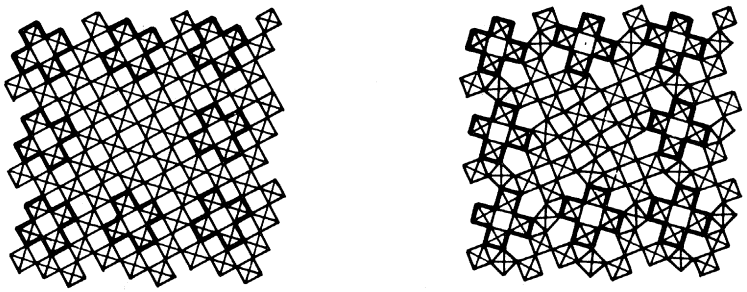

FIGURE 41. Derivation of the $Nb_4W_7O_{31}$ structure from that of ReO_3.

As the rotation centres become more widely spaced, and for structures derived by rotating squares by 45°, it may become more convenient to consider the derived nets as consisting of tiles of unchanged $\mathbf{4^4}$ and tiles containing the unit of rotation. This point is illustrated in figure 42, where a unit cell of net 19 is used as a tile. The net of the octahedron centres in $Nb_4W_7O_{31}$ is derived as a combination of this tile and tiles of $\mathbf{4^4}$. In figure 43 two other possibilities are shown: in figure 43(*a*) the net is no. 20 (that in Mn_2Hg_5) seen as an intergrowth of no. 19 tiles and small square tiles; and in 43(*b*) a new net is derived (by slip from net 20).

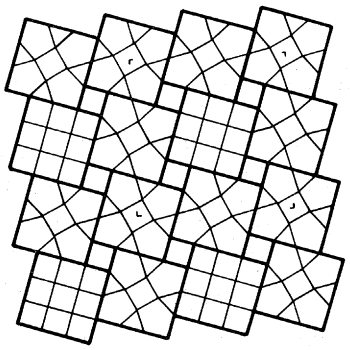

FIGURE 42. A tiling of units of net 19 and $\mathbf{4^4}$ giving the cation net of $Nb_4W_7O_{31}$.

It is of very great interest to distort the remaining squares in these last nets into rhombuses (as in $\mathbf{4^4 \rightarrow 3^2.4.3.4}$). In figure 44 this is done first in a distortion of the basic tile (figure 44(*a*)) and then to the net of figure 43(*b*) (figure 44(*b*)). The resulting net contains only pentagons

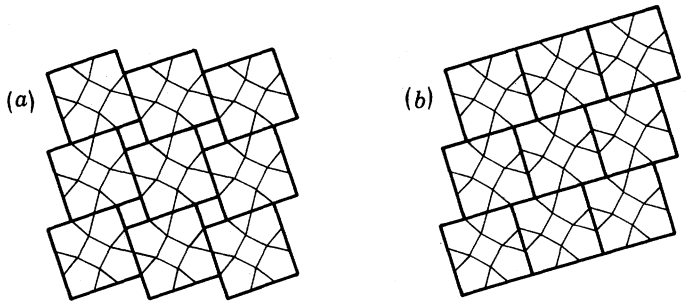

FIGURE 43 (*a*) AND (*b*). Tilings involving units of net 19.

and triangles and is the primary net of the μ-phase. The tiles of μ-phase (*μ-tiles*) can now be combined with rhombuses to give a distortion of net 20 shown as figure 45 (compare figure 43). This is the primary net of $W_6(Fe, Si)_7$ (Kripyakevich & Yarmolyuk 1971, quoted by Shoemaker & Shoemaker 1972). We shall further consider these and other related nets of 'topologically close-packed' structures below.

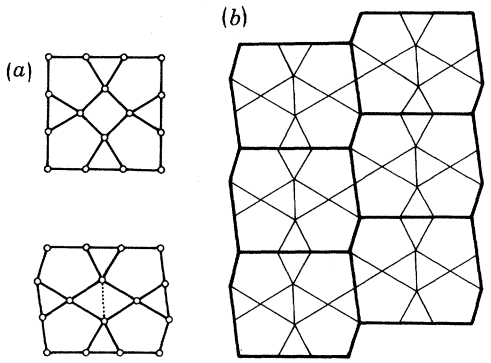

FIGURE 44. (*a*) Derivation of μ-tiles from those of figure 43.
(*b*) The primary net of μ-phase as a tiling.

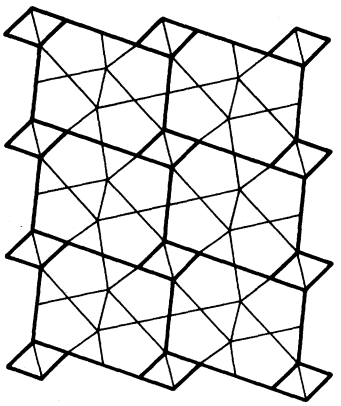

FIGURE 45. The primary net of $W_6(Fe, Si)_7$ as a tiling.

PHILOSOPHICAL TRANSACTIONS OF THE ROYAL SOCIETY A MATHEMATICAL, PHYSICAL & ENGINEERING SCIENCES

(ii) $A = 3$

The nets in this class appear, at least at first sight, not to be simply related to each other or to nets of other classes. The simplest one, shown in figure 46, is the only possible arrangement of three atoms in a cell with square symmetry. Its symmetry is $p4m$, and it has nodes at $1(b)$ and $2(c)$. Examples of the occurrence of this net are provided by (100) anion arrays in the structures proposed for Ag_2O_3 and Bi_2O_3 and the (100) Pt array in Pt_3O_4. It is also the arrangement of anions plus cations in (100) layers of $\mathbf{ReO_3}$, and so composite nets (of both ions) in structures derived from $\mathbf{ReO_3}$ and discussed in the previous section, also belong to this class. However, this is not a very useful or realistic way to consider the more ionic crystal structures, as anions and cations play quite distinct roles in the structure and should be considered separately. This is in contrast to alloy structures where we frequently consider nets composed of two different chemical elements (but cf. §6).

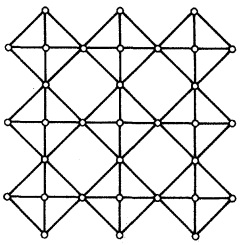

FIGURE 46. A simple square net with $A = 3$.

There are other, possibly useful, ways to consider this class. It may be seen that a square cell with 15 atoms also has $A = 3$ [$15 = 3(2^2+1^2)$]. Now an 'almost' (metrically) square cell can be chosen for $\mathbf{3^6}$ with 15 atoms per cell: this is shown in figure 47. It is actually oblique with $a = b = \sqrt{13}$ and $\gamma = 2\arctan\frac{3\sqrt{3}}{5} = 92.20°$. Also shown in the figure is a similar cell containing 60 atoms of $\mathbf{3^6}$ for which $a = b = \sqrt{52}$, and a rectangular cell of 30 atoms for which $a = 5$, $b = 3\sqrt{3} = 5.196$. It is possible therefore that some members of this square class may prove to be more usefully considered with the hexagonal nets, although we have discovered no simple connection with $\mathbf{3^6}$ for the square, $A = 3$ nets described in this paper.

A second, more fruitful, procedure is suggested by the net of figure 46. This may be described as $\mathbf{4^4}$ with one-quarter of the atoms removed ('vacancies'). The density of the net is

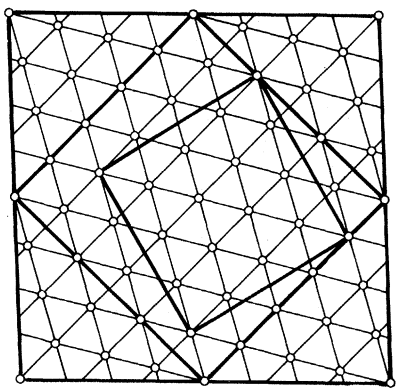

FIGURE 47. 'Almost' square cells of $\mathbf{3^6}$, with 15, 30 and 60 atoms.

low ($\rho = \frac{3}{16}\pi = 0.5890$). By way of contrast, the **U_6Mn** net (no. 12, which is also square, and may be regarded as **3^6** with 25% 'vacancies') has a much higher density, $\rho = 0.8418$, the same as **$3^2.4.3.4$**. It is interesting to see that the simple square cell containing three atoms is simply related to the **U_6Mn** net as shown in figure 48. Again, the atom movements are essentially rotations about four-fold symmetry axes.

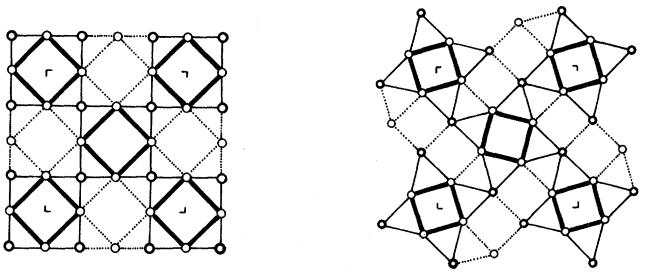

FIGURE 48. Transformation of the net of figure 46 to net 12 (**U_6Mn**).

This transformation may be used to relate structure types: in the proposed cubic Bi_2O_3 structure the cations are in cubic close-packing and the anions are on the net of figure 46, alternate layers being displaced by $\frac{1}{2}\frac{1}{2}$, forming the lattice complex J*. In the cubic bixbyite structure (C-type rare earth oxide structure) the same cation arrangement prevails, but the (100) anion layers approximate the **U_6Mn** arrangement, with successive layers displaced by $0\frac{1}{2}$, $\frac{1}{2}0$, $0\frac{1}{2}$, $\frac{1}{2}0$. (The above stacking of the idealized nets will not have cubic symmetry, but the relaxations to the real cubic structure are relatively small.) This arrangement results in all {100} planes being the same. Figure 48 therefore shows a relation between the structures of cubic Bi_2O_3 and bixbyite.

A related anti-structure is found for Cd_3As_2. The (001) layers of Cd are very similar to the anion layers in bixbyite but the stacking sequence is different. Specifically, the sequence of translations between layers is $\frac{1}{2}\frac{1}{2}$, $0\frac{1}{2}$, $\frac{1}{2}\frac{1}{2}$, $\frac{1}{2}0$, $\frac{1}{2}\frac{1}{2}$, $0\frac{1}{2}$, $\frac{1}{2}\frac{1}{2}$, $\frac{1}{2}0$.

We might mention that the B net of ThB_4 (no. 26) and the primary net of W_5Si_3 are closely allied to the **U_6Mn** net, which is not unexpected as they have the same number of atoms per unit cell (figure 49).

Net 18 ('MacMahon's net') is also a member of this family. Figure 50 shows the nodes of the net in figure 20, but with the vertices differently connected. The relationship to figure 46

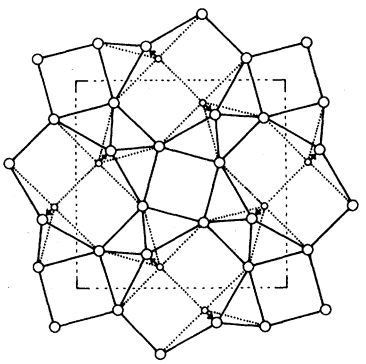

FIGURE 49. Relationship between the primary net of W_5Si_3 (full lines) and that of **U_6Mn** (dotted lines).

is readily apparent. With metal atoms in the centres of the squares, and anions at the corners, this net is of common occurrence (somewhat puckered) in chalcogenide and pnictide structures (Jeitschko 1974). The structure of pyrite, FeS_2, provides a good example. This way of regarding the net emphasizes that it is composed of two very different kinds of nodes and thus often occurs with two very different kinds of atoms at 5^3 and 5^4.

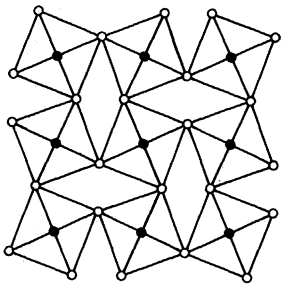

FIGURE 50. The nodes of net 18 differently connected (compare figure 46).

(*b*) *Hexagonal system*

(i) $B = 1$

The prototype of this class is the triangular net $\mathbf{3^6}$ and we find, as in previous sections, that many nets may be derived from the prototype by rotations of groups of atoms; in this instance triangles or groups of triangles. $\mathbf{3^6}$ occurs most notably in structures derived from close packing so that in many instances we will be able to relate structures with derived nets to those based on close-packing.

The next net in this class is the kagome net **3.6.3.6**. It may be rather obviously described as $\mathbf{3^6}$ with one-quarter of the atoms removed, but is much more elegantly and informatively

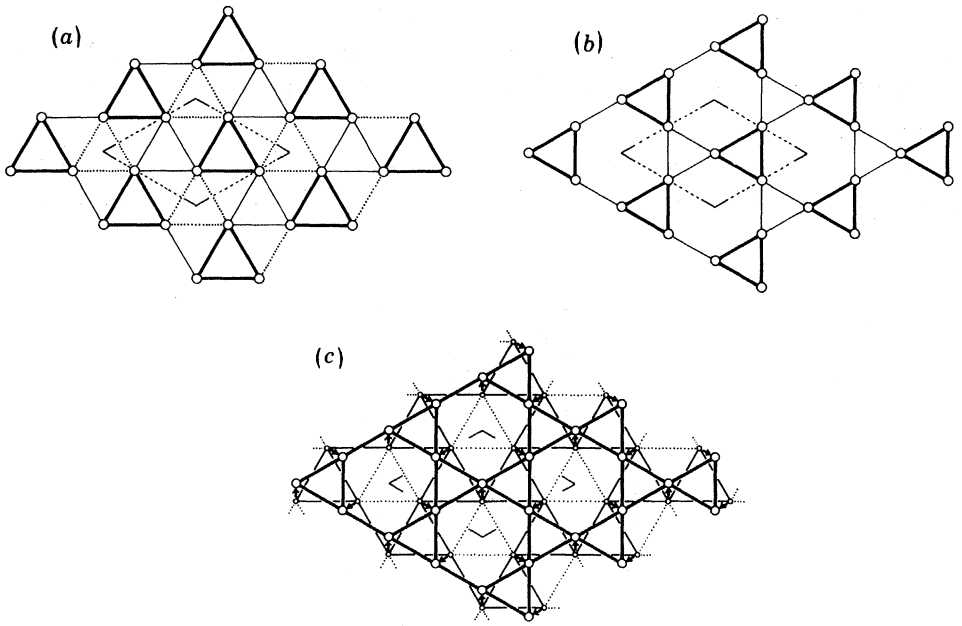

FIGURE 51. (*a*)–(*c*) Transformation between $\mathbf{3^6}$ and **3.6.3.6.**

related to $\mathbf{3^6}$ by rotations of triangular groups of atoms as shown in figures 51 (*a*) and (*b*). Figure 51 (*c*) shows that, once again, the process may also be described as expansion and contraction of the triangles (cf. transformation of $\mathbf{4^4 \leftrightarrow 3^2.4.3.4}$).

In non-metal structures the kagome net occurs most notably as the {111} anion net in $\mathbf{ReO_3}$; the J complex already mentioned above. Here the stacking of successive planes is as in cubic close packing, i.e. ...*a'b'c'*.... It can be seen from figure 52 that such a sequence of kagome nets can only be transformed (by using the operation of figure 51) to hexagonal close-packing (layer sequence ...*abab*...) or to primitive hexagonal packing ...*aaa*... or ...*bbb*..., or to a mixture of the two.

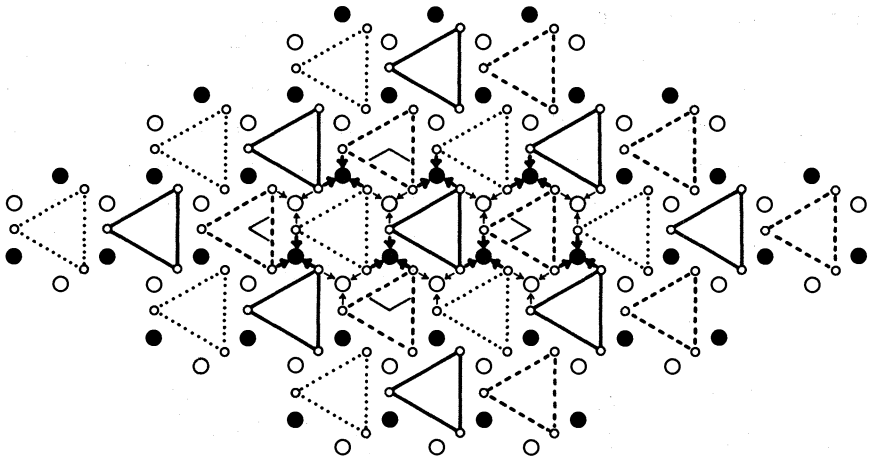

FIGURE 52. Transformations of kagome nets (small circles connected by heavy, dashed or dotted lines) in cubic stacking to $\mathbf{3^6}$ nets in positions *a* (large open circles) or *b* (large filled circles).

In the transformation J → h.c.p. the octahedral groups of atoms in the J complex remain unchanged. In $\mathbf{ReO_3}$, these octahedral holes are occupied by cations and the derived h.c.p. structure is $\mathbf{PdF_3}$. The correspondence between these two structures was pointed out by Jack & Gutmann (1951). It is elegantly described as alternate rotation of corner-connected octahedra by $\pm 30°$ about a trigonal axis, figure 53. The same, 'jack' operation (J → h.c.p.), but with rotation axes passing through the centres of empty octahedra, converts $\mathbf{AuCu_3}$ to $\mathbf{PdF_3}$. (A small shuffle, $\frac{1}{6}\langle 111\rangle_{\text{cubic}}$, is also necessary for **Au** → **Pd** since **Pd** is midway between the c.p. **F** planes while **Au** is in the centre of a $\mathbf{Cu_6}$ hexagon, i.e. in a **Cu** plane.)

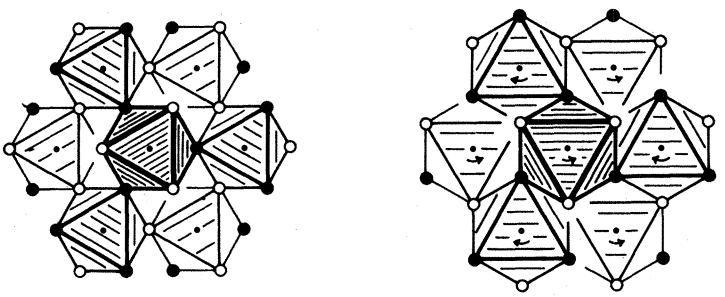

FIGURE 53. Transformation from the octahedral framework of ReO_3 (left) to that of PdF_3 (right). Arrows represent the sense of octahedral rotations for the reverse transformation.

There are several interesting corollaries:

(i) In the corundum structure type, two-thirds of the octahedral interstices in an h.c.p. anion array are occupied by cations. If the reverse, 'anti-jack', operation is applied and the rotation centres pass through the empty octahedra we get the (unlikely) structure proposed for $(Cr,W)_2O_3$ (Wyckoff 1963); idealized to $\alpha = 90°$, $u(2c) = \frac{1}{6}$, $u(3d) = \frac{1}{2}$ with cations in 9-coordination, one in each half of each cuboctahedron.

(ii) Topologically, the structure of $LiNbO_3$ is an ordered corundum type. By rotating one set of filled octahedra we combine the $\mathbf{PdF_3} \rightarrow \mathbf{ReO_3}$ and $\mathbf{PdF_3} \rightarrow \mathbf{AuCu_3}$ transformations: one set of cations remains in the rotated octahedra, the other set occupies the cuboctahedra, and $\mathbf{LiNbO_3} \rightarrow$ **perovskite** (Megaw 1957; O'Keeffe & Hyde 1977).

(iii) In **wurtzite** the cations occupy *tetrahedral* sites in an h.c.p. anion array. If the latter transforms from $\mathbf{3^6}$ to **3.6.3.6** and the cations move $\frac{1}{12}\langle 111\rangle + \frac{1}{6}\langle 1\bar{1}0\rangle = \frac{1}{12}\langle 3\bar{1}1\rangle$ (cubic indices), they arrive at the centres of the square faces of a cuboctahedron, and **wurtzite** $\rightarrow$ **NbO**. **NbO** may be similarly derived from **WC** and **NiAs**. It is normally described as 'deficit **NaCl**': an f.c.c. **NaCl** cell with Nb missing from the corners and O from the body centre of the cube. All atoms are in square planar coordination. This operation is more elegantly described as 'anti-jacking' *both* arrays: anions and cations. In each case h.c.p. $\rightarrow$ J: *in toto*, two interpenetrating h.c.p. arrays $\rightarrow$ two interpenetrating J complexes.

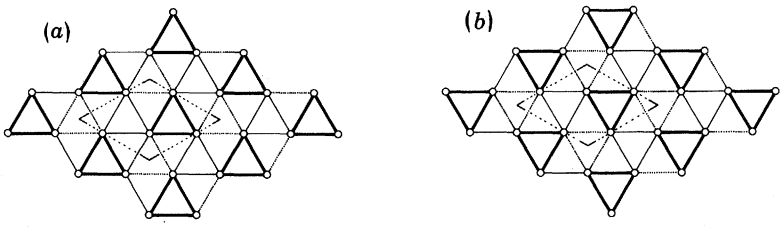

FIGURE 54. Change in stacking position of $\mathbf{3^6}$ accomplished by rotation of triangles.

If the rotation angle is doubled, i.e. the octahedra are rotated 60° instead of 30°, then $\mathbf{3^6} \rightarrow \mathbf{3^6}$ (obviously via **3.6.3.6**), figure 54. This is clearly jack = anti-jack except for a change of position: if the rotation axis is in the *a* position of a *b* net the product is in the *c* position and vice versa (cf. figure 52). If the rotation angle is halved (15° rotation or 'half-jack') the result is shown in figure 55. In this very common net the angles of the hexagons are alternately 90° and 150°. The anion nets in a group of transition metal trifluorides are one of $\mathbf{3^6}$, **3.6.3.6** or (for example, VF_3) this intermediate net (Hepworth *et al.* 1957; Michel *et al.* 1971). The same net appears in the structures of many other compounds, for example $Al_8FeMg_3Si_6$, Fe_2P, FeSi, $Y(OH)_3$ (very slightly deformed) and $LnCl_3$ (Ln = lighter lanthanides), δ'-Sb_3Cu_{10}, etc.

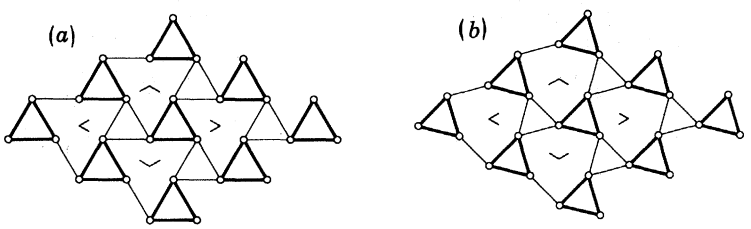

FIGURE 55. The 'half-jack' operation on $\mathbf{3^6}$.

The same operation on a 'substituted h.c.p.' array – AB_5, with A substituting for one third of the B atoms in alternate c.p. layers – but with rotation axes coinciding with the three-fold axes of the tetrahedra (parallel to **c**) so that the atoms of only half the layers are affected, transforms the twinned cuboctahedra to hexacapped hexagonal prisms. These are occupied by Ca in $CaZn_5$ (= $\mathbf{CaCu_5}$), the other atoms being at the transformed h.c.p. sites (cf. below, § 8*b*).

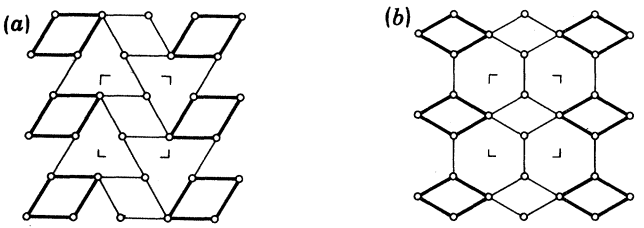

FIGURE 56. Transformation from 3^6 to net 14 (**β-W**).

This still does not exhaust the known possibilities. By rotating *pairs* of edge-shared triangles by 30°, $3^6 \rightarrow$ **β-W** (no. 14, figure 16), see figure 56. Finally, the strange, major anion layer in CrO_3 is also readily produced (slightly idealized) from 3^6 by rotating corner-shared triangles, figure 57.

Other nets can be derived from 3^6 by rotations of triangular groups of atoms, but these are of less importance than the anti-jack operation we have described. Figure 58 shows how net

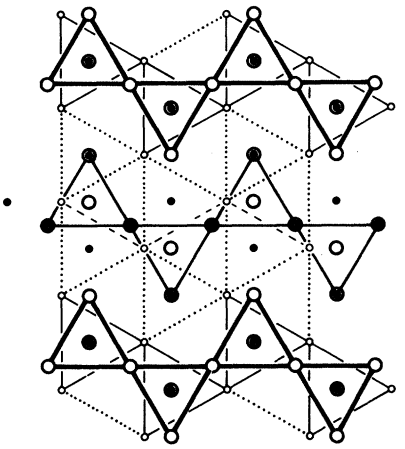

FIGURE 57. Transformation of h.c.p. to the anion array of CrO_3. The nodes of the two 3^6 nets are indicated by small circles, open at one level (*a*), filled at the other (*b*). (Only the *a* net is drawn.) The nodes of the transformed nets are indicated by large circles. In the transformation, triangles (actually tetrahedra) are rotated about axes normal to the plane of the diagram and passing through rotation centres indicated by double circles.

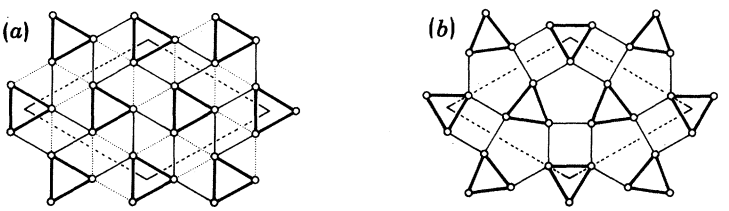

FIGURE 58. Transformation from 3^6 to net 23.

23 is derived by rotation from $\mathbf{3^6}$. The triangles to be rotated clockwise are the same as in figure 51 but the rotations are no longer all the same size. Figure 59 gives another example in which net 27 is derived from $\mathbf{3^6}$. Note that not all atoms are now involved in the rotation operation and that a considerable decrease in density results. (Note also that it is the net of figure 55, with half the triangles centred by an additional atom.)

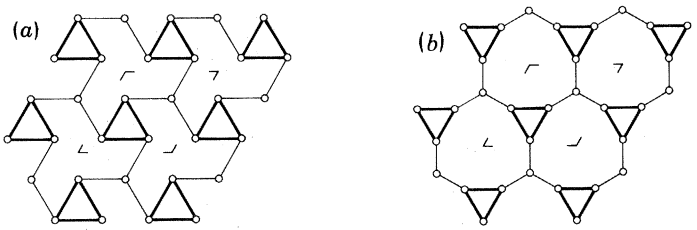

FIGURE 59. Transformation from $\mathbf{3^6}$ to net 27.

Other nets could be derived from $\mathbf{3^6}$ by varying the periodicity of spacing of rotation points (as was done with $\mathbf{4^4}$) but, in contrast to the earlier experience, this does not appear to be a fruitful line to pursue.

Of the other nets in this class, **4.6.12** (no. 11) seems to be of little importance in crystal chemistry, owing to the presence of the large polygon. The other two [nos 16(*a*) and (*b*)] are very simply related to each other by rotation of hexagonal groups of atoms as shown in figure 60. They are less readily related to $\mathbf{3^6}$ although, of course, they are compatible with it.

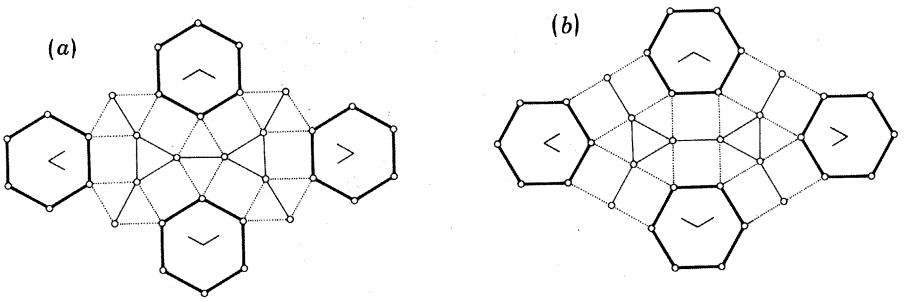

FIGURE 60. Transformation between nets 16*a* and 16*b*.

We have remarked that the **3.6.3.6** net can be derived from $\mathbf{3^6}$ by systematic removal of one-quarter of the atoms, and that in this sense the **3.6.3.6** $\rightarrow$ $\mathbf{3^6}$ transformation is elimination of 'vacancies' (the same is true of **β-W** $\rightarrow$ $\mathbf{3^6}$, figure 56). It is natural to enquire whether a net derived from $\mathbf{3^6}$ by removal of a smaller fraction of atoms can be converted to $\mathbf{3^6}$ in a similar manner. In general, it will be possible if the 'vacancy' net is in the $B = 1$ class. To illustrate this point, consider a net derived by removal of $\frac{1}{13}$ of the atoms from $\mathbf{3^6}$. Since $13 = 3^2 + (3 \times 1) + 1^2$, one can construct a supercell of $\mathbf{3^6}$ with 13 atoms per cell. If the atom at the origin of the cell is removed one has a hexagonal net with 12 atoms per cell, which is also in the $B = 1$ class ($p = 2, q = 2$). This latter net is shown in figure 61(*a*) in which groups of 12 atoms defining a hexagon and six triangles are picked out. Collapse of the hexagon in this group (a jack operation) to four triangles, as shown in figure 62, will result in a region of $\mathbf{3^6}$. The collapsed groups, suitably oriented as in figure 61(*b*), fit together to form a $\mathbf{3^6}$ net with the same number of atoms per cell as the original net.

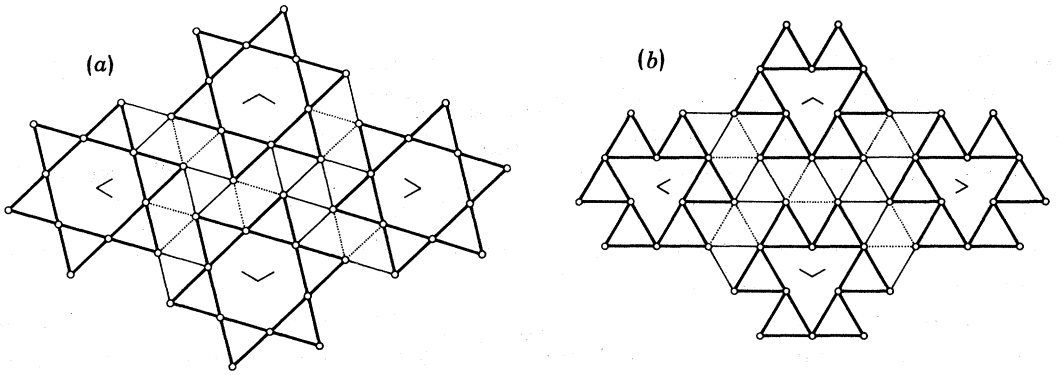

FIGURE 61. Transformation from (*a*) a net corresponding to 3^6 with $\frac{1}{13}$ of the atoms missing to (*b*) 3^6.

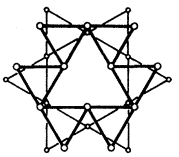

FIGURE 62. Relationship between the two groups of six triangles in figure 61.

The reasoning can be extended to higher numbers but the transformations will be less elegant. One could, for example, (to choose numbers arbitrarily) make a 3^6 net with 1/400 'vacancies' by taking an atom from the origin of a 20×20 supercell of 3^6. The resulting net, containing 399 atoms, is still in the $B = 1$ class ($p = 17$, $q = 5$ or $p = 13$, $q = 10$) and, in principle, can be transformed to 3^6 without any change in shape.

Thus, it may well be possible for vacant atom sites to be 'dissolved' or dispersed in a 3^6 net in a crystal structure: a possibility that seems not to have been considered. By the reverse operation 'vacancies' may be generated, also without the need for long-range diffusion.

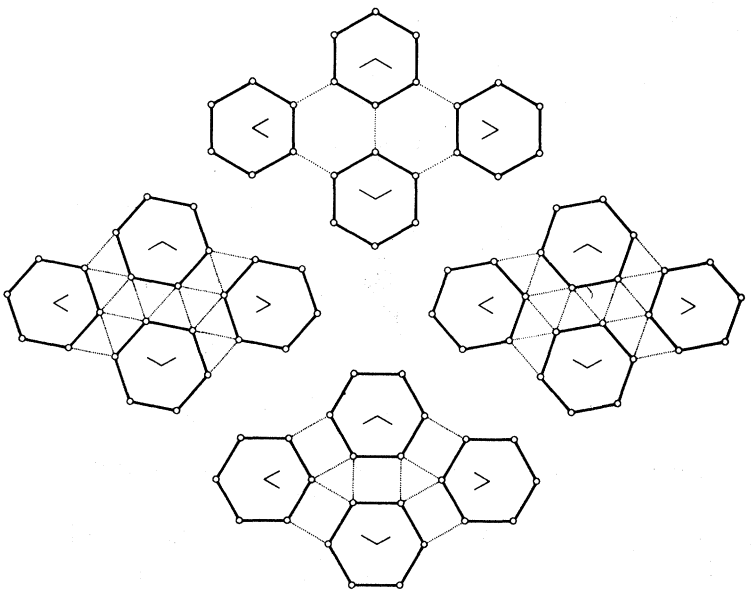

FIGURE 63. Transformation between 6^8, **3.4.6.4** and $3^4.6$.

PHILOSOPHICAL TRANSACTIONS OF THE ROYAL SOCIETY A MATHEMATICAL, PHYSICAL & ENGINEERING SCIENCES

(ii) $B = 2$

The prototype of this class is **6³**: three other semi-regular nets belong with it and they are all elegantly related. Figure 63 shows how **6³**, **3⁴.6** and **3.4.6.4** are related by rotations of hexagons. Starting with **6³**, we have picked out one-third of the hexagons. Rotation of each of these by $\pm \arctan \frac{\sqrt{3}}{5} = \pm 19.11°$ produces **3⁴.6**; rotation by another 10.89° will produce **3.4.6.4**. Thus, as the hexagons rotate, the sequence **6³**, **3⁴.6**, **3.4.6.4**, **3⁴.6** is repeated six times per revolution. (Note that the enantiomorphous forms of **3⁴.6** alternate, so that this is also a mechanism for 'inverting' this net.)

The relation between the structures of $TlSbF_6$ and $KOsF_6$ is just that between **3.4.6.4** and **3⁴.6**. In a manner analogous to the **$LiNbO_3$/perovskite** correspondence it is revealing also to consider this structural relation as a rotation of octahedral $[MF_6]$ groups, as shown in figure 64. (In this case the rotated octahedra are not connected.) Note that in these structures the stacking of the three anion layers is again ...$a'b'c'$... as for the kagome layers in **perovskite**; and that the large cations (Tl^+ or K^+) have the same environment in all three structures, a cuboctahedron of anions.

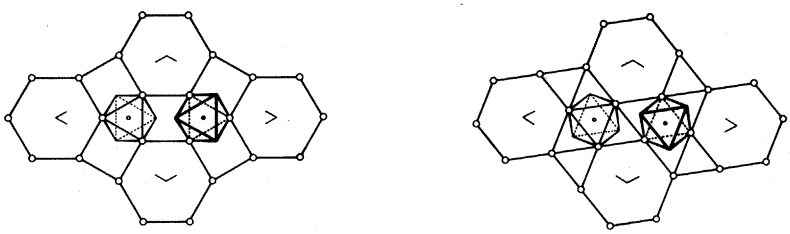

FIGURE 64. Transformations between the structures of $TlSbF_6$ (anion nets **3.4.6.4**) and $KOsF_6$ (anion nets **3⁴.6**).

To derive the last member of this class we again rotate the same group of hexagons and allow them to expand so that distances between atoms on one hexagon are larger than those on adjacent hexagons. This is shown in figure 65.

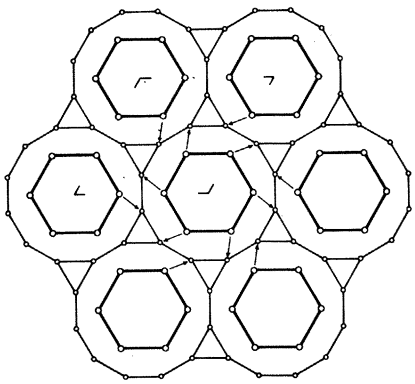

FIGURE 65. Transformation from **6³** (heavy lines) to **3.12²** (lighter lines).

It is interesting to apply the jack operation (in which a hexagon is converted to a group of four triangles) to **6³**. The result is shown in figure 66. One obtains a net with one group of four triangles and two deformed hexagons in the unit cell. The deformed hexagons are exactly

intermediate between regular hexagons and the group of four triangles, in the sense of having angles of 90° and 150° instead of all 120° for regular hexagons and 60° and 180° for the group of four triangles, i.e. they are identical to those produced in the half-jack operation on $\mathbf{3^6}$ (figure 55). However, the area of the deformed hexagon is closer to that of a regular hexagon than to that of the group of four triangles, so that the density of this net is less than that of $\mathbf{3^4.6}$ (which is made up of eight triangles and one hexagon) and is, in fact, equal to that of **3.4.6.4**. The net in figure 66 occurs, with only very slightly different angles, as the primary (001) nets in Mn_5Si_3 ($D8_8$) and, almost exactly, as the (0001) projection of the millerite (NiS) structure.

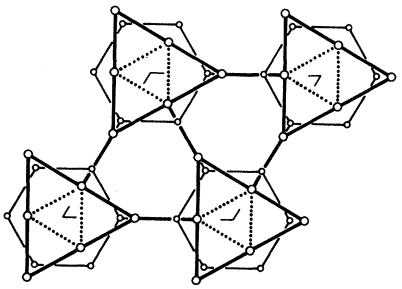

FIGURE 66. Deformation of $\mathbf{6^3}$ net (lighter lines) to a new net (heavier lines) described in the text.

It is worth noting too that $\mathbf{3^4.6}$ is not the densest net in the $B = 2$ family. In figure 67 (a) we show another net that can be considered as derived from $\mathbf{3^6}$ with one-ninth of the sites vacant. As shown in figure 67 (b), this is readily derived from $\mathbf{6^3}$ ($\equiv \mathbf{3^6}$ with one-third of the sites vacant!) by 30° rotations of hexagons (followed by a uniform contraction).

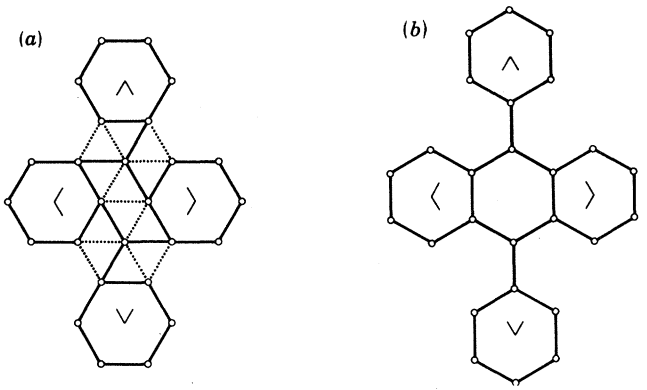

FIGURE 67. Derivation of $\mathbf{6^3}$ from a net derived from $\mathbf{3^6}$ by removing $\frac{1}{9}$ of the nodes.

There is an infinite number of such nets, derived from $\mathbf{3^6}$ with vacancies, compatible with $\mathbf{6^3}$. Thus, for example, a hexagonal cell with 999 atoms of $\mathbf{3^6}$ can be found ($B = 1$, $p = 30$, $q = 3$). Removing one atom (such as that at the origin) leaves a cell with 998 atoms, which is in the $B = 2$ class ($p = 18$, $q = 7$). (Doubtless larger numbers could be found. We need a number N such that $N = p_1^2 + p_1 q_1 + q_1^2$ and $(N-1) = 2(p_2^2 + p_2 q_2 + q_2^2)$ where p_1, q_1, p_2, q_2 are integers. Presumably, there is no limit to the value of N.) The 998 atoms per cell net will be very largely regions of $\mathbf{3^6}$, and it might seem at first sight that it is being claimed that a net that is essentially $\mathbf{3^6}$ is being transformed to $\mathbf{6^3}$ without change of shape while, at the same time, the transformation $\mathbf{3^6} \leftrightarrow \mathbf{6^3}$ is excluded, since these nets are in different classes. However,

within this large cell we will be transforming $\mathbf{3^6}$ to $\mathbf{6^3}$, presumably by a mechanism such as discussed later (p. 598), involving subcells that do change shape. The shape-change must be in different directions in different regions (i.e. multiple twinning on the subcell level) so that there is no overall change in shape in the supercell.

(iii) $B = 5$

We have described just two nets belonging to this class and they are simply related to each other. They are incompatible with the other hexagonal nets previously described, and thus cannot be transformed into them without adding or subtracting atoms. This observation suggests one means of deriving them originally proposed by Holmberg (1970) and by Loopstra (1970). In figure 68 we show how net 22 is derived from $\mathbf{6^3}$ by omission of one-sixth of the atoms. The structure of α-U_3O_8 is composed of primary layers of oxygen atoms on this net (5 atoms per cell) with uranium atoms centring the pentagons (3 U per cell). The remaining three oxygen atoms in the cell are on a secondary net with O above U. Adding one oxygen atom per cell (which converts this net to $\mathbf{6^3}$), one has approximately the structure of α-UO_3 (in which the $\mathbf{6^3}$ nets are appreciably puckered). The α-U_3O_8 structure thus provides another nice example of how a crystal structure may relax to eliminate 'ordered vacancies'.

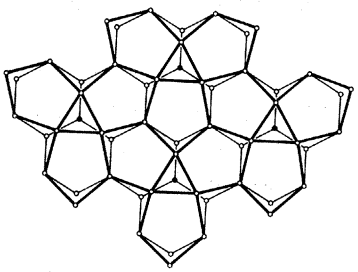

FIGURE 68. Derivation of net 22 (heavy lines) from $\mathbf{6^3}$ (light lines) by removal of one-sixth of the nodes (filled circles).

Figure 69 shows how net 22 is related to net 24* (the metrically hexagonal version of the primary anion net in β-U_3O_8). The operation is rotation of pentagonal groups of atoms, corresponding in the crystal structure to rotation of pentagonal bipyramidal $[UO_7]$ groups about a fivefold axis.

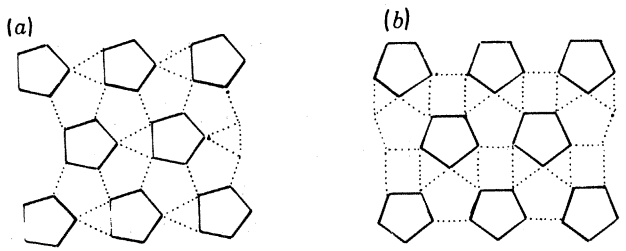

FIGURE 69. Relation between (*a*) net 22 ($\boldsymbol{\alpha}$-$\mathbf{U_3O_8}$) and (*b*) net 24* ($\boldsymbol{\beta}$-$\mathbf{U_3O_8}$).

8. Translation, or slip operations

(*a*) $3^6 \leftrightarrow 4^4$ (*and intergrowths*)

This is the prototype slip operation and was dealt with in a preliminary paper (Hyde *et al.* 1972). It allows transformation between the hexagonal class of nets and the square class. At its simplest, it involves a homogeneous deformation [figure 70 (*a*) → (*b*)]. The shear angle is 30°. If it is doubled, 3^6 is reproduced [figure 70 (*c*)]. Carrying out the double operation on alternate rows only also reproduces 3^6, but with a different change of shape (figure 71). Clearly, figure 71 (*b*) to figure 70 (*b*) changes 3^6 to 4^4 without changing the direction of the (macroscopic) crystal faces. If the single operation is carried out only on alternate rows of triangles, then $3^6 \rightarrow 3^3.4^2$ (figure 72). (Analogously, 4^4 can also be converted to $3^3.4^2$). Clearly, by varying the spacing and width of the deformed bands, any intergrowth of 4^4 and/or 3^6 with $3^3.4^2$ may be produced.

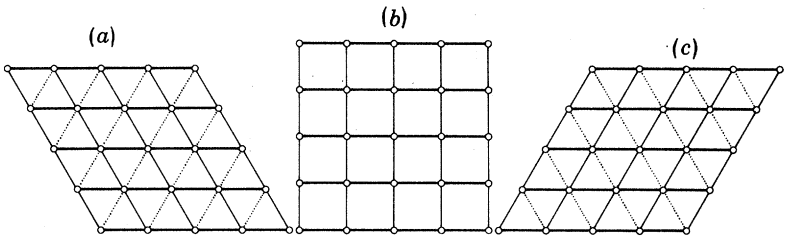

Figure 70. Transformation, by shear, from 3^6 to 4^4 to 3^6.

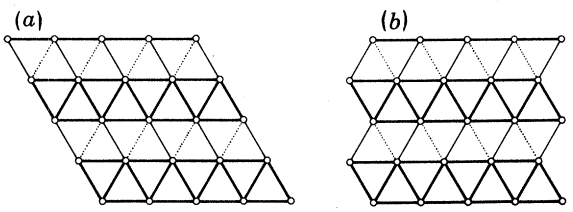

Figure 71. Change in shape of a 3^6 net (see text).

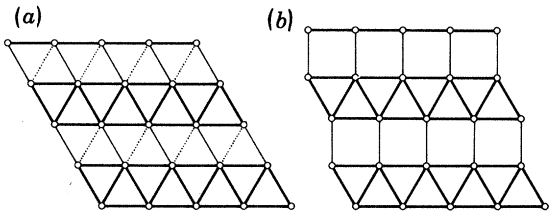

Figure 72. Transformation from 3^6 to $3^3.4^2$.

By appropriately stacking the various nets, and interleaving secondary nets, these operations lead more or less directly to relations between structure types. Starting with ... *aa*...stacking of primary nets with ...$\beta\beta$... secondary nets (also 3^6) figure 70 (*a*) → (*b*) converts **WC** to **CsCl**. If the secondary nets are ...$\beta\gamma\beta\gamma$... then anti-**NiAs** → **CsCl**. If the primary nets in figure 70 (*a*) are close-packed, and stacked ...*abcabc*... as in c.c.p., and the secondary nets are ...$\gamma\alpha\beta\gamma\alpha$..., then a primary stacking of ...*aaa*... in figure 70 (*b*) necessitates an additional slip of the primary layers. This is the well-known deformation of the primitive rhombohedral units cell of **NaCl** to the primitive cubic cell of **CsCl**. If the product primary net is ...*abab*... then, as well as slip, the secondary layers of cations drop into the primary layers to give **NaCl** in a different orientation.

Starting with ...*abab*... stacking, and filling alternate rows of octahedral interstices, gives the rutile structure idealized to h.c.p. anions. Figures 70 (*a*) → (*b*) → (*c*) then correspond to **rutile** → $\mathbf{CaF_2}$ → **rutile** twin, if the stacking in (*b*) is ...*aaa*..., and that in (*c*) is also

...abab.... Figure 72 (*a*) → (*b*) corresponds very approximately to **rutile** → monoclinic **zirconia**; and figure 71 (*a*) → (*b*) to **rutile** → **α-PbO_2** (with *...abab...* stacking). Similarly, the transformation figure 70 (*b*)–figure 72 (*b*) corresponds to high-TlI (= **CsCl**) → low-TlI (= anti-**CrB**).

These and similar transformations, and their relevance to, for example, phase transformations under high pressure, have been discussed in more detail elsewhere (Hyde *et al.* 1972; Hyde & O'Keeffe 1973*b*).

(*b*) $\mathbf{4^4 \leftrightarrow 6^3}$

This is less elegant, not being a homogeneous transformation. A simple mechanism is shown in figure 73. The square cell ($a = 2$) in (*a*) becomes the rectangular, 'orthohexagonal' cell ($a = \sqrt{3}$, $b = 3$) in (*b*).

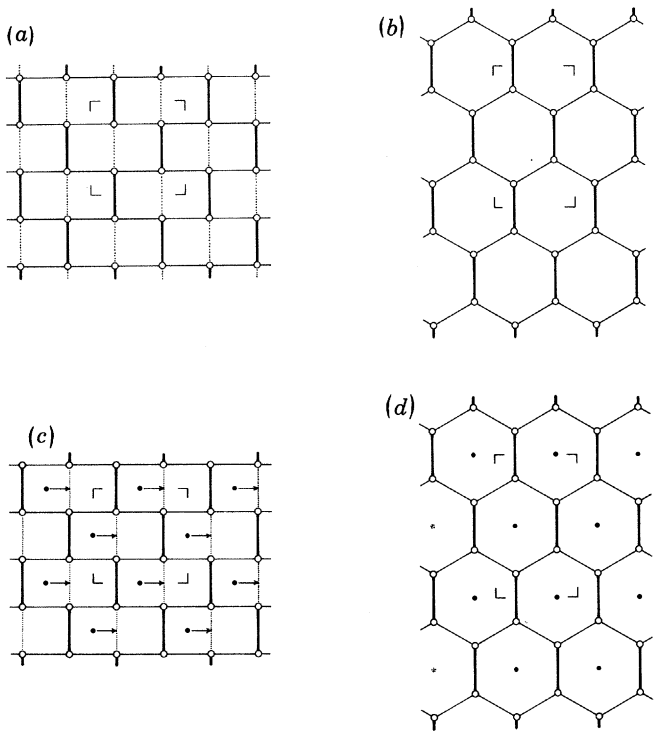

FIGURE 73. Transformation from (*a*) $\mathbf{4^4}$ to (*b*) $\mathbf{6^3}$, and (*c*) $\mathbf{Cu_3N}$ to (*d*) $\mathbf{Li_3N}$.

If the nets are stacked in superposition (i.e. *...aaa...*, normal to the net planes) then figure 73 (*a*) → (*b*) could represent a primitive cubic array transforming to a primitive hexagonal array. If the open circles are alternately M and X atoms this is **NaCl** → **BN** ('graphite' form). On the other hand, if the nets in figure 73 (*b*) are puckered, the same diagrams illustrate **α-Po** (primitive cubic) → **lonsdaleite** (= hexagonal diamond) or, with nets of alternate M and X atoms, **NaCl** → **wurtzite** (hexagonal ZnS, or zincite).

Similarly, figures 73 (*c*) and (*d*) represent $\mathbf{Cu_3N}$ (anti-$\mathbf{ReO_3}$) → $\mathbf{Li_3N}$. The filled circles represent –N–M–N–M– rows normal to the plane of the diagram, and the arrows indicate 'shuffles' accompanying the transformation, taking the rows from the centres of squares in (*c*) to the centres of hexagons in (*d*); thus converting $\mathbf{NCu_6}$ octahedra to $\mathbf{NLi_8}$ hexagonal

bipyramids. The same diagram describes a transformation of δ-UO_3 (**ReO_3**) to α-UO_3, though now the hexagons in figure 73(*d*) are grossly puckered, so that the hexagonal bipyramid is deformed to a cube compressed along the atom rows, which are now –M–O–M–O– (the nets being O atom arrays).

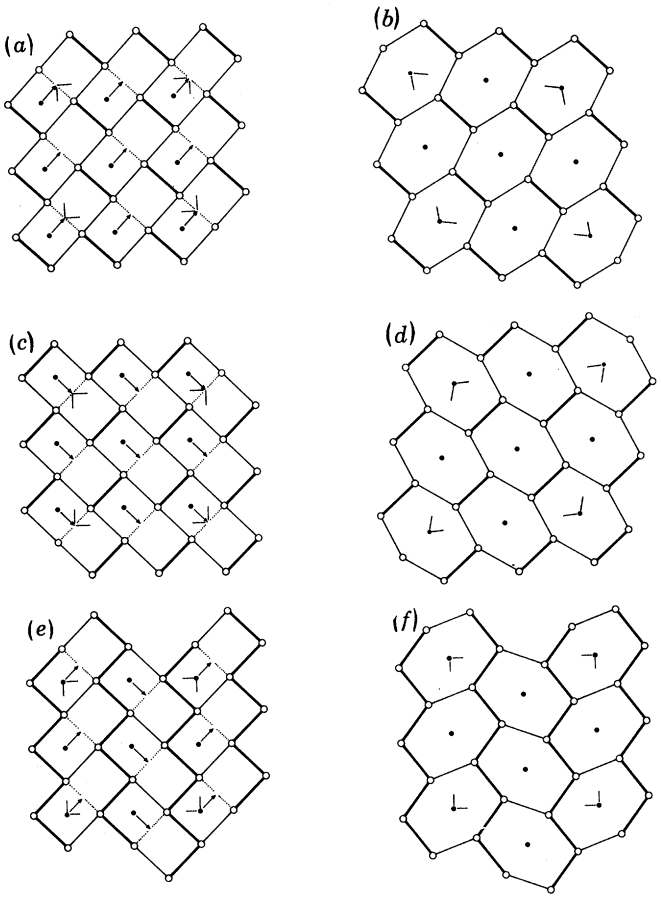

FIGURE 74. (*a*), (*b*), (*c*), (*d*) as (*a*), (*b*) but in a different orientation. (*e*), (*f*) intergrowth of (*b*) and (*d*).

In α-IrV and $BaZn_5$, for example, the nets lie between the two extremes of figure 73(*a*) and (*b*), cf. figure 74(*a*) and (*b*); $b/a = 1.167$ and 1.277 respectively, instead of 1.000 and 1.732. In this case it is clear that there are two equivalent orientations for the unit cell of the product net: figure 74(*b*) and (*d*). In any real case, strain would undoubtedly cause both orientations to occur, i.e. the product would be twinned so that shape change is minimized. Quite possibly twinning would be on the finest possible scale, see figure 74(*e*, *f*). The transformation from the major Zn net in $CaZn_5$ (= **$CaCu_5$**) to the corresponding Zn net in $BaZn_5$ is analogous to the actual transformation in figures 74(*a*) and (*b*), i.e. half that in figure 73(*a*) → (*b*). (There is also some shuffling of 20% of the Zn atoms.) The transformation **$CaZn_5$** → **$SrZn_5$** is that between figures 74(*e*) and (*f*), i.e. **$SrZn_5$** is finely twinned **$BaZn_5$**.

(*c*) $3^6 \leftrightarrow 6^3$

These different members of the hexagonal system are in different classes. They may, of course, be very simply related by a 'vacancy/interstial' mechanism: 6^3 is 3^6 with one-third of its atoms removed. Centring the hexagons in 6^3 restores the 3^6 nets, but a change in topology relates the two without adding or subtracting atoms, although, of course, it involves a change in the size of the unit cell (figure 75). In this case, the *a* axis of the unit cell remains unchanged, while *b* increases by 50%. It is readily apparent that $3^3.4^2$ is easily transformed to 6^3 (a hexagon $\approx$ 1 square + 2 triangles). Hence the transformation $3^6 \rightarrow 6^3$ may also be achieved via $3^3.4^2$.

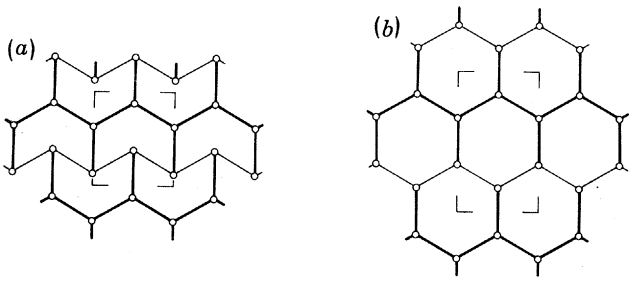

FIGURE 75. Transformation from 3^6 to 6^3.

These last are simple examples of the truism that any net may be converted to any other net by severing some links, or making new ones, and allowing the system to relax so that unlinked nodes become as far apart as possible.

(*d*) *Other slip relations*

There is a number of (fairly obvious) instances in which pairs of nets are related by slipping adjacent ribbons of net with respect to each other (as in $3^6 \leftrightarrow 3^3.4^2 \leftrightarrow 4^4$). For example, nets 7 and 14 (kagome net and **β-W**) are related in this way, by slipping the former by $\frac{1}{2}b$ on the (20) line at intervals of *a* (cf. figures 8 and 16). Similarly, net 19 is converted to a new net by slip of $\frac{1}{3}a$ along (01), as already mentioned (cf. figures 21 and 43(*b*)).

Only slightly less obvious is the transformation of the **HTB** net (no. 8) to that of $\mathbf{UVO_5}$ (no. 25) by slip of $\frac{1}{2}b$ along (10), repeated at unit cell intervals (figure 76). Here half-hexagons combine with half-squares so that alternate hexagon + square strips become the strings of edge-share pentagons that are so characteristic of the structures considered in §10.

There is another type of slip generally termed crystallographic shear (*CS*), in which the slip vector is no longer parallel to the slip line. Such transformations involve the elimination or

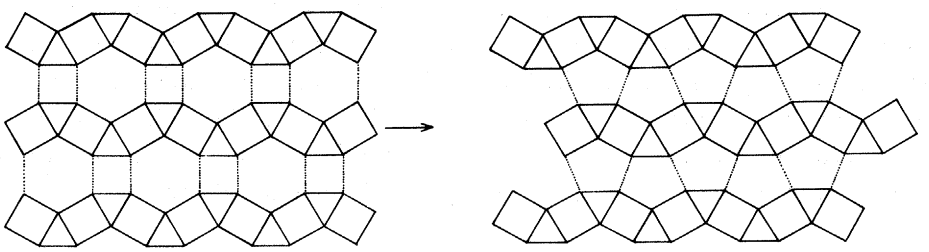

FIGURE 76. Production of net 25 from **3.4.6.4.**

addition of nodes/atoms, and appear at various places in this paper. They are specifically identified at several points in the next two sections.

9. Tetrahedrally close-packed (Frank–Kasper and Friauf–Laves) structures

(*a*) σ-*phase*

In this structure the primary (001) nets are kagome tiling, hexagon–triangle, with 11 atoms per tile (figure 77). Adjacent layers are rotated by $\frac{1}{2}\pi$ with respect to each other (so that the hexagons generate hexagonal antiprisms). The secondary layers are slightly puckered **3².4.3.4** nets.

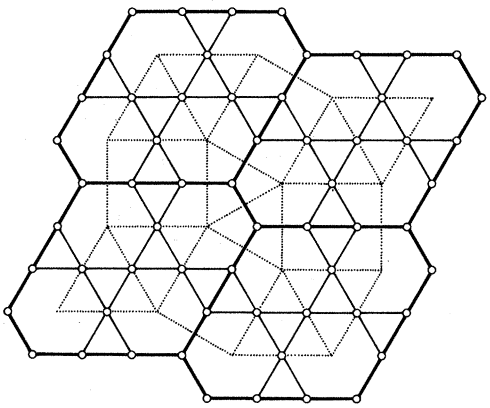

Figure 77. Secondary net (dotted lines) of kagome tiling (heavy lines).

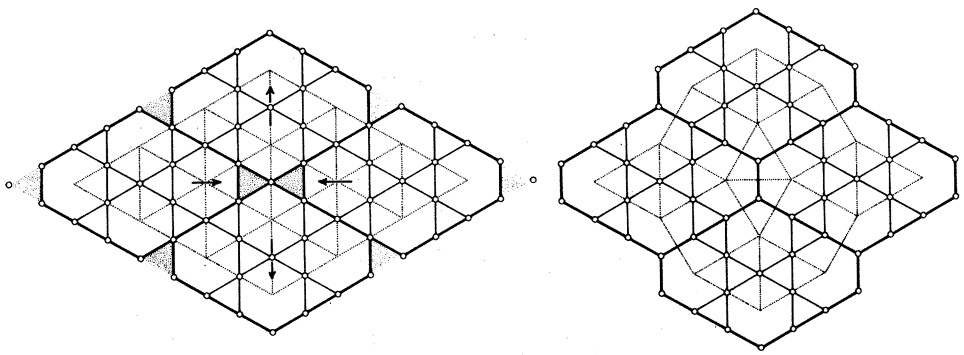

Figure 78. Transformation from the kagome net (left) to kagome tiling (right) by elimination of triangles (shaded).

The net in this tiling is closely related to the kagome net (**3.6.3.6**); each tile contains a segment of kagome net, and may be simply derived from it by collapse, eliminating one atom per large tile (= 4 unit cells of **3.6.3.6**) (figure 78). This operation converts the secondary nets from **3⁶** (for **3.6.3.6**) to **3².4.3.4** (for kagome tiling).

(*b*) $W_6(Fe,Si)_7$

This structure (by Kripyakevich & Yarmolyuk 1971; quoted by Shoemaker & Shoemaker 1972) has (001) pentagon–triangle primary nets consisting of what we might call KY tiles (figure 79). Two orientations alternate along **c** so that all the pentagons produce pentagonal antiprisms. The interleaved secondary nets are **3^2.4.3.4**.

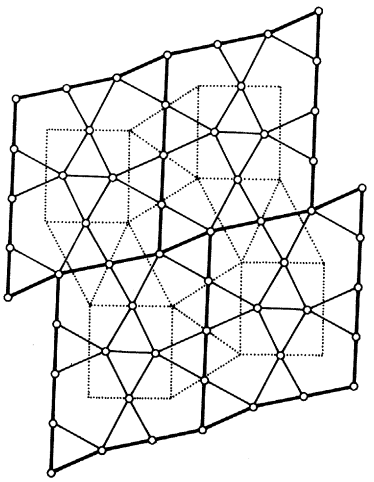

FIGURE 79. The primary net of $W_6(Fe,Si)_7$ as a tiling (heavy lines) with the secondary net (dotted lines).

We note that the KY tile is more conveniently regarded as a μ-tile (see μ-phase below) plus a pair of triangles, and that kagome tiling is readily converted to KY tiling by eliminating one atom per tile at the short edges (figure 80).

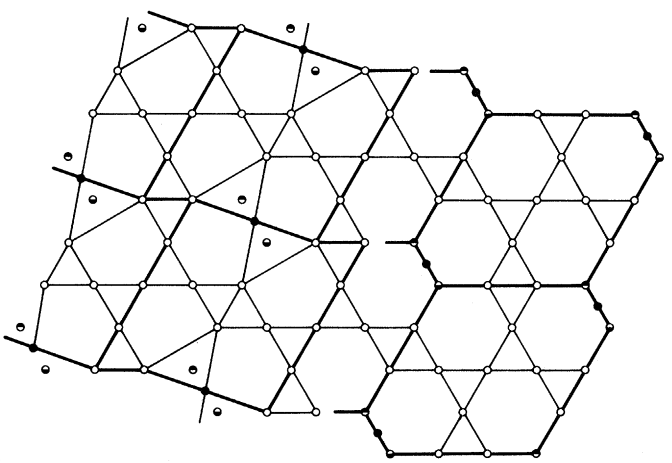

FIGURE 80. Comparison of KY tiling (on left) with kagome tiling (on right). The half-filled circles of kagome tiling are replaced by the filled circles of KY tiling.

(*c*) μ-*phase* (W_6Fe_7)

Parallel to (111) of the rhombohedral unit cell, the primary nets are kagome, and the secondary nets are **6^3** and **3^6** but, for our present purposes, it is better to concentrate on the layers parallel to (110). The primary nets are then pentagon–triangle, adjacent nets being

translated by $\frac{1}{2}[1\bar{1}0]$ so as to form pentagonal antiprisms and 'stellae quadrangulae'. They are readily resolved into a tiling (figure 81), the tiles being minor distortions of the unit cell of net 19 (Th_6Mn_{23}). They are also readily derived from KY tiling (= μ-tiles + triangles) by a simple slip/collapse (*CS*) that eliminates the triangles (figure 82). This converts the secondary net from $\mathbf{3^2.4.3.4}$ in KY tiling to $\mathbf{3^3.4^2}$ in the μ-phase.

We have already discussed the relation of the μ-tiling with net 20, etc. (§7 (*a*) (i)).

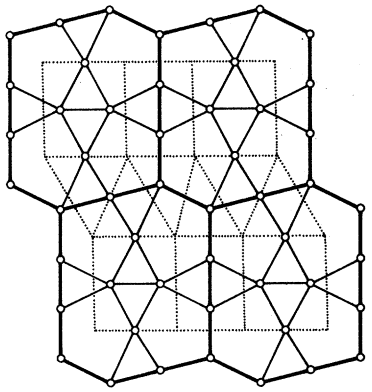

FIGURE 81. The μ-phase primary net as a tiling (heavy lines) with the secondary net (dotted lines).

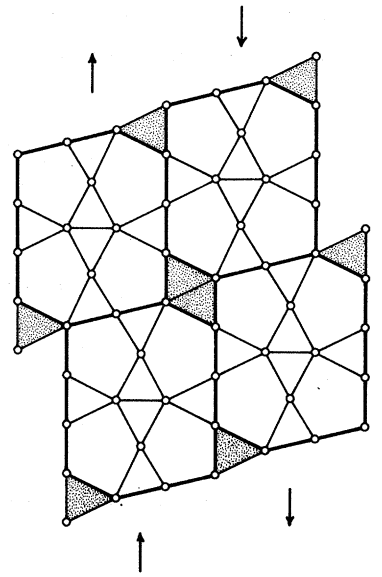

FIGURE 82. Transformation from the KY tiling (figure 79) to μ-tiling (figure 81) by shear (eliminating the shaded triangles).

(*d*) M-*phase*

The primary nets parallel to (001) again consist of pentagons and triangles, but they are more complex than in the previous two examples. They are, in fact, composed of strips of μ-net (infinite in the [10] direction), adjacent strips being twinned by glide reflexion across a line parallel to [10] – the twin and composition line (figure 83). There is considerable overlap between adjacent strips, i.e. many atoms near the composition line belong to both strips.

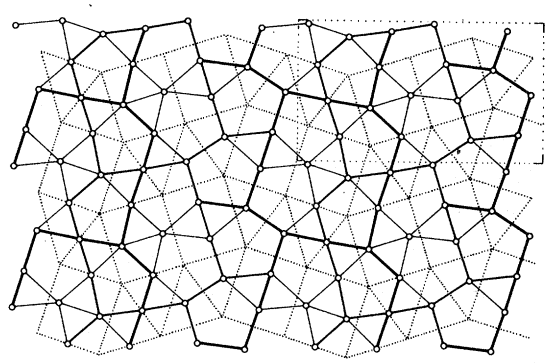

FIGURE 83. The primary net (light, medium and heavy full lines) of M-phase. Heavy and medium lines outline the edges of two sets of (twinned) μ-tiles. Dotted lines outline the secondary net.

PHILOSOPHICAL TRANSACTIONS OF THE ROYAL SOCIETY A MATHEMATICAL, PHYSICAL & ENGINEERING SCIENCES

The primary nets are, of course, stacked to give pentagonal antiprisms. The intervening secondary nets are (as they must be for twinned μ) twinned $\mathbf{3^3.4^2}$ which is, in fact, also twinned $\mathbf{3^2.4.3.4}$. They are net 13 (figure 14).

The primary nets may also be described as an intergrowth of one set of μ-tiles (in one of the twin orientations) with a differently shaped (μ′) tile (figure 84), or by a twinned arrangement of these μ′ tilings. It follows (*a*) that the μ-phase structure may itself be described as the μ′ tiling (figure 85) and (*b*) that the μ′ tile may be produced from a μ tile by a simple shear operation parallel to [10] (figure 86). Clearly, therefore, the M-phase structure may be produced from that of the μ-phase by mechanical twinning.

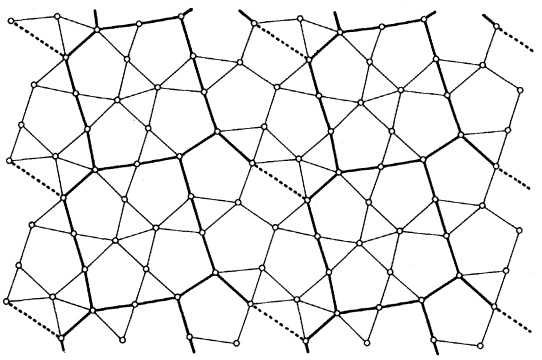

FIGURE 84. The M-phase net divided into tiles of two kinds.

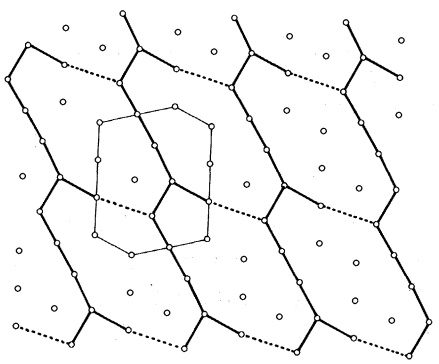

FIGURE 85. The μ-phase primary net as a μ′-tiling (see text). One μ-tile is lightly outlined.

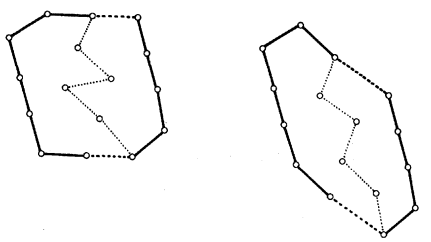

FIGURE 86. Relation between the μ-tile (left) and the μ′-tile (right).

(*e*) P-*phase*

The (001) primary layers, shown in figure 87 (*a*), are now hexagon–pentagon–triangle nets, with alternate nets superposed and the stacking arrangement such that all the hexagons form columns of hexagonal antiprisms and all the pentagons form columns of pentagonal antiprisms. They may be described in several ways:

(i) As twinned σ; the twin and composition lines being parallel to **a**. Within each twin there are hexagon–triangle nets (σ strips) which accommodate all the atoms; but the glide reflexion twinning operation generates pentagons in the boundary lines, figure 87 (*b*).

(ii) As twinned μ. Here the twin bands are pentagon–triangle nets, and the hexagons are generated in the boundaries by the glide reflexion, figure 87 (*c*).

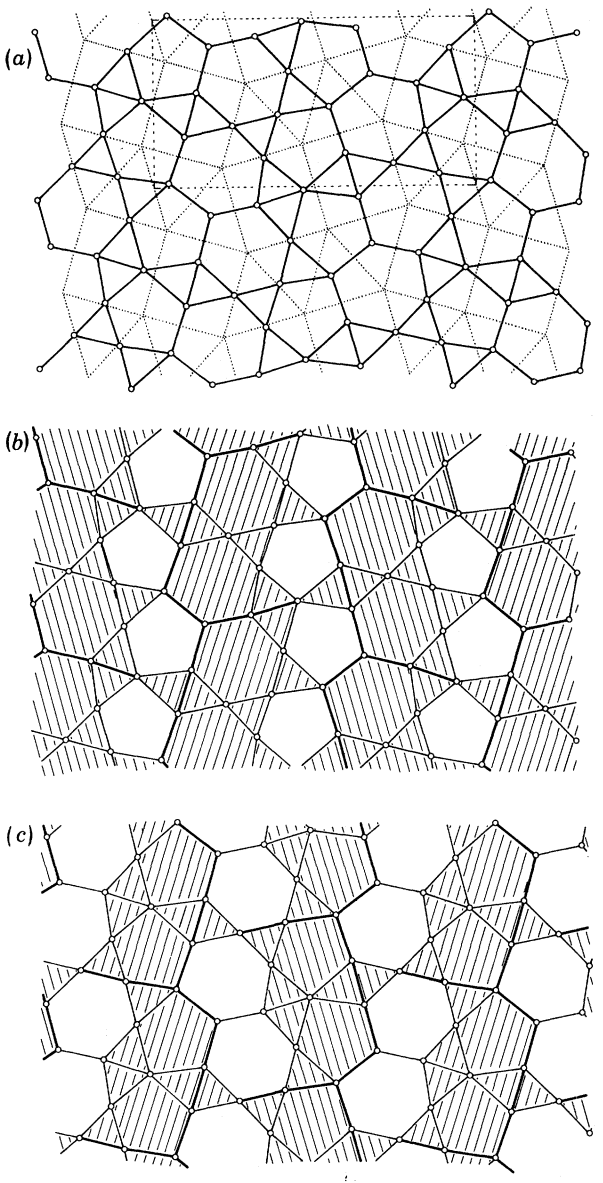

FIGURE 87. (*a*) The primary net of P-phase (heavy lines) and its secondary net (dotted lines). (*b*) The net in (*a*) divided into strips of σ-phase nets (shaded) related by glide-reflexion. (*c*) The net in (*a*) divided into strips of μ-phase nets (shaded) also related by glide-reflexion.

(iii) As an intergrowth of σ and μ strips.

The secondary nets (no. 18) are logically described as twinned $\mathbf{3^3.4^2}$ (twinned μ) = twinned $\mathbf{3^2.4.3.4}$ (twinned σ) or as an intergrowth of $\mathbf{3^3.4^2}$ and $\mathbf{3^2.4.3.4}$ (figure 87*a*).

(*f*) Zr_4Al_3

While this may be described, in terms of (0001) atom planes, as **3.6.3.6** primary nets of Al at $z/c = 0$ with secondary $\mathbf{6^3}$ layers of Zr at $z/c = \frac{1}{2}$ and (large) $\mathbf{3^6}$ nets of Zr at $z/c = \pm\frac{1}{4}$, it is also a Frank–Kasper structure. Parallel to $\{11\bar{2}0\}$ the primary nets are very symmetrical pentagon–triangle (figure 88). They are stacked in two orientations to form pentagonal anti-prisms. Intermediate secondary nets are $\mathbf{4^4}$.

PHILOSOPHICAL TRANSACTIONS OF THE ROYAL SOCIETY A MATHEMATICAL, PHYSICAL & ENGINEERING SCIENCES

The primary net is obviously closely related to those in $W_6(Fe,Si)_7$ (cf. (*b*) above), the μ-phase ((*c*) above), and net **19**.

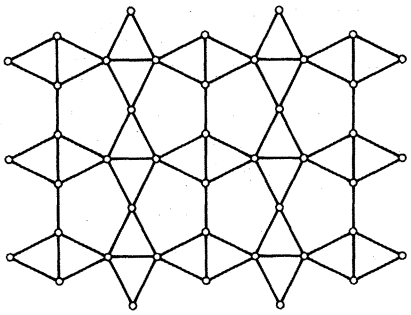

FIGURE 88. ($11\bar{2}0$) primary nets of $\mathbf{Zr_4Al_3}$.

(*g*) *Friauf–Laves phases*

These are incomplete close-packed structures, with **3.6.3.6** (kagome) primary nets normal to the three-fold axis. However, they may also be regarded as examples of Frank & Kasper's 'topologically close-packed structures', a description most obvious when one considers nets parallel to the prism planes, $\{11\bar{2}0\}$ in the hexagonal unit cell. All these structures then consist of pentagon–triangle primary nets (figure 89). In principle there is an infinite number of possibilities (polytypism in the stacking of the incomplete c.p. layers parallel to the basal plane of the hexagonal cell), but only two types of tile are involved. Furthermore, these are very easily interconverted by a 'place-exchange' mechanism (figure 90). (Clearly, as long as only one tile is used in a given $[\bar{1}100]$ row, rows of either type may be stacked along [0001].) The drawings (figure 89) show primary layers of (*a*) $MgCu_2$, (*b*) $MgZn_2$ and (*c*) $MgNi_2$, the three simplest polytypes. Two points may be noted: (i) the distorted hexagon tile corners are

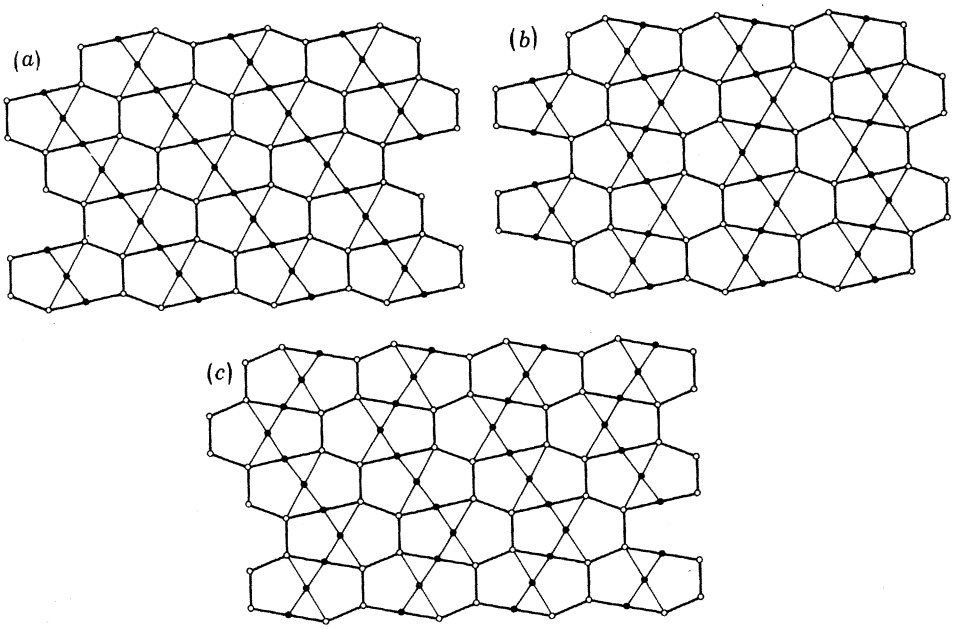

FIGURE 89. ($11\bar{2}0$) primary nets of (*a*) $\mathbf{MgCu_2}$ (*b*) $\mathbf{MgZn_2}$ (*c*) $\mathbf{MgNi_2}$.
In each case open circles are Mg.

all nodes of the type 3.5^3 and are always occupied by the (larger) Mg atom ($CN = 16$), the 3.5.3.5 nodes accommodating the smaller atom, Cu, Zn, Ni, etc.; (ii) In all cases the secondary nets (also of the smaller atoms) are 3^6.

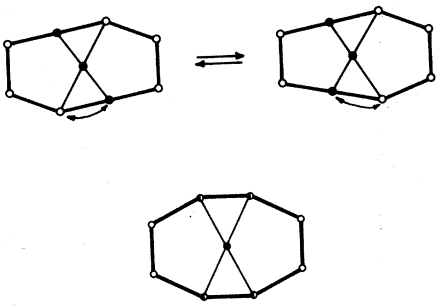

FIGURE 90. Top: relation between the tiles of $MgCu_2$ (left) and $MgZn_2$ (right). Bottom: a symmetrical, intermediate tile found in Zr_4Al_3, etc.

Very striking also is the fact that these same Friauf–Laves tiles (sometimes very slightly distorted, but still quite clearly recognizable) also occur in, and indeed dominate, all of the structures that we have already considered which contain pentagon–triangle nets (i.e. except σ) and will be encountered again in nets associated with the structures of oxides related to β-U_3O_8.

Figure 91 (*a*) shows the Zr_4Al_3 net in terms of Friauf–Laves tiles of the symmetrical form shown in figure 90. (In this tile the peripheral atoms are Zr and the central atom Al). In figure 91 (*b*) the μ-phase net is resolved into similar tiles and, in figure 91 (*c*), the net of $W_6(Fe,Si)_7$ is similarly described. Figures 91 (*a*) and (*b*) are obviously related by a simple slip/*CS* process between alternate horizontal rows of tiles. Slip between the remaining rows can produce figures 89 (*a*), (*b*) or (*c*) – the nets of the three simpler Friauf–Laves phases. Slip in a vertical direction relates figures 91 (*c*) and (*b*). In the M-phase structure (figure 91 (*d*)), not surprisingly, bands of similar tiles occur, with whole tiles bonded to half tiles at the sides of the bands; while in the P-phase, only fragments of tiles occur (figure 91 (*e*)). In both these cases, however, the whole structures are composed of these fragments. Again, it is not too difficult to see that figures 91 (*b*) and (*d*) are related by slip in a vertical direction. (This slip operation is analogous to the shear operation already described).

(*h*) *Conclusion*

The above discussion shows that the primary nets in all the topologically close-packed structures (table 3) need not be treated as isolated types. There are, in fact, very close relationships between them all, not unlike those between families of *CS* structures and 'column'

TABLE 3. CLASSIFICATION OF TOPOLOGICALLY CLOSE-PACKED STRUCTURES BY THEIR PRIMARY AND SECONDARY NETS†

	primary net		
secondary net	hexagon–triangle	pentagon–triangle	hexagon–pentagon–triangle
4^4	β-W	Zr_4Al_3	
3^6	ν	$MgCu_2$, $MgZn_2$, etc.	
$\alpha = 3^2.4.3.4$	σ	$W_6(Fe,Si)_7$	
$\beta = 3^3.4^2$		μ	
$\alpha\beta$		M	P

† Cf. Shoemaker & Shoemaker (1972).

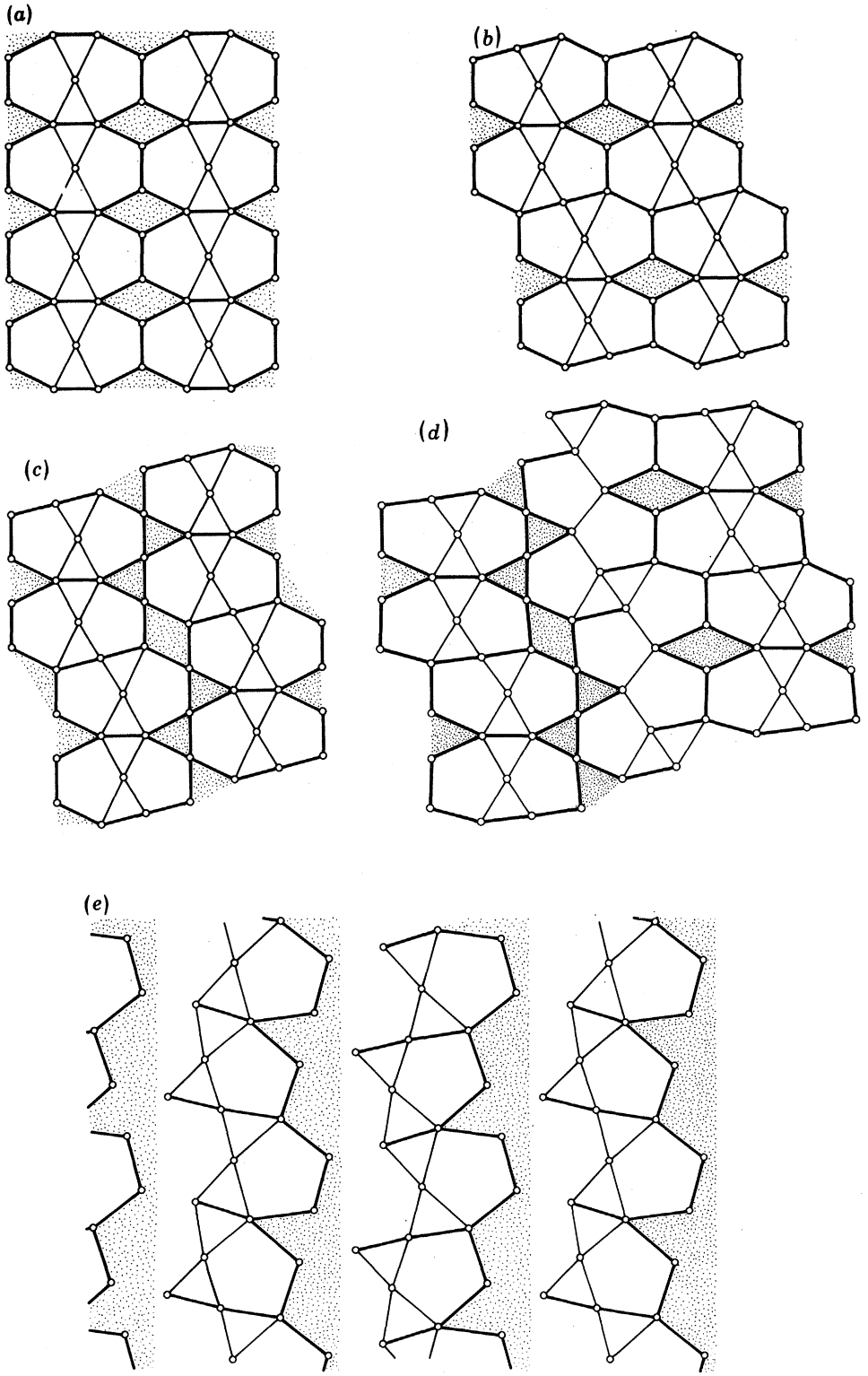

FIGURE 91. (*a*) $\mathbf{Zr_4Al_3}$ primary nets resolved into tiles. (*b*) A similar resolution of the μ-phase primary nets. (*c*) A similar resolution of the $W_6(Fe,Si)_7$ primary net. (*d*) The primary net of M-phase. (*e*) The primary net of P-phase.

PHILOSOPHICAL TRANSACTIONS OF THE ROYAL SOCIETY A MATHEMATICAL, PHYSICAL & ENGINEERING SCIENCES

structures in the transition metal oxides. The clue to the nature of the relationship between each pair is often made most readily apparent by comparing the related secondary nets. The relations between these, $\mathbf{4^4} \leftrightarrow \mathbf{3^6}$ and $\mathbf{4^4} \leftrightarrow \mathbf{3^2.4.3.4}$ etc., are quite simple translation or rotation operations that have been dealt with in earlier sections. These relationships extend to the crystal structures.

10. Nets derived from the β-U_3O_8 net

In this section we discuss a number of pentagon–square–triangle nets derived from that of β-U_3O_8 (no. 24, figure 26). These fall into a group rather as do the pentagon–hexagon–triangle nets characteristic of topologically close-packed structures and, as for those nets, it is more fruitful to concentrate on their topological rather than their metric aspects. A good account of many of the nets described here has been given earlier by Jahnberg (1971). We will find that the various operations (*CS*, twinning and rotation) previously discussed all come into play.

Many of these nets are four-connected, and we have already remarked that for such nets equation (1) shows that the fraction of triangles, f_3, is equal to the fraction of pentagons, f_5. In metal oxide structures, in which they largely occur, the metal atoms centre the squares and pentagons; and oxygen atoms in a secondary net are over the metal atoms so that the metal coordination is either octahedral or pentagonal bipyramidal. Per polygon the number of metal atoms is f_4+f_5, and this is also the number of oxygen atoms in the secondary net. The composition of the primary net is $\frac{3}{4}f_3+f_4+\frac{5}{4}f_5$. Using the condition $f_3 = f_5$, one readily finds that the composition is MO_x with $x = (2-f_3)/(1-f_3)$. In principle, x can range from 2 ($f_3 = 0$) to 3 ($f_3 = \frac{1}{2}$); here we consider only nets in which f_3 ranges from $\frac{1}{3}$ to $\frac{3}{7}$.

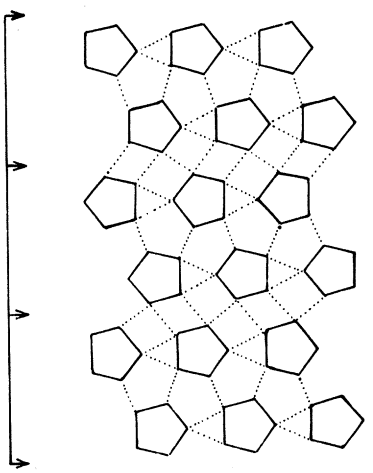

Figure 92. The primary oxygen net of U_2MoO_8.

In going from the net of β-U_3O_8 to that of α-U_3O_8 one-half of the pentagons of the β-U_3O_8 net are rotated in the same sense by 18° (figure 69). If instead, rows of pentagons are rotated in opposite senses new nets are obtained. In figure 92 we derive the net of U_2MoO_8 (Serezhkin *et al.* 1973) from that of β-U_3O_8 by rotations of the same group of pentagons but with the sense of rotation changed every second row. The resulting net contains strips of the α-U_3O_8 net in two different orientations separated by composition/twin lines indicated by the arrows.

Clearly this new net is one of a family of nets (differing in the widths of **α-U_3O_8** strips) that might be expected to occur in the U_2MoO_8–U_3O_8 system.

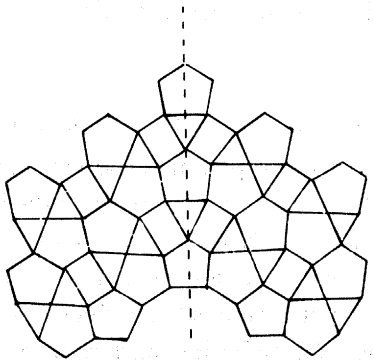

FIGURE 93. Reflexion twinning of **β-U_3O_8**.

The **U_2MoO_8** nets might (in two senses) be called rotation-twinned **α-U_3O_8**. There are other nets to be derived from that of **β-U_3O_8** by reflexion twinning. In figure 93 we show a possible mode of twinning the **β-U_3O_8** net. In this the fraction of triangles is decreased so that, if we are dealing with a metal oxide in which metal atoms centre the squares and pentagons, the O/M ratio also decreases. Indeed, the closest possible periodic twinning of this type produces the anion net of **UVO_5**, shown in figure 94. There is a series of nets derived from that of **β-U_3O_8** which differ only in the spacing of the twin planes. Another such net is shown in figure 95. It corresponds to the primary anion net of a hypothetical oxide M_5O_{13} ($M_3O_8 + M_2O_5$), and could be described as an intergrowth of **β-U_3O_8** and **UVO_5**. It has been proposed that structures of phases in the Ta_2O_5–WO_3 system are derived along these lines (Stephenson & Roth 1971).

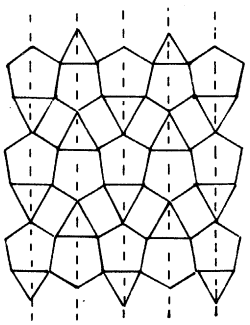

FIGURE 94. **UVO_5** primary oxygen net as a periodic twinning of the **β-U_3O_8** net (cf. figure 93).

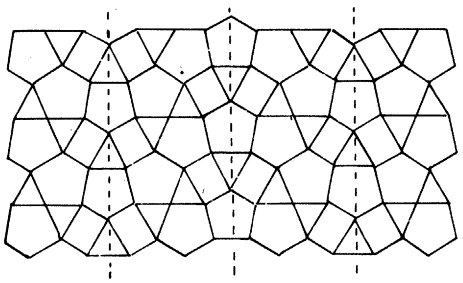

FIGURE 95. Periodic twinning of the **β-U_3O_8** net (see text).

There is a second, quite distinct, relation between the **UVO_5** and **β-U_3O_8** structures. In figure 96 we show how an element of the **β-U_3O_8** structure is introduced into that of **UVO_5** by crystallographic shear (*CS*). The operation eliminates one node of the net (●) and one square (occupied by M in an oxide) which, together with an O atom above the square in the secondary net, constitute the elements of MO_2. The limiting composition is $2M_2O_5$–MO_2 = M_3O_8: thus the **β-U_3O_8** structure is the end member of a homologous series of structures

derived from that of **UVO_5** by *CS*. The general formula is $M_{4n+3}O_{10n+8}$, where n is an integer. The $n = 1$ member of this family is shown in figure 97. Although an oxide with this structure (e.g. $U_5V_2O_{18}$) has not yet been discovered, the same primary net is found in alloy structures such as those of $FeAl_3$ and Fe_4Al_{13}.

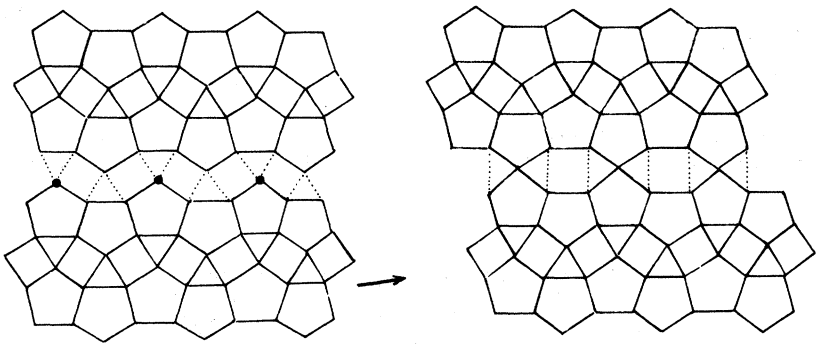

FIGURE 96. *CS* of **UVO_5** (see text).

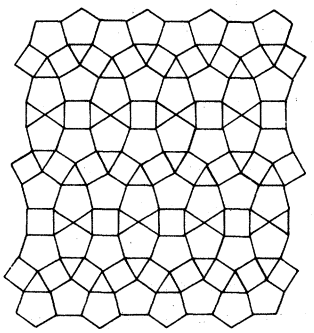

FIGURE 97. A net formed by periodic *CS* of **UVO_5**.

Jahnberg (1971) has called attention to a second kind of twinning that is possible with the **β-U_3O_8** structure: it is illustrated in figure 98. The relative orientation of the twins is the same as in the first kind, and the twin/composition planes are parallel (compare figures 93 and 98); but groups of three pentagons united by edge-sharing are now introduced. Figure 99 shows a new net derived from **β-U_3O_8** by multiple twinning of this second kind. It is analogous to that of **UVO_5**, produced by twinning of the first kind, but the composition is M_4O_{11}. The fraction of triangles in the new net is $\frac{3}{7}$, close to the maximum value of $\frac{1}{2}$. Remarkably, this latter structure can be intergrown with **α-U_3O_8**. A structure is known which is based on this principle (though not so described): it is shown in figure 100; units of M_4O_{11} (the wider strips) are intergrown with units of M_3O_8 (the narrower strips, with **α-U_3O_8** structure). The composition is M_7O_{19} in accord with that of the actual compound, $Zr_7O_9F_{10}$ (Holmberg 1970).

Other possibilities for intergrowth should be apparent. We have already described how the **UVO_5** net may be derived by slip from **3.4.6.4** so that, obviously, these two nets can intergrow having a square-triangle strip in common. This same strip occurs in **3^2.4.3.4**, so that this net

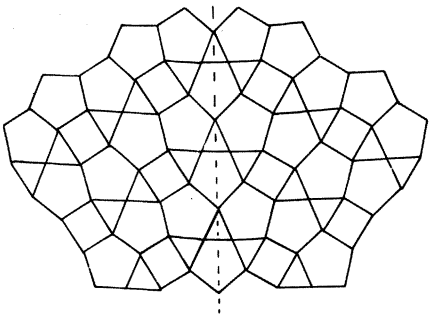

FIGURE 98. A second type of reflexion twinning of the **β-U_3O_8** net (compare figure 93).

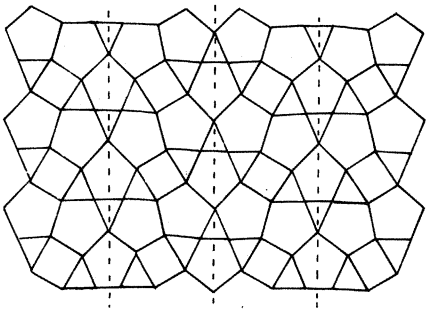

FIGURE 99. Periodic twinning of the second kind on the **β-U_3O_8** net (compare figure 95).

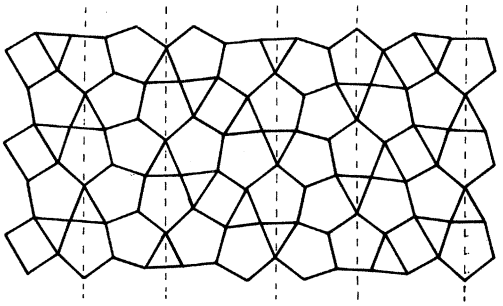

FIGURE 100. The primary anion net of $Zr_7O_9F_{10}$.

can also intergrow with the other two as shown in figure 101. In this connection we might cite γ-$U_3Mo_{20}O_{64}$ (Serezhkin *et al.* 1974) as an example of a compound with a primary net that is an ordered intergrowth of **3.4.6.4** and **3^2.4.3.4**. (Similar intergrowths involving HTB have also been observed by Hussain & Kihlborg 1976).

Note that the **UVO_5** and **β-U_3O_8** nets can intergrow in two different orientations illustrated

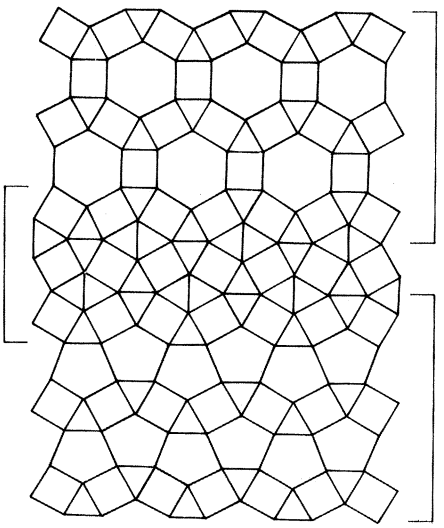

FIGURE 101. **3.4.6.4** (top) intergrown with **3^2.4.3.4** (centre) and the **UVO_5** net (bottom).

in figure 102 (corresponding to the two derivations of $\mathbf{UVO_5}$ from $\mathbf{\beta\text{-}U_3O_8}$ by *CS* and twinning respectively).

Finally, it may be pointed out that many of the primary nets occurring in topologically close-packed structures, notably those of $MgCu_2$ and $MgZn_2$, already discussed, might be

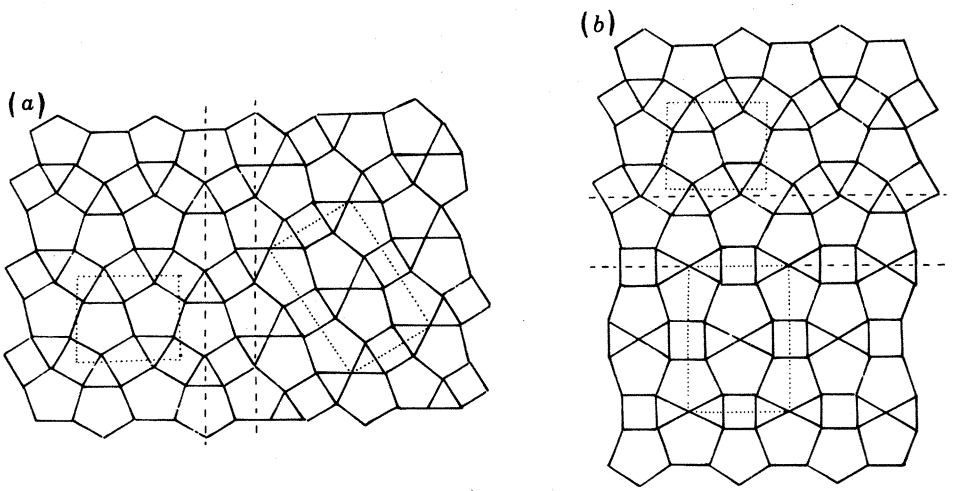

FIGURE 102 (*a*) AND (*b*). $\mathbf{UVO_5}$ and $\mathbf{\beta\text{-}U_3O_8}$ intergrown in two different orientations.

expected to be found in oxides also. For example, the $\mathbf{MgCu_2}$ net (figure 89 (*a*)) contains only 3.5^3 and 3.5.3.5 vertices and has a $\mathbf{3^6}$ secondary net. Applied to oxides of the type currently under discussion it would be the primary net of an oxide MO_3. Net 24, $\mathbf{\beta\text{-}U_3O_8}$ contains Friauf–Laves tiles (two pentagons and two triangles) combined with squares (figure 26). The squares of the $\mathbf{\beta\text{-}U_3O_8}$ net lie on ⟨11⟩ directions and can be eliminated by *CS* with a displacement vector of approximately $\frac{1}{3}\mathbf{a}$ in this plane (figure 103). Clearly, a series of hypothetical oxide structures with compositions ranging from M_3O_8 to MO_3 can be derived by periodic *CS* of $\mathbf{\beta\text{-}U_3O_8}$.

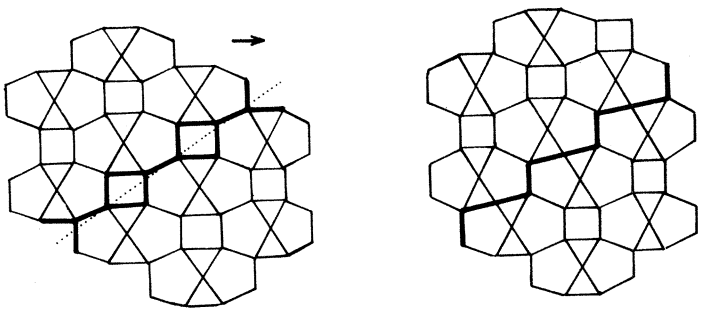

FIGURE 103. Elimination of squares from the $\mathbf{\beta\text{-}U_3O_8}$ net by *CS*.

It is of interest that the nets of this section are also elegantly related to $\mathbf{4^4}$ ($f_3 = 0$, hypothetical oxide MO_2) by periodic twinning. Figure 104 (*a*) shows $\mathbf{4^4}$ twinned about (21); about the composition line one now has pentagons and triangles rather than squares. Applied to oxides (in which MO groups centre squares and pentagons) this results in a decrease in the M/O ratio and is an example of 'chemical twinning' (Andersson & Hyde 1972; Hyde *et al.*

1974). Periodic twinning produces different nets according to the spacing between twin lines; thus figure 104(*b*) shows the net of $\mathbf{UVO_5}$ as a periodic twin of $\mathbf{4^4}$, and figure 104(*c*) similarly shows the derivation of the $\boldsymbol{\beta}$-$\mathbf{U_3O_8}$ net. The closest possible such twinning (figure 104(*d*)) produces a net topologically equivalent to that of $\mathbf{MgCu_2}$ (corresponding to the hypothetical oxide MO_3 already mentioned). Another example is provided by the structure of $BaNb_2O_6$ (Galasso *et al.* 1959), with which one form of $CaTa_2O_6$ is isostructural. The square net of anions is twinned by reflexion on every fourth (21) row, and the nets stacked so as to superimpose. Nb–O–Nb–O rows fill the square tunnels, forming $[NbO_6]$ octahedra, and the Ba atoms lie between the nets and in the pentagonal tunnels, so that the Ba coordination polyhedron is a pentagonal prism.

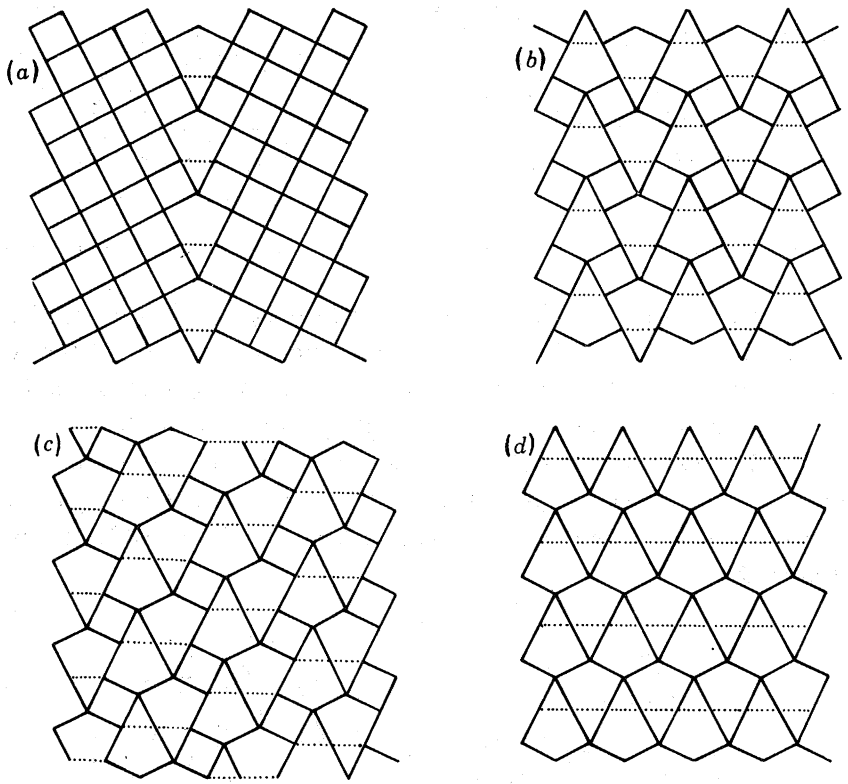

FIGURE 104. (*a*)–(*d*) (21) twinning of $\mathbf{4^4}$ (see text).

11. COLLAPSE

The foregoing discussion has been restricted almost entirely to operations on nets confined to the plane. However, the interest is largely in three-dimensional crystal structures, many of which contain nets in two layers in very close proximity.

An example is provided by the familiar cubic and hexagonal structures of diamond. Here one has $\mathbf{3^6}$ nets of unit edge-length occurring a distance of $\frac{1}{\sqrt{24}}$ apart in pairs, the distance between pairs (of nets) being $\sqrt{\frac{3}{8}}$. If these pairs are enclosed in parentheses the stacking is ...(*ab*) (*bc*) (*ca*)... in cubic diamond and ...(*ab*) (*ba*)... in hexagonal diamond. If alternate

nets are cations and anions we have of course the **zinc blende** and **wurtzite** structures respectively.

An alternative description of the double layers is that they are puckered honeycomb (6^3) layers of skew hexagons with vertex angles of arccos $(-\frac{1}{3}) = 109° 28'$ (such as occur in the 'chair' form of cyclohexane). Clearly only a small distortion is required to make the pairs of 3^6 into planar 6^3 layers, i.e. by collapsing the two layers into one. We represent this symbolically by $(ab) \rightarrow C$, etc., capital letters here being used for 6^3 nets and lower case for 3^6 nets.

Such an operation applied to the **wurtzite** structure will convert it to **BN** (figure 105), with 6^3 nets stacked prismatically. Applied to cubic **diamond**, it will convert it to rhombohedral **graphite**: 6^3 nets stacked in the sequence ...*ABC*... (figure 106). Both transformations correspond to transforming the bonding orbitals from sp^3 to $sp^2 + p$. Production of hexagonal graphite (stacking sequence ...*ABAB*...) requires slip of adjacent layers in addition to collapse.

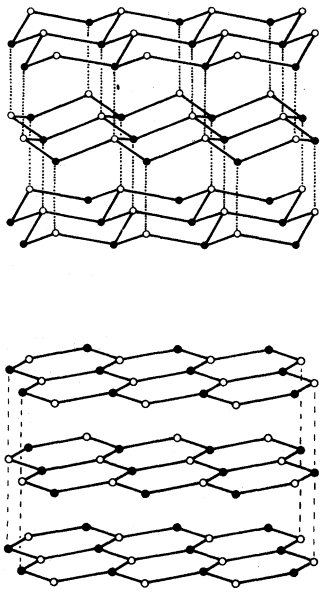

FIGURE 105. The relation between **wurtzite** (top) and **BN** (bottom).

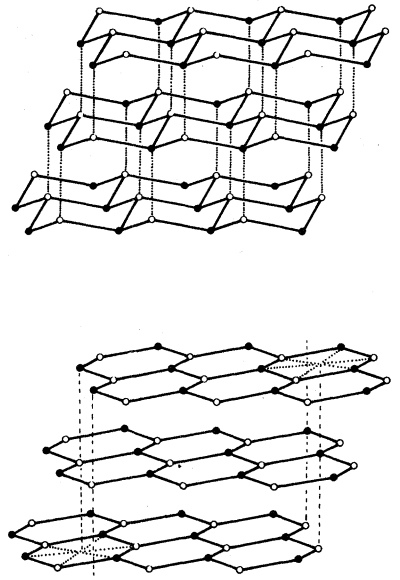

FIGURE 106. The relation between **zinc blende** (or cubic **diamond**, top) and rhombohedral **graphite**.

The body-centred cubic array can also be decomposed into (111) 3^6 nets stacked in the sequence ...*abc*..., but now every inter-net spacing is the same, $\frac{1}{\sqrt{24}}$. Pairs of (111) nets in the **b.c.c.** structure thus form the same puckered 6^3 nets as in **diamond**. The nets can be divided in the sequence ...$(ab)\,c\,(ab)\,c$.... Collapse of the (ab) pairs to 6^3 in the C orientation yields the structure of the ω phase (Silcock 1958): ...*CcCc*.... This is the $\beta \rightarrow \omega$ transformation often observed on quenching b.c.c. alloys. The $\mathbf{AlB_2}$ structure type (alternating 3^6 of **Al** and 6^3 of **B**) is formally the same.

The simple cubic and face-centred cubic arrays can be decomposed into (111) 3^6 nets in a similar manner but with spacings of $\frac{1}{\sqrt{6}}$ and $\sqrt{\frac{2}{3}}$ respectively. The anion arrangement in α-$\mathbf{UO_3}$ can be derived from simple cubic in a manner somewhat analogous to the $\beta \rightarrow \omega$ transformation although the 6^3 nets are now very puckered. The structure of Li_3N has planar 6^3 nets of Li alternating with 3^6 nets of Li. Here the interlayed spacing suggests that it might

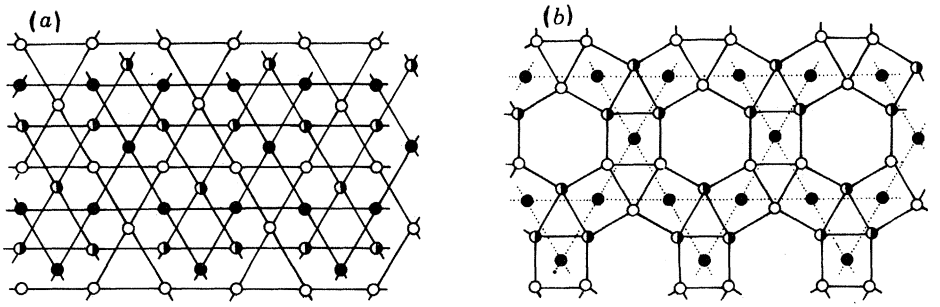

FIGURE 107. Relationship between the anion arrangement of $\mathbf{ReO_3}$ (left) and that of **HTB** (right).

be more appropriate to consider Li_3N as derived from f.c.c. Li with N in octahedral holes on every third (111) layer. These octahedra then collapse to hexagons.

There is a group of structures that may be derived by collapse of kagome (**3.6.3.6**) nets. It may be recalled that the anions of $\mathbf{ReO_3}$ may be described in terms of kagome nets with an $\ldots a'b'c'\ldots$ stacking. The spacing between nets of unit bond length is as in cubic close packing, namely $\sqrt{\frac{2}{3}}$. In figure 107 (*a*) we show in projection three kagome nets with $\ldots a'b'c'\ldots$ stacking. In figure 107 (*b*) two of the nets are collapsed to be coplanar and minor displacements made in the plane to change rectangles into squares. The collapsed net is now **3.4.6.4**, the primary anion net of (ideal) hexagonal tungsten bronze (**HTB**). The third kagome net centres the squares in just the position of the secondary anion net of **HTB**. Thus the transformation of the anion net of $\mathbf{ReO_3}$ to that of **HTB** involves the collapse of two-thirds of the kagome nets to **3.4.6.4**, leaving the remaining kagome nets unchanged.

If the third, undeformed kagome net of X atoms (say a') is centred by A atoms, then figure 107 (*a*) → (*b*) corresponds to an ordered, A-deficient **perovskite** $A_{\frac{1}{3}}Bx_3 \rightarrow$ **HTB** of the same stoichiometry (with no A-deficiency). (At the same time the B atoms shuffle from the octahedral sites in (*a*) to those in (*b*) – rather small, cooperative movements.)†

In figure 108 we show the **3.4.6.4** net decomposed into two adjacent, deformed kagome nets. The deformation is such as to enlarge the octahedral sites in the plane between them. On collapse, these octahedra become the hexagons of **3.4.6.4**. In the kagome → **3.4.6.4** deformation alternate triangles in two of the three kagomes become larger and smaller, by $\pm 26.8\%$ in edge length. The whole array (of three nets) is then expanded by 36.6%.

To complete the structural correspondence of $\mathbf{ReO_3}$ to the octahedral network of **HTB** the octahedrally coordinated cation layers must collapse in a concerted manner. The cations in $\mathbf{ReO_3}$ are in a simple cubic array. If all three layers collapse as in figure 109 (*a*) → (*b*) and simultaneously transform to kagome by the 'jack' operation as in figure 109 (*b*) → (*c*) the array of octahedrally coordinated cations in **HTB** is obtained.

The collapse of the anion and cation nets must of course be considered to occur simultaneously: then the mechanism appears quite plausible.

The deformed kagome nets of figure 108 occur in another structure type, that of **pyrochlore**.

† In reality the layers of corner-connected octahedra in **HTB** are puckered (by tilting the octahedra about their two-fold axes in the plane of the drawing) so that, in fact, the true situation is between those in figure 107 (*a*) and (*b*). The two combined kagomes are not quite coplanar, and their distortion is more equally distributed over all three kagomes. Closely similar relations occur between the AX_3 structures (with empty octahedra) of $AuCu_3$ and a number of other alloys, such as Mn_3Al_9Si (= Mn_3Al_{10}), Fe_3NiAl_{10} (= Co_2Al_5, Pd_2Mg_5, Rh_2Al_5 and Rh_2Mg_5), etc. (Andersson *et al.* to be published).

PHILOSOPHICAL TRANSACTIONS OF THE ROYAL SOCIETY A MATHEMATICAL, PHYSICAL & ENGINEERING SCIENCES

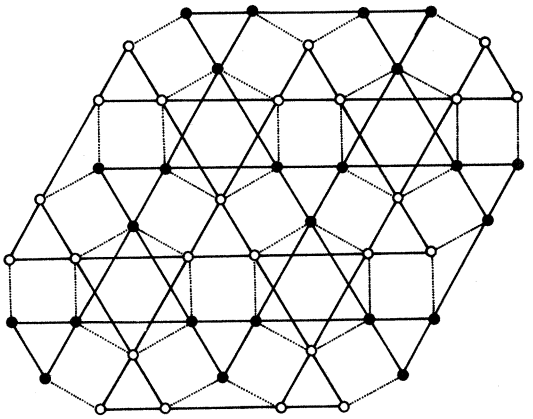

FIGURE 108. **3.4.6.4** decomposed into two kagome nets (open and filled circles).

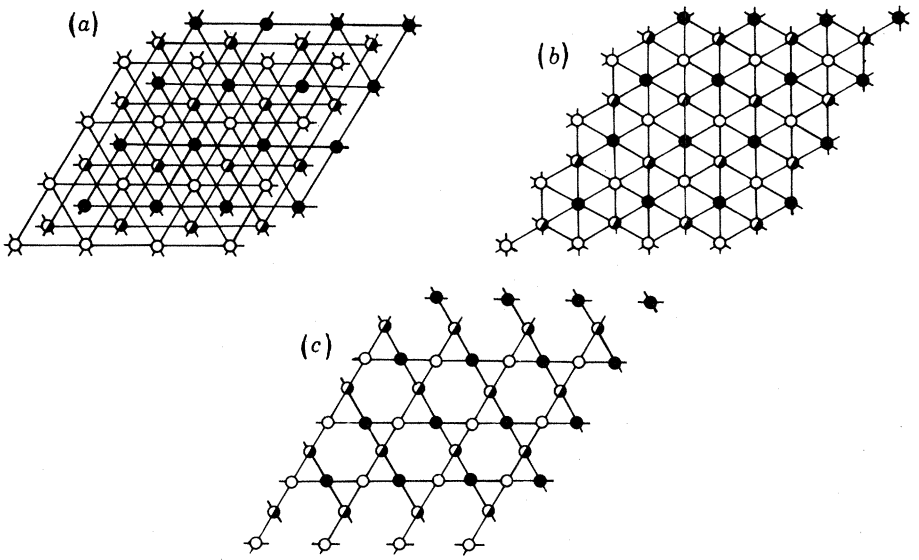

FIGURE 109. Production of a kagome net from three superimposed $\mathbf{3^6}$.

This structure is best considered as a network of corner-connected metal–oxygen octahedra with composition BO_3. Cavities in the structure can be filled by large cations as in $Ag(SbO_3)$ or cation + anion groupings as in $La_2O(TiO_3)_2 = La_2Ti_2O_7$. We consider here just the BO_3 network. Parallel to (111), the anion array consists of unequally spaced deformed kagome nets of the type just described. Pairs of such nets are almost coplanar (cf. footnote on **HTB**) so that they may be considered as slightly puckered **3.4.6.4** nets. The cation arrangement is alternately **3.6.3.6** and $\mathbf{3^6}$. Clearly the **pyrochlore** structure is related to $\mathbf{ReO_3}$ in much the same way as is **HTB**. Figure 110 shows the sequence of anion and cation planes in **HTB** (along [0001]) and in **pyrochlore** (along [111]) and their relationships to $\mathbf{ReO_3}$. Clearly the octahedral framework of the **pyrochlore** structure may be considered as an intergrowth of the framework of $\mathbf{ReO_3}$ and **HTB** and one might expect intergrowth of any one of these structures with another. Once again these relations are illuminating in the context of metal alloy structures, e.g. the V + Al alloys: VAl_{10}, V_4Al_{23}, V_4Al_{45} etc. (Andersson, Hyde and Nyman, to be published).

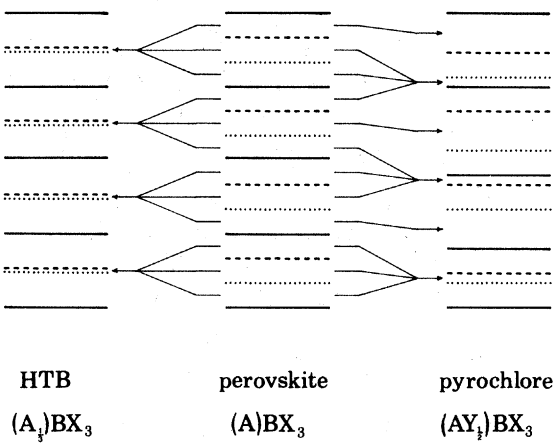

FIGURE 110. The sequence of cation planes (light lines) and anion planes (heavy lines) in the BO_3 frameworks of **HTB**, **ReO_3** and **pyrochlore**. The three types of heavy lines (full, broken and dotted) represent the (relative) positions *a′*, *b′* and *c′*. The arrows indicate the movements of the cation layers from **ReO_3** or **perovskite**, in the centre, to **HTB**, on the left, and to **pyrochlore**, on the right: groups of three coalescing cation layers correspond to the transformation process in figure 109 (see text).

12. CONCLUSION

In this paper we have attempted to give a rather wide-ranging, but by no means complete, analysis of planar nets and their application in crystal chemistry. Formal definitions were followed by some mathematical results, but the emphasis is on nets observed in and useful in understanding crystal structures, whether or (more often) not they are regular enough to be of formal mathematical interest. The major part of our thesis, and where we differ most from earlier investigators in this field, is that net types may often be simply and conveniently related/transformed into one another by rather straightforward operations that may be termed 'crystallographic', for example translation and rotation. Elimination or addition of nodes from or to a net may also produce another net – an operation corresponding to the production of 'point defects' in crystals. It transpires that, frequently, this may equally be achieved by the 'crystallographic' operations – a mode which in the crystal case circumvents the need for long-range diffusion in order to achieve a structure containing 'point defects'. The former is cooperative, the latter is not. This suggests the possibility of new models for 'cooperative diffusion processes', which seem not to have been previously taken into account, at least in the standard texts on diffusion in solids.

Throughout the paper, nets have been related to the structures of specific compounds. These range through a wide variety, from metal alloys such as the Frank–Kasper and Friauf–Laves phases, through intermediate cases such as metal borides, to inorganic materials such as transition and actinide metal oxides, and to minerals such as silicates. The customary but artificial and limiting division of structures into separate groups, of interest largely to *only* metallurgists or *only* inorganic chemists or *only* mineralogists, is self-defeating, and to be deprecated.

The approach is of course essentially geometrical: it leaves aside important questions such as the binding between atoms in crystalline solids. Our justification is simply that it seems logical to develop *description* as an essential preliminary to *explanation*. A coherent and unified

approach to crystal chemistry and physics has not yet been achieved, although we would argue that the sort of approach used here (relating structures by simple, geometrical–crystallographic operations) is enabling one to be developed. Elsewhere a number of people have been using a similar approach in correlating structures described in terms of coordination polyhedra, i.e. in three dimensions. Different descriptive methods have different advantages; and all that are found useful should be used and developed.

The last section departs somewhat from the others in explicitly introducing the third dimension to nets. This results in new insights. It also raises the whole question of three-dimensional nets – a subject on which A. F. Wells has published a number of papers and, after this work was completed, a monograph (Wells 1977), but in which progress has not been spectacularly useful. It seems to us that this is an area of very great importance; and the need for its development as an essential adjunct to topology in crystal science is extreme. But it is also very difficult.

We therefore end by saying that the present paper provides only an introduction to the application of planar nets to crystal science. *A fortiori* it serves only to introduce the *need* for a similar development in three-dimensional nets. We suggest that both areas are worthy of considerable effort. If this is made, it is likely that it will then become even clearer that, contrary to general, implicit assumption, crystal structures are not many thousands of almost arbitrary atom arrays, but rational architectural constructs with their own logic, and based on a few rather simple arrays plus a few rather simple relations/operations which are, nevertheless, able to yield an impressively large collection of structures – which appear to be of great complexity only if the underlying principles (relations) are not recognized.

This work was carried out with the assistance of research grants from Z.W.O. (the Dutch Organization for the Advancement of Pure Scientific Research) and N.A.T.O., to whom we are grateful.

Addendum

Since this text was completed (in 1977) two papers concerning part of its subject matter have appeared: Papiernik *et al.* (1978) on structures related to **β-U_3O_8** (§10), and Andersson (1978) on tetrahedrally close-packed alloy structures (§10), although these are described therein as connected coordination polyhedra rather than as stacks of planar nets.

References

Andersson, S. 1978 *J. Solid State Chem.* **23**, 191.
Andersson, S. & Hyde, B. G. 1972 *J. Solid State Chem.* **9**, 92.
Bursill, L. A. & Hyde, B. G. 1972 *Nature, phys. Sci.* **240**, 122.
Chevalier, R. & Gasperin, M. 1970 *Bull. Soc. fr. Minér. Cristallogr.* **93**, 18.
Coxeter, H. S. M. 1948 *Regular polytopes*. London: Methuen.
Coxeter, H. S. M. 1961 *Introduction to geometry*. New York: John Wiley.
Cundy, H. M. & Rollet, A. P. 1961 *Mathematical models*, 2nd edn. Oxford: Clarendon Press.
Fejes Tóth, L. 1964 *Regular figures*. London: Pergamon Press.
Fisher, W., Burzlaff, H., Hellner, E. & Donnay, J. D. H. 1973 *Space groups and lattice complexes*, N.B.S. monograph 134. Washington, D.C.: U.S. Government Printing Office.
Flahaut, J. & Laruelle, P. 1970 In *The chemistry of extended defects in non-metallic solids* (ed. L. Eyring & M. O'Keeffe), p. 109. Amsterdam: North-Holland.
Frank, F. C. & Kasper, J. S. 1958 *Acta crystallogr.* **11**, 184.
Frank, F. C. & Kasper, J. S. 1959 *Acta crystallogr.* **12**, 483.
Galasso, F., Katz, L. & Ward, R. 1959 *J. Am. chem. Soc.* **81**, 5898.
Geller, S. 1972 *Science, N.Y.* **176**, 1016.

Glazer, A. M. 1972 *Acta crystallogr.* B **28**, 3384.
Haag, F. 1929 *Z. Kristallogr. Kristallgeom.* **70**, 353.
Henry, N. F. M. & Lonsdale, K. 1965 *International Tables for X-ray Crystallography*, 2nd edn. Birmingham: Kynoch Press.
Hepworth, M. A., Jack, K. H., Peacock, R. D. & Westland, G. J. 1957 *Acta crystallogr.* **10**, 63.
Holmberg, B. 1970 *Acta crystallogr.* B **26**, 830.
Hussain, A. & Kihlborg, L. 1976 *Acta crystallogr.* A **32**, 551.
Hyde, B. G., Bagshaw, A. N., Andersson, S. & O'Keeffe, M. 1974 *Ann. Rev. Mater. Sci.* **4**, 43.
Hyde, B. G., Bursill, L. A., O'Keeffe, M. & Andersson, S. 1972 *Nature, Lond.* **237**, 35.
Hyde, B. G. & O'Keeffe, M. 1973*a* *Acta crystallogr.* A **29**, 243.
Hyde, B. G. & O'Keeffe, M. 1973*b* In *Phase Transitions – 1973* (ed. L. E. Cross). New York: Pergamon Press.
Iijima, S. & Allpress, J. G. 1974*a* *Acta crystallogr.* A **30**, 29.
Iijima, S. & Allpress, J. G. 1974*b* *Acta crystallogr.* A **30**, 22.
Jack, K. H. & Guttmann, V. 1951 *Acta crystallogr.* **4**, 246.
Jahnberg, L. 1963 *Acta chem. scand.* **17**, 2548.
Jahnberg, L. 1970 *J. Solid State Chem.* **1**, 454.
Jahnberg, L. 1971 *University of Stockholm chem. Commun.* nr XIII.
Jamieson, P. B., Abrahams, S. C. & Bernstein, J. L. 1968 *J. chem. Phys.* **48**, 5048.
Jeitschko, W. 1974 *Acta Crystallogr.* B **30**, 2565.
Kripyakevich, P. I. & Yarmolyuk, Ya. P. 1971: see Shoemaker & Shoemaker 1972.
Kuz'ma, Yu. B. 1970 *Soviet Phys. Crystallogr.* **15**, 312.
Kuz'ma, Yu. B. & Svarichevskaya, S. I. 1972 *Soviet Phys. Crystallogr.* **17**, 569.
Loopstra, B. O. 1970 *Acta crystallogr.* B **26**, 656.
Lundberg, M. 1971 *University of Stockholm Chem. Commun.* Nr XII.
MacMahon, P. A. 1921 *New mathematical pastimes.* Cambridge: The University Press.
Magnéli, A. 1949 *Ark. Kemi* **1**, 213.
Mahe, R. 1967 *Bull. soc. chim.* fr. **6**, 1879.
Megaw, H. D. 1957 *Ferroelectricity in crystals*, p. 104. London: Methuen.
Michel, C., Moreau, J. M. & James, W. J. 1971 *Acta crystallogr.* B **27**, 501.
Miller, J. C. P. 1930 *Phil. Trans. R. Soc. Lond.* A **229**, 336.
Moore, P. B. 1967 *Science, N.Y.* **156**, 1361.
Moreau, J. M. & Parthé, E. 1974 *Acta crystallogr.* B **30**, 1743.
Niggli, P. 1926 *Z. Kristallogr. Kristallgeom.* **65**, 341.
Niggli, P. 1928 *Z. Kristallogr. Kristallgeom.* **68**, 304.
O'Keeffe, M. & Hyde, B. G. 1976 *Acta crystallogr.* B **32**, 2923.
O'Keeffe, M. & Hyde, B. G. 1977 *Acta crystallogr.* B **33**, 3802.
Papiernik, R., Gaudreau, B. & Frit, B. 1978 *J. Solid State Chem.* **25**, 143.
Pearson, W. B. 1972 *The crystal chemistry and physics of metals and alloys.* New York: Wiley.
Povarennykh, A. S. 1972 *The crystal chemical classification of minerals.* New York: Plenum Press.
Schubert, K. 1964 *Kristallstrukturen Zweicomponentiger Phasen.* Berlin: Springer-Verlag.
Serezhkin, V. N., Kovba, L. M. & Trunov, V. K. 1973 *Dokl. Akad. Nauk SSSR* **210**, 1106.
Serezhkin, V. N., Kovba, L. M. & Trunov, V. K. 1974 *J. struct. Chem. U.S.S.R.* **14**, 689.
Shannon, J. & Katz, L. 1970 *J. Solid State Chem.* **1**, 399.
Shoemaker, D. P. & Shoemaker, C. B. 1968 In *Structural chemistry and molecular biology* (ed. A. Rich & N. Davidson). San Francisco: Freeman.
Shoemaker, C. B. & Shoemaker, D. P. 1972 *Acta crystallogr.* B **28**, 2957.
Silcock, J. M. 1958 *Acta metall.* **6**, 481.
Sinha, A. K. 1972 *Prog. Mater. Sci.* **15**, 79.
Smith, C. S. 1968 In *Hierarchical Structures* (ed. L. L. Whyte, A. G. Wilson & D. Wilson). New York: Elsevier.
Spinat, P., Brouty, C., Wheeler, A. & Herpin, P. 1975 *Acta crystallogr.* B **31**, 541.
Stephenson, N. C. & Roth, R. S. 1971 *Acta crystallogr.* B **27**, 1010.
Sturm, J. & Gruehn, R. 1975 *Naturwissenschaften* **6**, 296.
Watanabe, D., Terasaki, O., Jostsons, A. & Castles, J. R. 1970 In *The chemistry of extended defects in non-metallic solids* (ed. L. Eyring and M. O'Keeffe), p. 249. Amsterdam: North-Holland.
Wells, A. F. 1954*a* *Acta crystallogr.* **7**, 535.
Wells, A. F. 1954*b* *Acta crystallogr.* **7**, 545.
Wells, A. F. 1954*c* *Acta crystallogr.* **7**, 842.
Wells, A. F. 1970 In *Models in structural inorganic chemistry.* Oxford: Clarendon Press.
Wells, A. F. 1977 *Three-dimensional nets and polyhedra.* New York: John Wiley.
Wyckoff, R. W. G. 1963 *Crystal structures*, 2nd edn. New York: John Wiley.

PHILOSOPHICAL TRANSACTIONS OF THE ROYAL SOCIETY A MATHEMATICAL, PHYSICAL & ENGINEERING SCIENCES